The Use of Conventional and Advanced Magnetic Resonance Techniques in the Assessment of Primary Brain Tumours

Gisele Duwe Brasil Caseiras

A thesis submitted to the University College London for the degree of

Doctor of Philosophy

June 2008

Department of Brain Repair and Rehabilitation

Institute of Neurology, University College London

Queen Square

London WC1N 3BG

United Kingdom

Declaration

I, Gisele Duwe Brasil Caseiras, confirm that the work presented in this thesis is my own. Where information has been derived from other sources, I confirm that this has been indicated in the thesis.

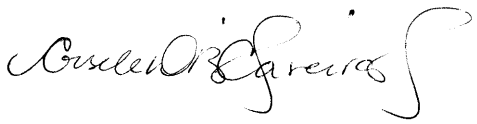

Abstract

The aim of the work described in this thesis was to investigate the value of conventional, perfusion- and diffusion-weighted magnetic resonance imaging (MRI) in patients with histology-proven low-grade gliomas (LGG), and the potential role of these methods in the management of patients with these brain tumours.

Thirty-six patients were studied at the National Hospital for Neurology and Neurosurgery using conventional, perfusion-weighted and diffusion-weighted MRI at study entry and 6 monthly intervals thereafter. At each visit, tumour volume, maximum rCBV and ADC histogram measures were calculated. This is a unique cohort, as patients were treatment free until malignant transformation was diagnosed, which translates the natural history of these brain tumours. It is unlikely to find such a specific cohort as most of the patients receive treatment after the initial diagnosis of low grade gliomas.

Chapters 1 and 2 of this thesis describe the theoretical basis of the MRI techniques used, and summarise the natural history and imaging aspects of cerebral gliomas. Chapter 3 describes a methodological study relating to tumour perfusion measurement: since the inclusion or exclusion of intratumoural vessels may influence the quantification of relative cerebral blood volume (rCBV), a study was conducted to choose the best ROI placement technique to be used for the rCBV measurements included in this thesis. It was shown that only the approach which excluded intratumoural vessels demonstrated a significant association between rCBV values and tumour subtypes (astrocytomas, oligodendrogliomas and oligoastrocytomas) and therefore this technique was used in all subsequent rCBV measurements.

In chapter 4, it was investigated whether rCBV is a useful outcome predictor in patients with low-grade gliomas. We found that in LGG susceptibility-weighted MR perfusion imaging not only allows differentiation between histological tumour subtypes but also between two different outcome groups. More importantly, rCBV at study entry can be used to predict time to transformation in these patients.

To complement these studies we assessed the utility of rCBV in predicting clinical response in 2 patient groups with low-grade glioma, studied at two separate institutions. The results presented in chapter 5 suggested that glioma rCBV correlates with time to progression or death, independently of institution, despite different approaches to patient management at the two sites.

Finally, in chapter 6 we analyzed which quantitative MRI measure (tumour volume, rCBV and ADC) was the best predictor of outcome (stable, progressive disease or death). We found that tumour volume at study entry, at 6 and at 12 months, and its short-term changes were stronger predictors of outcome in patients with low-grade glioma than, and independent of, rCBV, diffusion histogram parameters, age, gender, histology and treatment. Moreover tumour growth was the best predictor of time to transformation and tumour volume was the only independent predictor of time to death. Since this parameter can readily be obtained in any MRI centre and be quantified with an automated method, it may become a useful prognostic factor in clinical practice.

Acknowledgements

I would like to thank my supervisors Dr. Rolf Jäger, Prof. Tarek Yousry and Dr. John Thornton for giving me the opportunity to do this PhD, for carefully reading my thesis, and for their encouragement.

A special thanks to Dr. Olga Ciccarelli, for her invaluable advice, support and guidance, without which I would not have been able to write and finish my thesis, and for being such good and supportive friend.

A warm thank you to Dr. Zhaleh Khaleeli, Dr. Benedetta Bodini and Dr. Tom Jenkins, who gave me much appreciated support and a deeper knowledge in neurology, and for the lessons in English and Italian culture, and especially tea making.

Thanks to Mr. Chris Benton for scanning the patients and Dr. Daniel Altman for his much needed statistical advice.

I would like to thank the patients, without whom this thesis would not have been possible. I truly appreciate their commitment and effort in helping the scientific field.

A big “obrigado” and love to all my family in Brazil, and in London, for their support, especially to my mother who inspired me to pursue a career in academia and to my father who inspired me to be a doctor.

Most of all I would like to thank my dear husband Paul for his unconditional support, for learning everything about brain gliomas, rCBV, ADC and statistics, and for his encouragement and listening skills. Finally, a loving thank you to my sweet baby daughter Beatriz for allowing me the time to finish my thesis.

Publications associated with this thesis

Brasil Caseiras G, Thornton JS, Yousry T, Benton C, Rees J, Waldman A, D., et al. Inclusion or exclusion of intratumoural vessels in relative cerebral blood volume characterization in low-grade gliomas: does it make a difference? *American Journal of Neuroradiology* 2008.

Caseiras *GB*, Chheang S, Babb J, Rees J, Pecerrelli N, Tozer D, Benton C, Zagzag D, Johnson G, Waldman AD, Jäger HR, Law M. Relative Cerebral Blood Volume Measurements of Low-Grade Gliomas Predicts Patient Outcome in a Multi-institution Setting. *European Journal of Radiology* 2008.

Gisele Brasil Caseiras, Olga Ciccarelli, Daniel R Altmann, Christopher Benton, Daniel J Tozer, Paul S Tofts, Tarek Yousry, Jeremy Rees, Adam D Waldman, and Hans Rolf Jäger. Tumour growth and volume predict patient outcome in conservatively treated low-grade gliomas better than ADC and rCBV measurements. Submitted to *Radiology*.

Jäger HR, **Caseiras GB**, Rich PM. Grainger and Allison's Diagnostic Radiology, Chapter 56. 2007; 2: 1271-1294.

Danchaivijitr N, Waldman AD, Tozer DJ, Benton CE, **Brasil Caseiras G**, Tofts PS, et al. Low-grade gliomas: do changes in rCBV measurements at longitudinal perfusion weighted MR imaging predict malignant transformation? Radiology 2008; 247: 170-8.

Table of Contents

List of Figures

Page

Chapter 1

Chapter 2

Chapter 3

Chapter 4

Chapter 5

Chapter 6

List of Tables

Abbreviations

1H	hydrogen nuclei
B0	external magnetic field
ADC	apparent diffusion coefficient
AC	astrocytoma
CI	confidence interval
CT	computed tomography
D	self diffusion constant of the tissue
DSC-MRI	dynamic susceptibility contrast MRI
DWI	diffusion-weighting imaging
EORTC	European organization for research and treatment of cancer
FLAIR	fluid-attenuated inversion recovery
FSE	fast spin echo
GE-EPI	gradient-echo echo-planar imaging
GBM	glioblastoma multiforme
GRE	gradient recalled echo
HGG	high-grade glioma
ION	Institute of Neurology
LGG	low-grade glioma
M	magnetization
MRI	magnetic resonance imaging
MTT	mean transient time
NEX	number of excitations
NYUMC	New York University Medical Centre
NMR	nuclear magnetic resonance

RF	radio frequency
OA	oligoastrocytoma
OD	oligodendroglioma
PET	positron emisson tomography
PGSE	pulse gradient spin echo
rCBF	relative cerebral blood flow
rCBV	relative cerebral blood volume
ROC	receiver operating characteristic
ROI	region of interest
SD	standard deviation
SE	spin echo
SE-EPI	spin-echo echo-planar imaging
SNR	signal to noise ratio
SPGR	spoiled gradient echo
T1	longitudinal relaxation time
T1W	T1 weighted
T2	transversal relaxation time
T2*	loss of phase due to inhomogeneity within the magnetic field
T2W	T2 weighted
TE	echo time
TR	repetition time
VEGF	vascular endothelial growth factor
WHO	World Health Organization

Chapter 1

An introduction of the principles of MRI, diffusion-weighted and perfusion-weighted imaging

1.1. Principles of magnetic resonance imaging (MRI)

1.1.1 Basic Physics of MRI

Nuclear magnetic resonance (NMR) provides a non-invasive means of constructing a spatial representation human tissue *in vivo* and relies on the magnetic properties of certain atomic nuclei. Nuclei with an odd number of protons and neutrons possess the property of spin and, since atomic nuclei are electrically charged, their spinning motion produces a magnetic moment in the direction of the spin axis. The strength of the magnetic moment is a property of the type of nucleus: since hydrogen nuclei (^{1}H) possess the strongest magnetic moment and are present in high abundance in biological material, ^{1}H-imaging is the most widely used MRI procedure.

In the absence of an externally applied magnetic field, thermal motion causes the magnetic moments of individual nuclei to have random orientations (Figure 1.1 (a)). However, if an externally supplied magnetic field B_0 is imposed, the magnetic moments have a tendency to align with the external field (Figure 1.1 (b)).

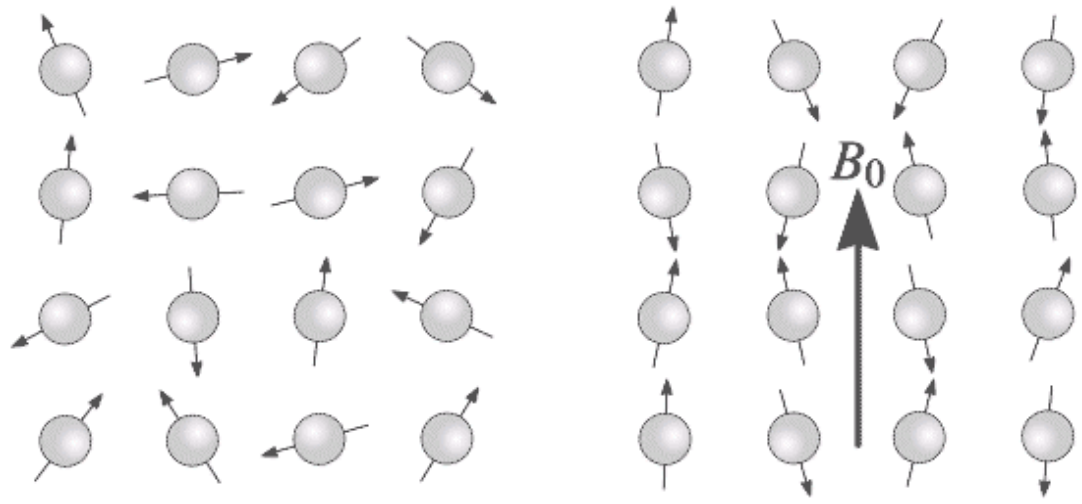

a) b)

Figure 1.1: (a) A collection of spinning protons in the absence of an externally applied magnetic field. The magnetic moments have random orientations. (b) An external magnetic field B_0 is applied which causes the nuclei to align themselves in one of two orientations with respect to B_0.

The spin axes are not exactly aligned with B_0, they precess around B_0 with a characteristic angular frequency as shown in Figure 1.2.

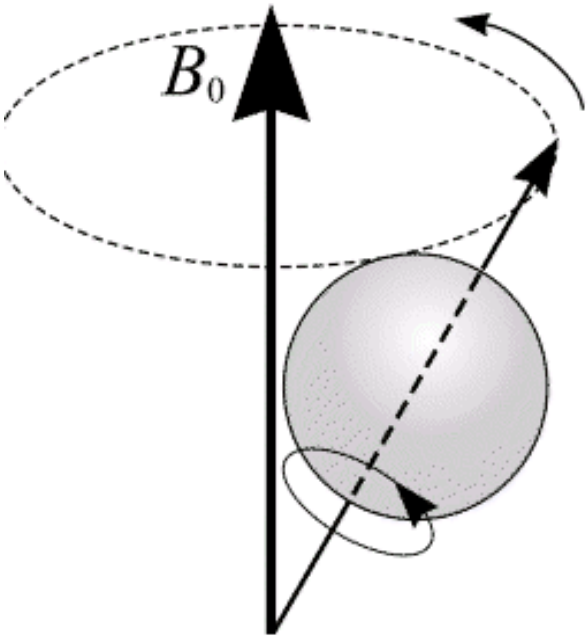

Figure 1.2: A magnetic moment precessing around B_0. Its path describes the surface of a cone.

The angular precession frequency depends on the strength of the magnetic field according to the Larmor equation:

$\omega = \gamma B_0$

where γ is the gyromagnetic ratio of the nucleus; B_0 is the external magnetic field given in Tesla and ω is the precessional, or Larmor, frequency in radians per second. The equation shows that the precession frequency increases linearly with the magnetic field strength.

In order to detect a signal from ^{1}H nuclei, radio frequency (RF) energy must be applied in the form of a magnetic field (B_1) rotating at the Larmor frequency. This causes M to rotate away from its equilibrium orientation parallel to B_0 towards the *x-y* plane.

The angle through which M has rotated away from the z-axis is known as the flip angle: the flip angle is proportional to the strength and duration of B_1. A 180^{o} pulse rotates M into an orientation anti-parallel to B_0. If the B_1 field is applied indefinitely, M tilts away from the z-axis, through the x-y plane towards the negative z direction, and finally back towards the x-y plane and z-axis (where the process begins again) (McRobbie et al., 2005). Figure 1.3.

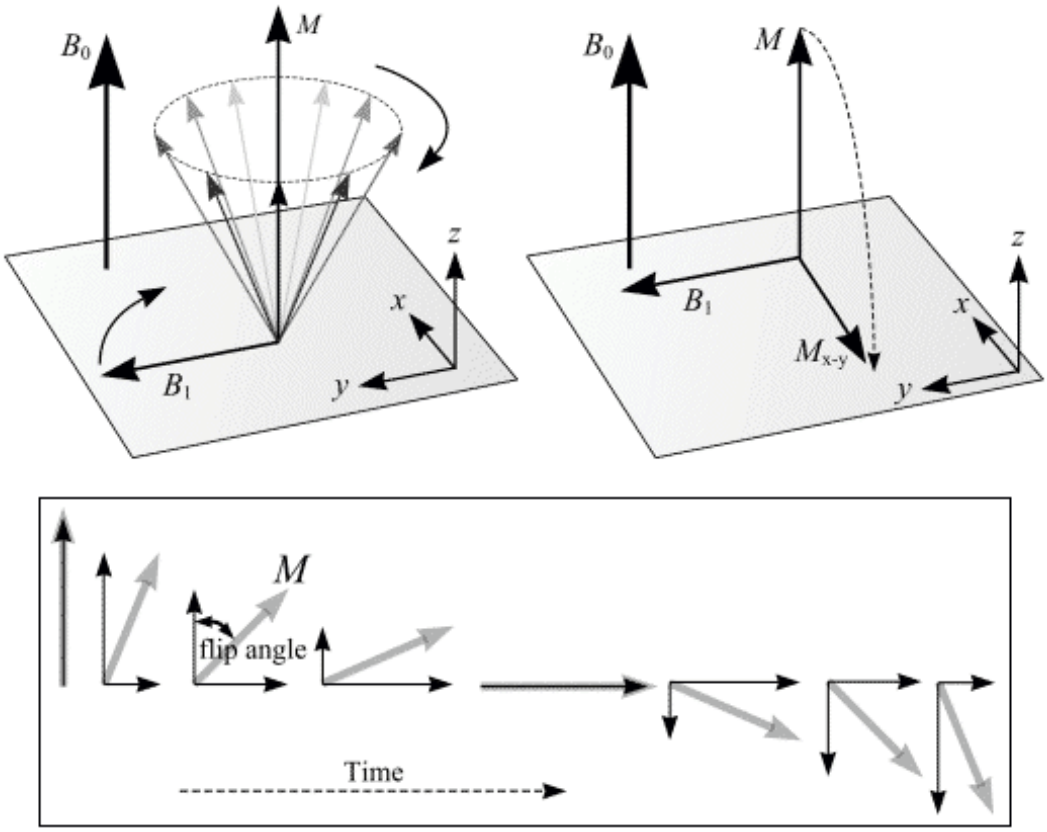

Figure 1.3: Top: the effect of RF radiation on the net magnetization M is to produce a component of M, $M_{x\text{-}y}$, orthogonal to B_0. M is tilted from its original longitudinal z-axis orientation, parallel to the direction of the external magnetic field B_0, into the transverse x-y plane. Bottom: an illustration of flip angle, which is the angle through which M has rotated away from the z-axis. Figure after Mike Puddephat 2005.

Figure 1.4 (a) shows the situation after a RF pulse is applied that causes the net magnetization vector M to flip by 90 degrees. M lies in the x-y plane and continues to precess about the B_0 direction. M will induce an electromotive force (voltage) in a receiver coil. This is the principle of NMR signal detection. It is from this received RF signal that an MR image can be constructed. Figure 1.4(b) shows a graph of the voltage or signal induced in a receiver coil verses time. Such a graph, or waveform, is termed the free induction decay (FID). The magnitude of the generated signal depends on the number of nuclei contributing to produce the transverse magnetization and on the NMR relaxation times.

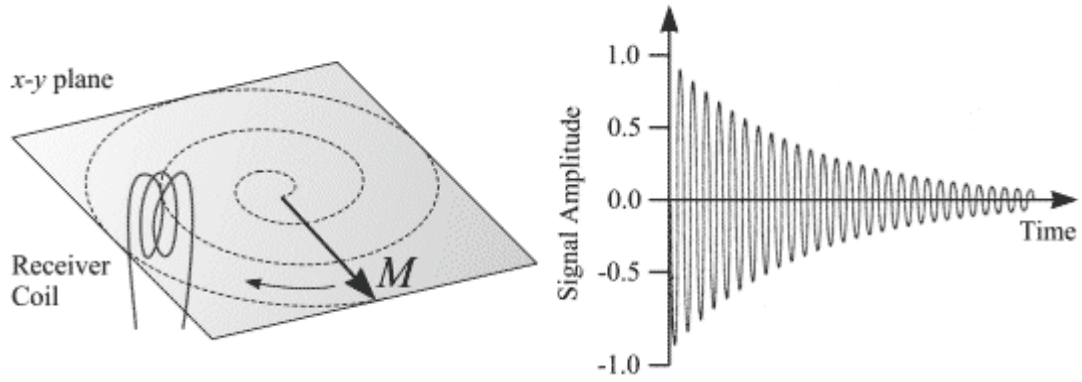

(a) (b)

Figure 1.4: (a) After a 90 degree RF pulse, M lies in the x-y plane and rotates about the z-axis. The component of M in the x-y plane decays over time. An alternating current, producing the voltage signal shown in Figure (b), is induced in the receiver coil. Figure after Mike Puddephat 2005.

1.1.2 Relaxation Processes

The return of M to its equilibrium state (i.e. aligned parallel to B_0) following an RF pulse is known as relaxation, which is influenced by three processes: the longitudinal T1 relaxation, transverse T2 relaxation and signal decay caused by magnetic field inhomogeneities. T1 relaxation (also known as spin-lattice relaxation) is the realignment of spins (and so of M) with the external magnetic field B_0 (z-axis). T2 relaxation (also known as T2 decay, transverse relaxation or spin-spin relaxation) governs the irreversible decrease of the x-y component of M.

1.1.2.1 T1 relaxation

Following termination of an RF pulse, nuclei will dissipate their excess energy as heat to the surrounding environment (or lattice) and revert to their equilibrium orientations. Realignment of the nuclei along B_0, through a process known as recovery, leads to a gradual increase in the longitudinal magnetization. The time taken for the nuclei to relax back to the equilibrium state depends on the rate that excess energy is dissipated to the lattice. Figure 1.5.

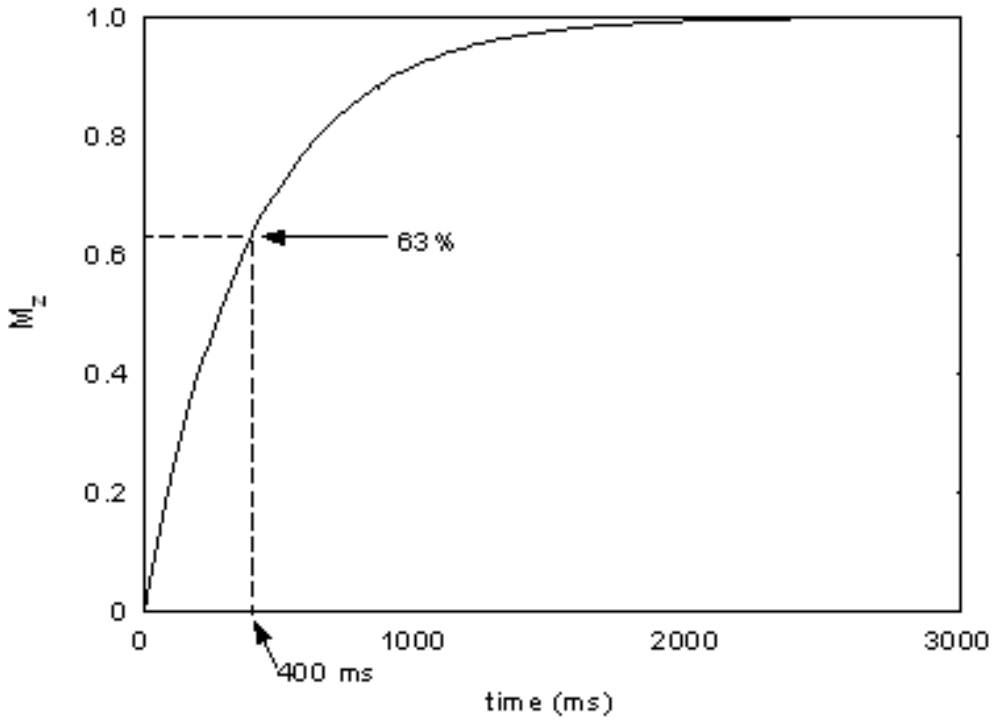

Figure 1.5: T1 is the time taken for the M_z magnetization to recover to 63% of its equilibrium value following a 90^o pulse. M_z represents the component of the net magnetization parallel to the main magnet field B_0.

1.1.2.2 T2 relaxation

While nuclei dissipate their excess energy to the lattice following an RF pulse, the magnetic moments also interact with each other causing a decrease in transverse magnetization. Each nucleus is influenced by the fluctuating magnet fields produced by its neighbours, causing transient changes in the Larmor frequency resulting in a loss of phase coherence. The resulting decrease in M_{xy} (which does not involve the emission of energy) is generally considered to be an exponential decay with time constant T2: T2 is the time it takes for the transverse magnetization to decay to 37% of its original magnitude in the absence of magnetic field inhomogeneities. Figure 1.6.

It is virtually impossible to construct an NMR magnet with perfectly uniform B_0. Much additional hardware is supplied with NMR machines to assist in producing a homogenous B_0 field. However, it is inevitable that an NMR sample will experience different B_0's across its body so that nuclei within the sample (that exhibit spin) will exhibit different precessional frequencies (according to the Larmor equation). Immediately following a 90^o pulse, all regions within the sample will have $M_{x\text{-}y}$ coherent. However, as time goes on, phase differences across the sample will evolve due to nuclei precessing at different frequencies. These phase differences will increase with time and the vector addition of these out of phase moments will progressively reduce $M_{x\text{-}y}$.

Therefore in addition to decay governed by the T2 time constant, there is an additional contribution to the decay of the M_{xy} from magnetic field inhomogeneities, and the overall signal decay is described by a time constant T2* which characterizes dephasing due to both B_0 inhomogeneity and transverse relaxation.

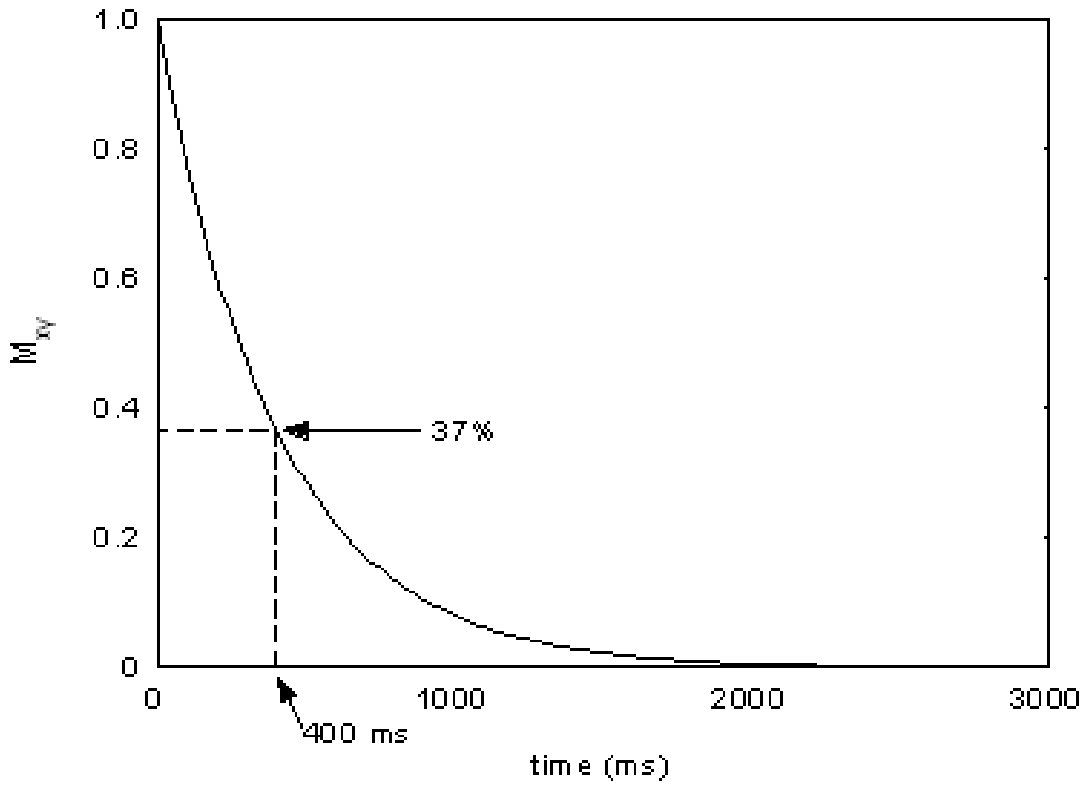

Figure 1.6 T2 is the time taken for the transverse magnetization to drop to 37% of its initial size in the absence of magnetic field inhomogeneities.

Field gradients and spatial localisation

In MRI, a field gradient is a linear variation in B_0 produced by pulsing current in special gradient coils, which can produce field gradients in 3 orthogonal directions corresponding to the x, y and z axes. Since the Larmor frequency is linearly dependent on B_0, the application of field gradients causes the Larmor frequency to be dependent upon position: this is the basis of spatial discrimination in MRI.

1.1.3 MRI Pulse Sequences

A pulse sequence is an appropriate combination of one or more RF pulses and gradients with intervening periods of recovery. A pulse sequence is characterized by several parameters, of which the main ones are the TR, TE, flip angle, the number of excitations (NEX), bandwidth and acquisition matrix.

1.1.3.1 Spin Echo Pulse Sequence

In order to obtain signal with a T2 dependence rather than a T2* dependence, the spin-echo (SE) pulse sequence is used which reverses the effects of B_0 inhomogeneity on $M_{x\text{-}y}$. The SE sequence is the most commonly used pulse sequence in clinical imaging. It comprises 2 RF pulses - the 90^o pulse that creates the detectable magnetization and the 180^o pulse that refocuses it at TE. The selection of TE and TR determines resulting image contrast.

The SE sequence is shown pictorially in Figures 1.7 and 1.8. Figure 1.7 is a graph of pulsed RF and received signal verses time, while Figure 1.8 is a phase diagram of the magnetization vector M. After a 90^o pulse, a signal is produced which decays with T2* characteristics. This is illustrated by the top right ellipse in Figure 1.7 which shows three spins at different phases due to their different precessional frequencies. The fastest spin is labelled f and the slowest s. At time TE/2, an 180^o pulse is applied to the sample (see bottom left ellipse in Figure 1.8) which causes the three spins to be reflected about the x axis. After this, the order of the spins is reversed with the fastest lagging behind the others. At time TE, the spins become coherent again so that a signal (known as the spin echo) is produced.

If a further 180^{o} pulse is applied at time TE/2 after the peak signal of the first spin echo, then a second spin echo signal will form at time TE after the first spin echo. The peak signal amplitude of each spin echo is reduced from its previous peak amplitude due to T2 dephasing which cannot be reversed by the 180^{o} pulses. Figure 1.9 shows how the signal from a spin echo sequence decays over time. A line drawn through the peak amplitude of a large number of spin echoes describes the T2 decay, while individual spin echoes exhibit T2* decay.

Signal strength decays with time to varying degrees depending on the different materials in the sample. Different organs have different T1s and T2s and hence different rates of decay of signal.

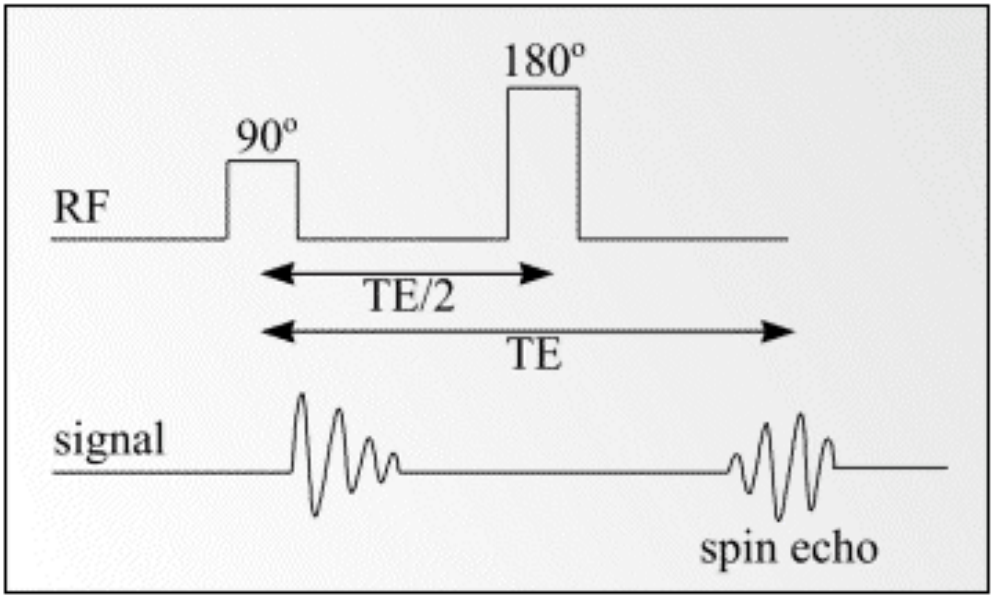

Figure 1.7: Formation of a spin echo at time TE after a 90^{o} pulse. Figure after Mike Puddephat 2005.

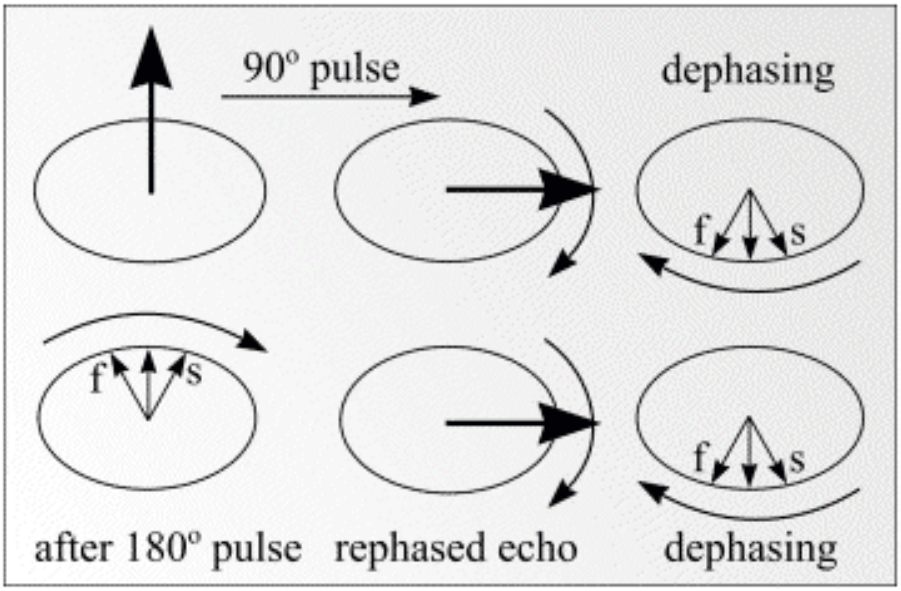

Figure 1.8: Dephasing of the magnetization vector by T2* and rephasing by an 180° pulse to form a spin echo. Figure after Mike Puddephat 2005.

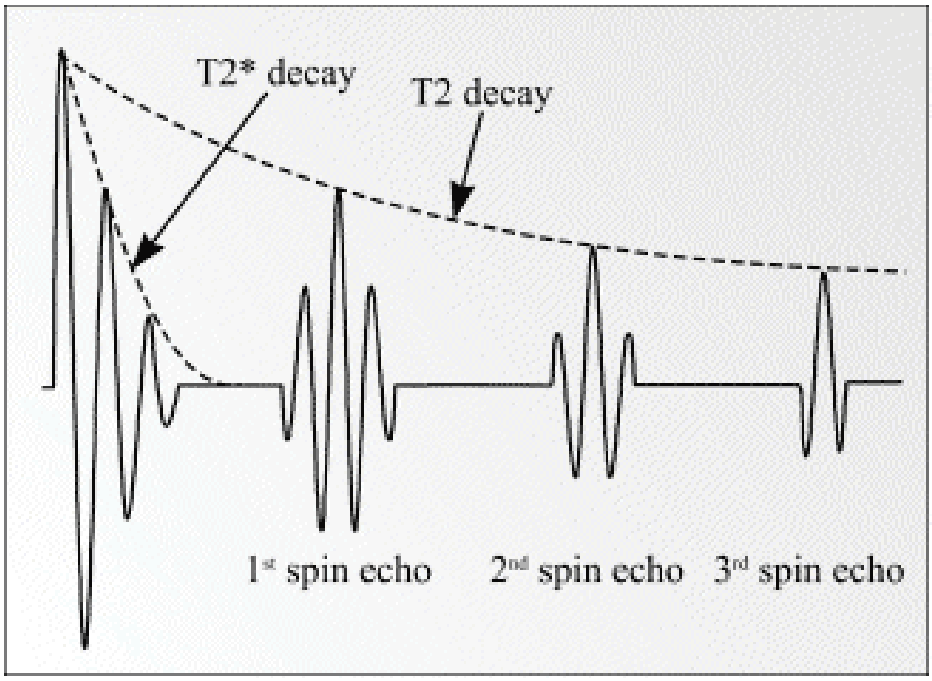

Figure 1.9: Decay of signal with time in a spin echo sequence. Figure after Mike Puddephat 2005.

Spin-echo sequences can produced both T1- or T2-weighted contrast according to the choice of TR and TE. The repetition time (TR) is the time between 2 consecutive 90^{o} RF pulses and determines the amount of T1 relaxation occurring between them. The longer the TR, the more the longitudinal magnetization is recovered. For short TRs (< 1s), tissues with short T1 have greater signal intensity than tissues with a longer T1 at a given TR. A long TR allows more magnetization to recover and thus reduces the degree of T1-weighting in the image contrast. Thus a pulse sequence with short TR and short TE produces a T1-weighted image. Conversely, a long TE and long TR will allow almost complete T1-relaxation, but allow considerable T2 signal decay, resulting in a T2-weighted image.

In short TR T1-weighted images, tissues that have short T1 relaxation times (such as fat) present as bright signal. Tissues with long T1 relaxation times (such as cysts, cerebrospinal fluid and oedema) show as dark signal. In T2-weighted images, tissues that have long T2 relaxation times (such as fluids) appear bright.

In cerebral tissue, differences in T1 relaxation times between white and grey matter permit the differentiation of these tissues on heavily T1-weighted images. Proton density-weighted images also allow distinction of white and grey matter, with tissue signal intensities mirroring those obtained on T2-weighted images. In general, T1-weighted images provide excellent anatomic detail, while T2-weighted images are often superior for detecting pathology.

1.1.3.2 Gradient Recalled Echo Pulse Sequences

Gradient recalled echo (GRE) sequences, which are significantly faster than SE sequences, differ from SE sequences in that there is no 180^{o} refocusing RF pulse. In addition, the single RF pulse in a GRE sequence is usually switched on for less time than a 90^{o} pulse, in order to obtain an adequate signal-to-noise ratio (SNR) despite a short TR used to reduced the total scan time. Depending upon the TE and TR, the GRE sequence produces T1- or T2*-weighted contrast at the expense of the SNR which drops due to incomplete relaxation and magnetic susceptibility variations. At the interface of bone and tissue or air and tissue, there is an apparent loss of signal that is heightened as TE is increased. Nevertheless, GRE sequences are widely used for obtaining T1-weighted images for a large number of slices or a volume of tissue in order to keep scanning times to a minimum. GRE sequences are often used to acquire T1-weighted 3D volume data that can be reformatted to display image sections in any plane.

1.1.3.3 FLAIR (Fluid attenuation inversion recovery)

FLAIR uses a variation on the SE sequence called “inversion recovery”, which has an extra 180^{o} RF pulse separated by the inversion recovery time (TI) before the 90^{o} pulse.

The action of the inversion RF pulse is to invert the starting magnetization, which then returns to its equilibrium value (M_0) according to T1 relaxation (Figure 1.10). TI is chosen so that when the 90° pulse is applied, there is no longitudinal magnetization to be flipped into the x-y plane from liquid (Figure 1.11).

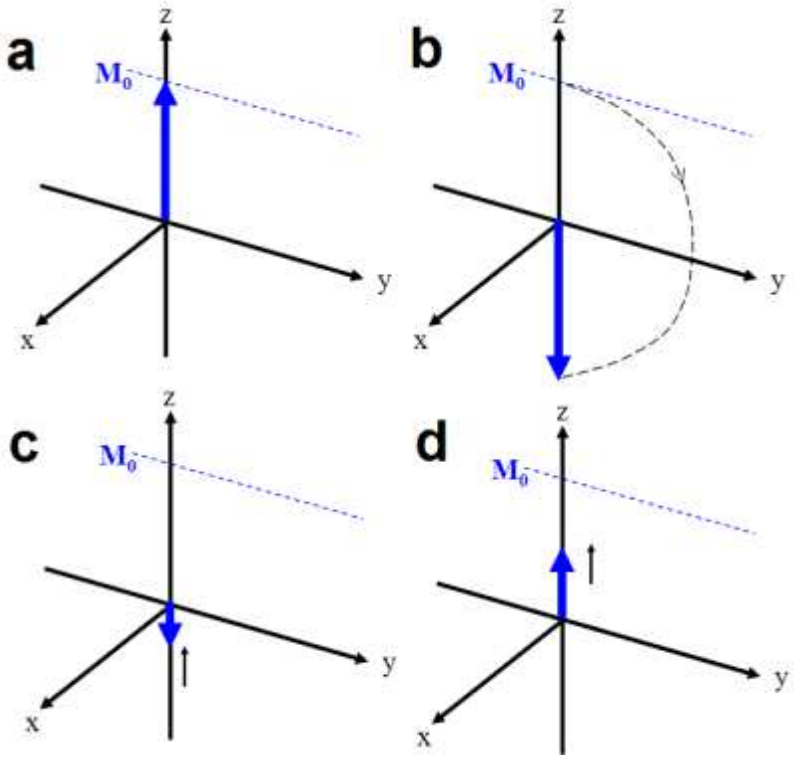

Figure 1.10: (a) Initially the nuclear spins are aligned along z and (b) a 180º pulse inverts the magnetization. Note that no transverse magnetization is produced at this stage (c,d) T1 relaxation occurs and at the chosen inversion time TI a 90º pulse is applied to generate the MR signal.

.

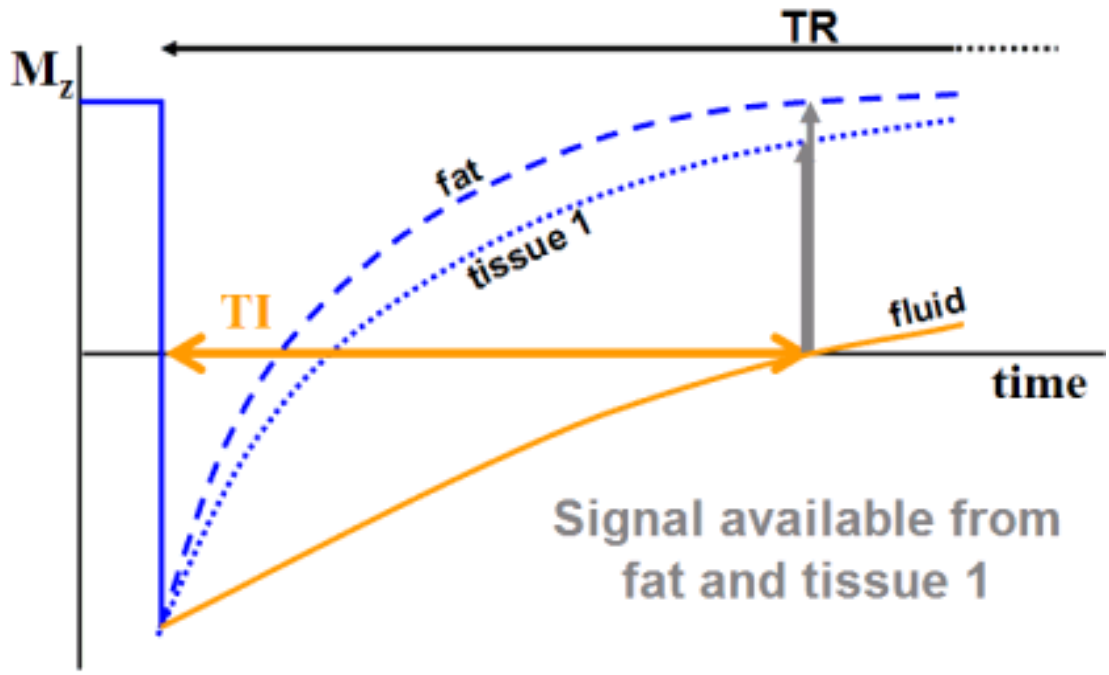

Figure 1.11: TI is chosen so that the 90° pulse is applied at the null point of fluid.

Thus fluid signals are suppressed in FLAIR imaging, meaning that in brain imaging, CSF appears dark, and does not produce a strong signal that may contaminate that from adjacent parenchyma.

1.1.3.4 Diffusion-weighted imaging

Diffusion phenomena are the consequence of a microscopic random molecular motion, known as Brownian motion. Due to molecular thermal energy, each particle in a fluid is constantly moving and is occasionally struck by other molecules. With every hit, a particle changes direction randomly, so that, over time, its path can be described as a random walk. In free water, molecular diffusion is isotropic, i.e. independent of direction. In biological tissues the situation is different because diffusing molecules may be reflected, or have their mobility interrupted, by the interactions with the cell membranes and other intracellular and extracellular structures. Therefore, water diffusion becomes anisotropic, meaning that the molecular motion is restricted or hindered by cellular structures in a geometrically-dependent manner.

The most common method for producing diffusion-weighted contrast is the pulse gradient spin echo (PGSE) method. It consists of a 90° - 180° pair of RF pulses (i.e. an SE sequqnce) with large and equal field gradients placed on either side of the 180° pulse (Figure 1.12).

The first 90° pulse excites the sample, whilst the second 180° pulse reverses the phase of the spins and refocuses the magnetization. In the absence of motion or diffusion of the water molecules, the dephasing that occurs after during the first gradient pulse is exactly rephased after the 180° pulse and the signal will be unchanged. If, instead, there is a random motion of the spins between dephasing and rephasing, then the refocusing of the spins is incomplete and there is a loss in the transverse magnetization and a reduction in the signal amplitude (Schaefer et al., 2000). The extent of this attenuation depends on: 1) the diffusion properties of the tissue and 2) the magnetic field and the time during which the diffusion process takes

place. As a result, where there is free water movement, for example, cerebral spinal fluid or in areas of vasogenic oedema, there is a drop in signal. Where there are regions of water trapping, for example within swollen cells in areas of cytotoxic oedema, there is an increase in signal. In summary, structures with fast (high) diffusion are dark, because they are subject to greater signal attenuation, whereas structures with slow (low) diffusion are bright (Le Bihan et al., 1992).

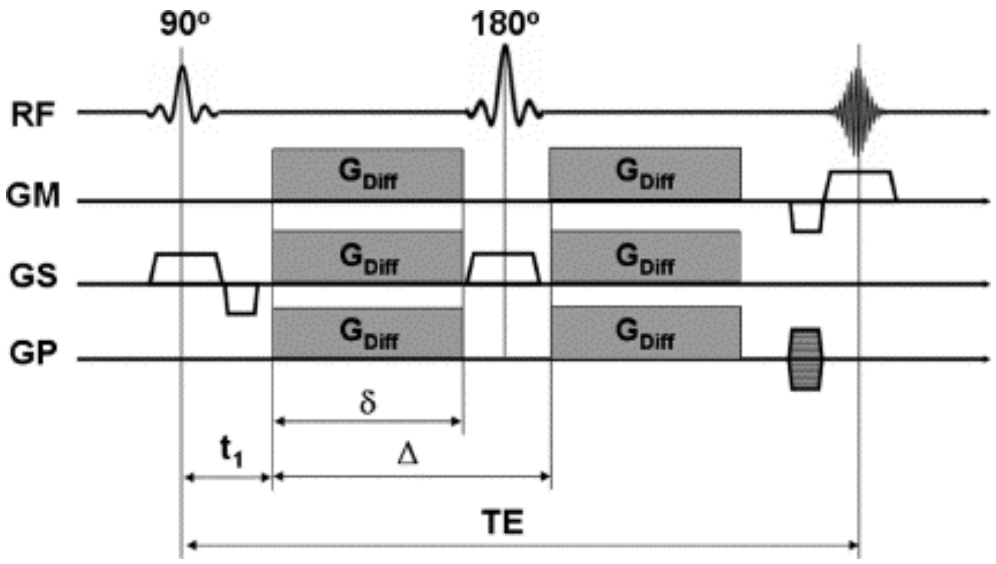

Figure 1.12: Basic pulsed gradient spin echo (PGSE) sequence for diffusion-weighted imaging (DWI). Diffusion-weighting gradients of strength G_{Diff}, duration δ, and spacing Δ are applied during each TE/2 period. The diffusion-weighted echo is sampled at the time t=TE when the spin echo is formed. The diffusion attenuation is only dependent on the parameters G_{Diff}, Δ, and δ but does not depend on t_1. Large gradient amplitudes are highly advantageous because their use means that the TE can be minimized reducing signal loss by T2 decay. Figure after Mike Puddephat 2005.

Since the signal change with DWI is also dependent on the underlying T2-weighted signal, it is not possible to use DWI signal changes alone to quantify diffusion process. Instead the gradient of the signal intensity obtained with different degree of diffusion-weighting (b value) is plotted. This yields the diffusion coefficient, which is a measure of all random motional processes such as diffusion and incoherent flow. In practice what we measure in PGSE is not the free-water (unrestricted) diffusion coefficient: since diffusion is frequently reduced by microscopic tissue structures which hinder the free motion of eater molecules, *in vivo* we usually refer to apparent diffusion coefficient (ADC).

In areas of increased diffusion (vasogenic oedema) there is an increase in ADC, and DWI signal intensity is decreases. In areas of restricted water diffusion (e.g. cytotoxic oedema) ADC decreases and DWI signal intensity increases. To reiterate: a high value of D (the self diffusion constant of the tissue) or ADC implies rapid motion and therefore low signal in DWI. The corresponding ADC map will be bright (McRobbie et al., 2005).

1.1.3.5 Perfusion-weighted imaging

Perfusion is a term that has different meanings to different professionals. Biotechnologists use it to mean the process of keeping tissues alive in a solution containing all the vital nutrients. In cardiology, perfusion means the use of artificial blood pumps to propel open-heart surgery patients' blood through their body tissue, replacing the function of the heart while the cardiac surgeon operates. In imaging, perfusion is the process of nutritive delivery of arterial blood to a capillary bed in the biological tissue (McRobbie et al., 2005).

There are three measures commonly used to quantify perfusion using MRI or other imaging techniques: cerebral blood volume (CBV), cerebral blood flow (CBF) and mean transit time (MTT). Often these terms are prefixed with “r” (rCBV, rCBF and rMTT), since it is difficult to quantify them absolutely and it is usually preferable to find a ratio between the ipsi- and contra-lateral sides.

There has been much development in the study of blood flow in animals. Since the late 1960s the use of plastic, radioactive microspheres was introduced for measurement of regional organ perfusion (Rudolph and Heymann, 1967). In 1968 Makowski et al.(Makowski et al., 1968) the microsphere method was used extensively to measure regional blood flow in laboratory animals. Small diameter microspheres injected into the left atrium distribute throughout the body and become trapped in capillaries of target tissue based on regional blood flow patterns. The quantity of microspheres lodged in the tissue of interest is proportional to the reference blood flow sample and allows the calculation of regional blood flow in ml/g/min (Bartoli et al., 2008). Using this technique, radioactive-labelled microspheres have been used to determine relative blood flow in both acute and

chronic preparations. In acute experimentation, these microspheres may slightly underestimate relative blood flow due to the difference in density between radioactive-labelled microspheres and erythrocytes (Hale et al., 1988). Fluorescent-labelled microspheres are more useful for chronic experimentation, do not pose health risks for investigators, and avoid the high disposal costs of radioactive tissues and cadavers (Hale et al., 1988; Hoffmann et al., 2002).

In the neurological field, numerous imaging techniques have also been developed and applied to evaluate brain hemodynamics. The main imaging techniques dedicated to brain hemodynamics are positron emission tomography (PET), single photon emission computed tomography (SPECT), dynamic perfusion computed tomography (PCT), MRI dynamic susceptibility contrast (DSC), MRI dynamic contrast enhanced (DCE) and arterial spin labeling (ASL) (Wintermark et al., 2005). All these techniques give similar information about brain hemodynamics in the form of parameters such as cerebral blood flow (CBF) or cerebral blood volume (CBV). They use different tracers diffusible or non diffusible, endogenous or exogenous and have different technical requirements.

Positron emission tomography is able to quantify blood flow and different PET tracers are available. Among them, $^{15}0$ labeled-water has the major advantage of being freely diffusible and its short half-life (2.1 min) allows sequential measurements with a low radiation dose for patients. However, it has the disadvantage of a poor signal-to-noise ratio, which hinders its use in clinical routine (Merlet et al., 1993). It is mainly used to assess myocardial blood flow (Sheikine and Di Carli, 2008).

Single photon emission computed tomography (SPECT) using technetium-99m hexamethylpropylene amine oxime (^{99m}Tc-HMPAO) is a well-recognized method of

detecting changes of cerebral perfusion (Lee et al., 2003). SPECT perfusion agents such as [123I]IMP, [99mTc]HMPAO, [99mTc]ECD have been successfully used to detect various cerebrovascular diseases such as stroke, Parkinson disease, Huntington's disease, epilepsy, dementia, and psychiatric disorders (Saha et al., 1994). Furthermore, a reduction in blood flow in the parietal and temporal regions is considered to be the definitive SPECT finding in Alzheimer disease (Nitrini et al., 2000).

Dynamic CT perfusion imaging uses equipment available in most radiology departments to measure the first pass of a bolus of iodinated contrast medium. The method has been used to study the hemodynamics in acute stroke and has been validated in animal and human studies (Nabavi et al., 1999; Wintermark et al., 2001). Perfusion CT provides an imaging correlate for tumour vascularity that can be used to discriminate benign and malignant lesions, indicate tumour aggressiveness, reveal occult tumour and improve the delineation of tumours during radiotherapy planning, and can also be used as a functional assessment of tumour response to therapy (Miles, 2006). Perfusion CT is used for preoperative grading of gliomas with relative CBV being the best parameter correlating with glioma grades (Ellika et al., 2007). A study showed good correlation between CT and MR for CBF and MTT abnormalities (Eastwood et al., 2003). However, dynamic CT perfusion studies presently are limited to either a 1-cm- or a 2-cm-thick section of tissue per acquisition, depending on whether a single-slice CT scanner or a multislice CT scanner is used.

Perfusion-weighted imaging (PWI) methods can be divided into three main categories depending on the type of imaging used to acquire the data. First, dynamic susceptibility contrast MRI (DSC-MRI) is a first pass technique that uses rapid measurement of T2- or T2*-weighted signal change after injection of a bolus of

paramagnetic compound (i.e. gadolinium-based contrast material). This technique will be described with more detail bellow. Secondly, dynamic contrast enhanced MRI (DCE-MRI) is based on the T1-weighted signal change produced after an interval of 5-10 minutes following injection of gadolinium-based contrast material. Thirdly, arterial spin labeling (ASL) uses water as a freely diffusible endogenous tracer of the blood's entry into the imaging volume (Jenkinson et al., 2007). It tags proton in the arterial blood supply with a magnetic "label", then images the required slices with or without the labelling. When images are then acquired from slices in the brain, there will be a very small signal loss compared with unlabelled images. This is because there is an inflow enhancement even in the capillaries (McRobbie et al., 2005). The label decays in only 4-5 seconds due to T1 relaxation of the blood protons, so EPI id used for the image acquisition. There are several different ASL techniques, differing mainly in the way they apply the labelling and control pulses, one of them is flow-sensitive alternating inversion recovery (FAIR). In the FAIR labelled images, an inversion pulse is applied to the whole brain before a single-slice EPI image is acquired. For the control experiment the inversion pulse is applied only to the imaged slice. In the labelled image, inverted protons in the arterial supply are carried into the capillary bed of the imaged slice and exchange with protons in the tissues. It has been shown that the FAIR signal may depend on hemodynamic parameters other than perfusion, the most important one being transit delays of labelled spins to the observed tissue. (Schepers et al., 2004). Although a slower technique with poor signal to noise ratio, it is completely non-invasive and can be repeated as often as required without having to wait for the excretion of the gadolinium (McRobbie et al., 2005) (Tofts, 2004). Although recent developments at

3T have improved results, ASL has been slow to emerge as a technique sufficiently robust for clinical use.

Since DSC-MRI was the technique used in this thesis, the method will now be described in greater detail. DSC-MRI required rapidly repeated multi-slice imaging during the first pass of a gadolinium bolus: a volume of tissue, usually only a few slices, is imaged repeatedly using an echo-planar imaging (EPI) sequence. After a few images have been collected to establish an equilibrium baseline, a bolus of gadolinium is injected as rapidly as possible. During the first pass through the intracranial circulation the high concentration of gadolinium in the vasculature causes a reduction of T2 and T2* in the surrounding tissue, which is seen as a drop in signal intensity on T2-weighted or T2*-weighted images (Figure 1.13 A, B and C). This drop in signal is proportional to the concentration of the contrast agent and the tissue vascularity. The whole imaging sequence takes no more than 2-3 minutes. The signal intensity curve is used to determine the rCBV, the relative cerebral blood flow (rCBF), the time of arrival, the time to peak and the mean transient time (MTT) of the contrast–agent (Chaskis et al., 2006). The time to peak is not often used in brain tumours since, unlike in infarcts, there rarely is much of a delay in blood flow within tumours (Price, 2007). In the evaluation of intracranial mass lesions, CBV appears to be the most useful parameter (Cha et al., 2002) and this will be emphasized in this thesis.

The passage of gadolinium causes changes in both T2 and T2* so that both spin-echo and gradient-echo echo-planar imaging sequences provide robust measurements of CBV. Originally gradient-echo EPI sequences were used for DSC-MRI since they are most sensitive to changes in T2*. When a paramagnetic contrast agent such as gadolinium passes through the cerebral vascular system, it induces differences in

local magnetic susceptibility between vessels and the surrounding tissue. Although the vascular space is a small fraction of the total tissue blood volume, this compartmentalization of contrast agent causes targeted paramagnetism within the intravascular spins as well as the surrounding spins within a given voxel. Thus, both intravascular and extravascular spins experience a reduction of T2* that leads to a large transient signal loss of approximately 25% in normal white matter with a standard dose of contrast (0.1 mmol/kg of body weight). T2-weighted spin-echo images are less sensitive and require double or even quadruple the contrast agent dose to give substantial signal changes during the bolus passage. On the other hand, gradient-echo sequences are more prone to magnetic susceptibility artefacts. Thus, when imaging lesions near brain-bone-air interfaces such as the temporal lobes or posterior fossa where these artefacts are more pronounced, spin echo sequences may be preferable. However, artefacts in gradient-echo images can be overcome to a large extent by reducing the slice thickness (Cha, 2004).

There should be at least five images in the baseline section for analysis purposes: since a bolus injection in the antecubital vein typically takes 8-10 seconds to reach the brain, the injection should be started soon after the start of the imaging sequence. It is useful to have a power injector as an injection rate of 3-5ml s-1 is necessary to achieve a good bolus which may be difficult by hand. Repeated imaging of the volume should continue for a total of 2-3min.

In the absence of recirculation and contrast leakage, CBV is proportional to the area under the contrast concentration-time curve (Figure 1.13). The effects of the recirculation can be reduced by manually choosing the beginning and end of the bolus. While the area under the corrected contrast concentration-time curve is proportional to the CBV, this approach does not yield an absolute measurement. It is

therefore necessary to express the measurement relative to a standard reference, usually contralateral white matter. We refer to this as relative CBV (rCBV).

In order to determine absolute values of CBV and CBF it is necessary to deconvolve the arterial input function (AIF) from the tissue response curve, in order to account for variations in the bolus shape and timing. However, the unambiguous determination of an appropriate AIF is challenging, the calculations may be sensitive to the details of the analysis method, and the necessary assumptions regarding the relationship between contrast agent concentration and signal intensity may be hard to support in the atypical microvascular environment of many tumours (Calamante et al., 1999). For this reason absolute quantification of these haemodynamic measures was not attempted in the present work. In this thesis we will consider only the use of rCBV acquired with DSC MRI.

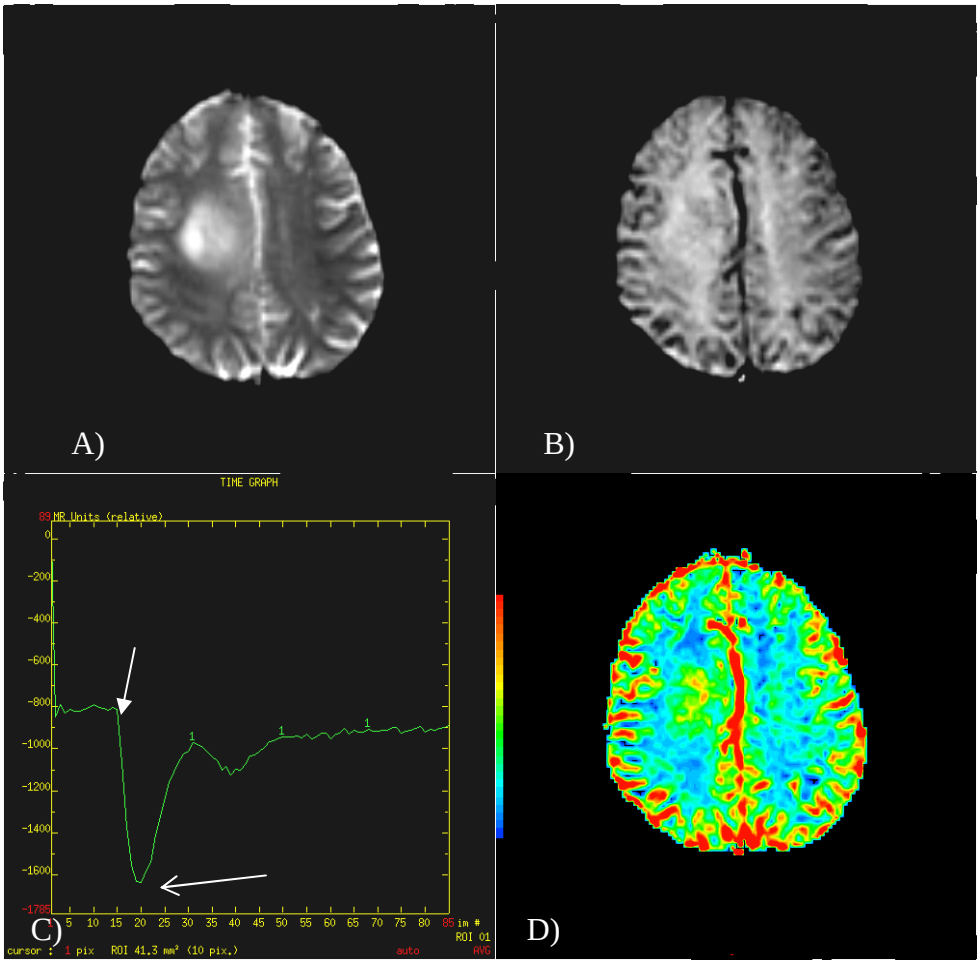

Figure 1.13: T2*-weighted image before the injection of a bolus of gadolinium, B) T2* weighted with drop of signal intensity, during the first pass of the gadolinium bolus, C) signal-intensity/time graph showing the arrival of the first pass of the bolus of gadolinium (closed arrow) and peak height (open arrow). D) rCBV map of a right frontal low-grade glioma.

Analysis of DSC-imaging cerebral perfusion data is frequently performed at a clinical workstation using proprietary software. Most software produce pixel-by-pixel maps of the required parameters and use colour scales for display (Figure 1.13 D).

1.2. Conclusion

This chapter has described the basic physics of MRI and the most relevant sequences used within this thesis. Chapters 3, 4, 5 and 6 while describe the application of conventional, perfusion- and diffusion-weighted MR imaging in patients with histology proven low-grade gliomas in order to provide further insight into their role in the management of patients with these brain tumours.

Chapter 2

An introduction to brain gliomas and clinical applications of magnetic resonance imaging

2.1 Brain Gliomas

The World Health Organization (WHO) classification (Kleihues et al., 1993; Kleihues P, 2000; Louis et al., 2007) classifies brain tumours in: neuroepithelial tumours, cranial nerves tumours, meningial tumours, lymphoma and haemopoietic tumours, germ cell tumours, tumours of the sellar region and metastatic tumours. The fourth edition of the World Health Organization (WHO) classification of tumours of the central nervous system, published in 2007, lists several new entities, including angiocentric glioma, papillary glioneuronal tumour, rosette-forming glioneuronal tumour of the fourth ventricle, papillary tumour of the pineal region, pituicytoma and spindle cell oncocytoma of the adenohypophysis. However when the work of this thesis was performed, WHO classification of 2000 was used. In the 2000 edition the main contribution to brain gliomas was the recognition of the emerging role of molecular diagnostic approaches to tumour classification, as in the distinct subtypes of glioblastoma and the already clinically useful 1p and 19q markers for oligodendroglioma.

In this thesis the main attention will be given to gliomas, which are the commonest neuroepithelial tumours. They can be divided into three types, depending on the cell type they originate from: astrocytomas, oligodendrogliomas and oligoastrocytomas (Behin et al., 2003). These gliomas can be subdivided in low (WHO grades I and II) and high-grade tumours (WHO grades III and IV), reflecting their biological behavior.

Caution should be taken when interpreting the incidences for each subtype of astrocytoma, oligodendroglioma and oligoastrocytoma, since histologic sampling error and inter- or intrapathologist variability could result in tumour misclassification.

The use of diffusion- and perfusion-weighted imaging has been used widely in the study of brain gliomas. Section 2.2 of this chapter will further consider this technique and its neuroimaging characteristics will be discussed in detail.

2.1.1 Astrocytomas

Astrocytomas account for approximately 75% of glial tumours. They can be divided into four histological grades, according to the WHO classification, ranging from the benign pilocytic astrocytomas (Grade I) to glioblastoma multiforme (Grade IV), which is the most malignant astrocytic tumour. The incidence of the various types of astrocytic tumours varies with age. In children, most of these are relatively benign tumours (pilocytic or low-grade astrocytomas), in young adults low-grade astrocytomas predominate, whereas anaplastic astrocytomas have a peak incidence around 40 years and glioblastoma multiforme usually occurs after 40 years (Behin et al., 2003).

2.1.1.1 Pilocytic astrocytomas (WHO grade I)

These are well-circumscribed, potentially resectable lesions with a low proliferative potential and a predilection for the posterior fossa. They are primarily seen in children and are rare in adults. Infratentorial pilocytic astrocytomas in adults are frequently mistaken for haemangioblastomas, which have a similar appearance and represent the commonest primary intra-axial tumour below the tentorium cerebelli in adults (Jäger et al., 2007).

Clinical Features

Seizures are uncommon, since the tumour does not usually involve the cerebral cortex. These tumours produce focal neurological deficits, such as macrocephaly, headache, endocrinopathy or increased intracranial pressure. Other focal deficits could be present, depending on the location of the tumour.

Neuroimaging

Pilocytic astrocytomas are primarily a paediatric neoplasm and rare in adults. They are well circumscribed tumours and have a predilection for the posterior fossa, optic nerves and hypothalamus. Infratentorial pilocytic astrocytomas in adults may be mistaken for haemangioblastomas. On computed tomography (CT) they often appear as a cystic lesion with an eccentric mural nodule that strongly enhances after the administration of contrast agent. On MRI, low-grade astrocytomas are typically hyperintense on T2-weighted images. They usually have a significant cystic component and show enhancement which can be nodular or ring-like (Dixon et al., 2007).

2.1.1.2 Diffuse astrocytomas (WHO grade II)

Diffuse astrocytomas are infiltrating low-grade tumours which occur typically in the hemispheres of young adults, involving cortex and white matter. However, focal, grossly circumscribed lesions can also occur. They have less well defined borders than pilocytic astrocytomas and contrast enhancement is usually absent. WHO grade II astrocytomas show a low mitotic activity but have a propensity to progress to a higher histological grade. They represent 10 to 15% of all astrocytomas and the median survival time is 10 years (Osborn, 1994).

Clinical Features

Seizures are a common manifestation of the tumour. Other abnormalities could be present, such as speech difficulties, changes in sensation, vision or some motor changes as well. The focal deficit will depend on the location of the tumour. With frontal lobe tumours, changes in behaviour or personality may be the presenting feature.

Neuroimaging

CT and MRI: These tumours appear as an iso- or hypodense mass on CT and could show calcification in up to 20% of cases. MRI (and specifically a FLAIR sequence) is better in defining the extent of the low-grade gliomas, which are hyperintense on FLAIR and T2-weighted images (Figure 2.1.) and hypo/isointense on T1-weighted images. The margins of many tumours are poorly delineated. Cystic degeneration may happen, but necrosis is usually absent. Haemorrhage is also unusual and the surrounding oedema is generally kept to a minimum (Osborn, 1994). Gadolinium enhancement is not common in low-grade diffuse astrocytomas, but tends to appear during tumour progression. Low-grade astrocytomas have higher ADC than oligodendrogliomas (Tozer et al., 2007).

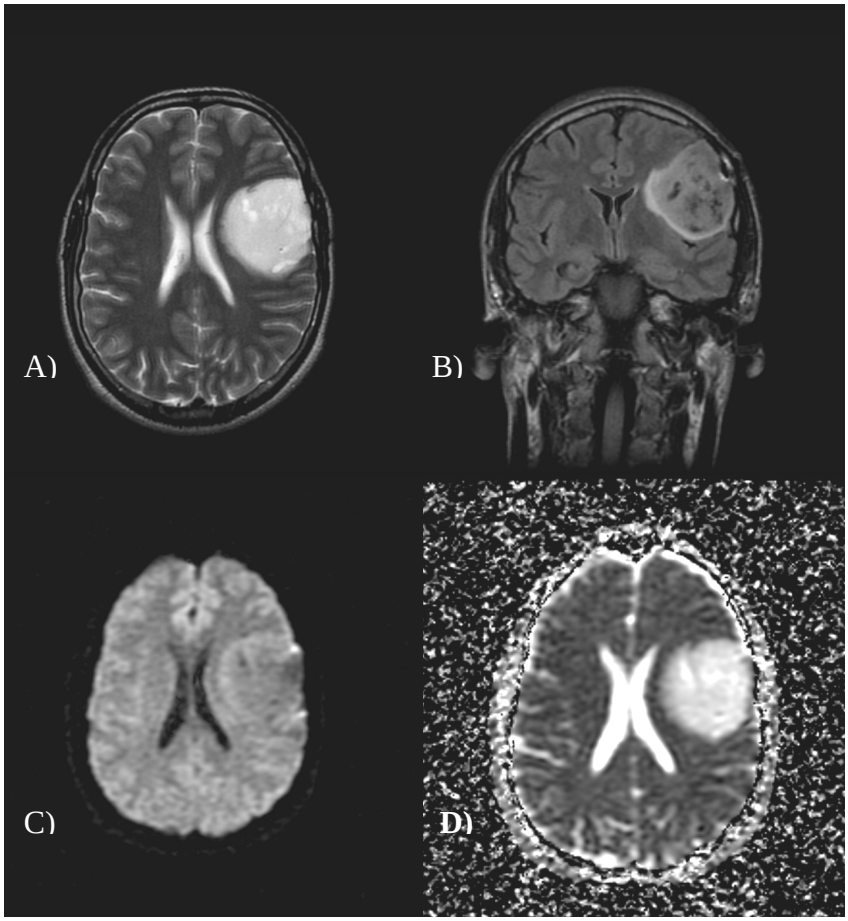

Figure 2.1. WHO grade II astrocytoma. Axial T2W (A), FLAIR (B) images showing a left frontal hyperintense mass lesion with well defined borders and small cystic areas. On the trace-weighted DWI (C) the tumour is not very conspicuous as T2 effects and diffusion effects cancel each other out. On the ADC map (D) the glioma is easily identified as an area of increased diffusivity compared to normal brain parenchyma.

2.1.1.3 Anaplastic astrocytomas (WHO grade III)

WHO grade III astrocytomas represent 33% of astrocytomas and they are usually present in patients from 40 to 60 years old (Osborn, 1994). They have an increased mitotic activity and may arise from low-grade astrocytomas, but are also diagnosed at first biopsy, without indication of a less malignant precursor lesion. The prognosis is poor, with a medium survival of 2 years (Osborn, 1994). These tumours have a tendency for malignant progression to glioblastoma multiforme.

Clinical Features

Symptoms are similar to those of patients with diffuse astrocytoma. Not infrequently there are signs of a recurrent glioma, following initial resection of a diffuse low-grade astrocytoma. These signs could be increasing neurological deficits, seizures and/or intracranial pressure.

Neuroimaging

The tumour can appear very heterogeneous, with haemorrhagic areas within the tumour and show more extensive infiltration of the peri-tumoural tissues than WHO Grade II lesions (Wilms et al., 2005; Young and Knopp, 2006). This leads to a mixed density and intensity on both CT and MRI (Figure 2.2). These tumours usually have moderate mass effect. Contrast enhancement is usually observed and a rapid tumour growth with development of oedema may lead to mass shifts and increased intracranial pressure (Figure 2.2). Anaplastic astrocytomas typically spread through white matter tracts. In most cases, tumour cells can be found in the oedematous areas and beyond it as well (Earnest et al., 1988; Watanabe et al., 1992). These tumours can also spread along the ependyma, leptomeninges and the cerebrospinal fluid (Grabb et al., 1992).

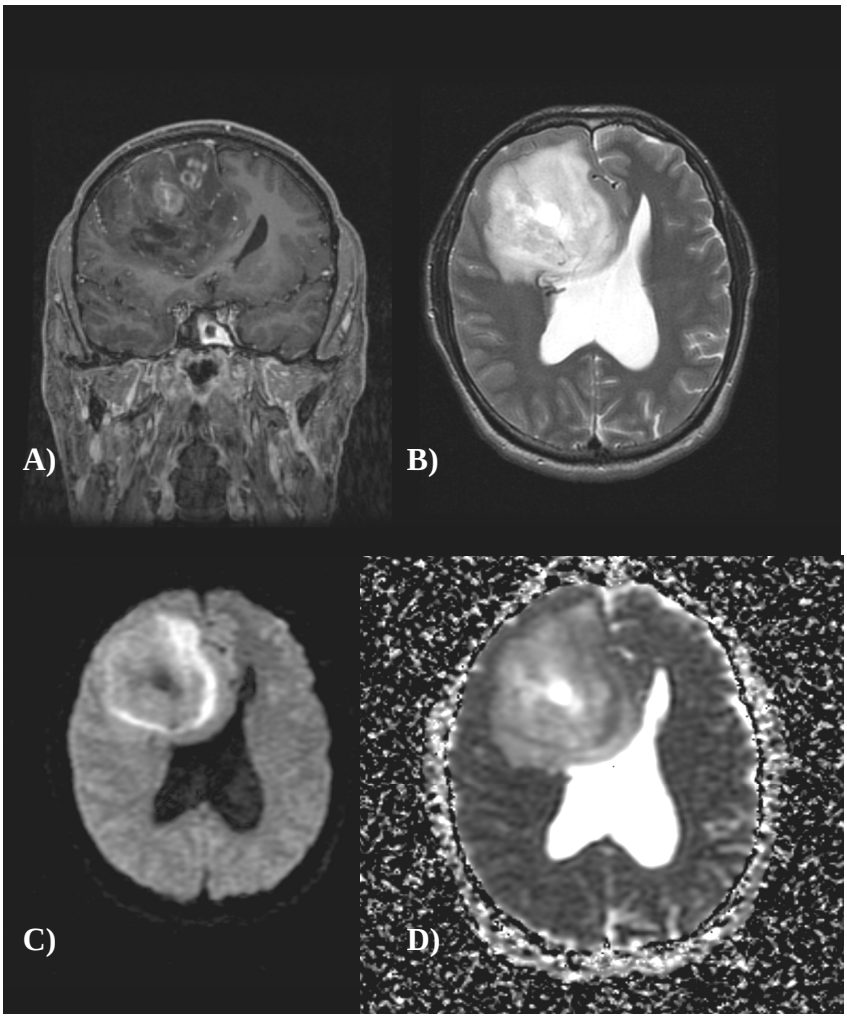

Figure 2.2. WHO grade III astrocytoma. Coronal T1W post-contrast image (A) of a frontal irregularly enhancing mass with some cystic areas, which appears inhomogeneous on T2W images (B). The latter showing also associated vasogenic oedema at the posterior margin of the tumour. There is marked mass effect with midline shift. The trace-weighted DWI (C) and ADC map (D) appear inhomogeneous with cystic areas and more restricted diffusion peripherally.

2.1.1.4 Glioblastoma multiforme (WHO Grade IV)

Glioblastoma multiformes (GBMs) show poorly differentiated, often highly pleomorphic glial tumour cells with vascular proliferation and necrosis. Unfortunately it has the worst prognosis and is also the commonest primary intracranial neoplasm in adults (Nelson and Cha, 2003). These rapidly growing, highly mitotic tumours may arise from pre-existing lower grade astrocytomas or occur de novo (particularly in older patients) (Behin et al., 2003).

Clinical Features

Unless the neoplasm has developed from a WHO grade III tumour, the clinical history is usually less than 3 months in more than 50% of cases (Kleihues P, 2000). Patients can present with seizures and non-specific neurological symptoms, but the most aggressive aspect is the rapid development of increased intracranial pressure.

Neuroimaging

This tumour may arise from pre-existing lower grade astrocytomas or occur de novo (primary), particularly in older patients (Behin et al., 2003). Vasogenic oedema and contrast enhancement are usually much more extensive than in anaplastic astrocytomas. These tumours have a mixed density on CT and a mixed signal mass in MRI.

Tumour necrosis is a hallmark of GBM and appears on MRI as areas of non-enhancing T1 hypointensity, frequently surrounded by a ring-like zone of contrast enhancement (Figure 2.3). Studies have showed that this contrast area does not represent the outer tumour border, as infiltrating glioma cells can be easily identified within a 2cm margin (Burger and Bigner, 1988). Enhancement is usually strong and very inhomogeneous. Intratumoural haemorrhage of different ages contributes to the heterogeneous MR appearance of GBM. Their usual location is the cerebral white

matter, particularly the frontal and temporal lobes. Basal ganglia involvement may be present. GBMs have a rapid, infiltrative growth and tend to extend through the corpus callosum into the contralateral hemisphere, creating the image of a bilateral symmetrical lesion, known as “butterfly glioma”. A small number of GBMs may show evidence of subarachnoid seeding.

The presence of true multiple independent gliomas is controversial. Post-mortem studies may not show a connection between apparently multifocal gliomas, as the infiltrating cells are often small and undifferentiated. However, this type of tumours can only be proven by molecular markers which will allow a distinction between tumours of common or independent origin (Kleihues P, 2000).

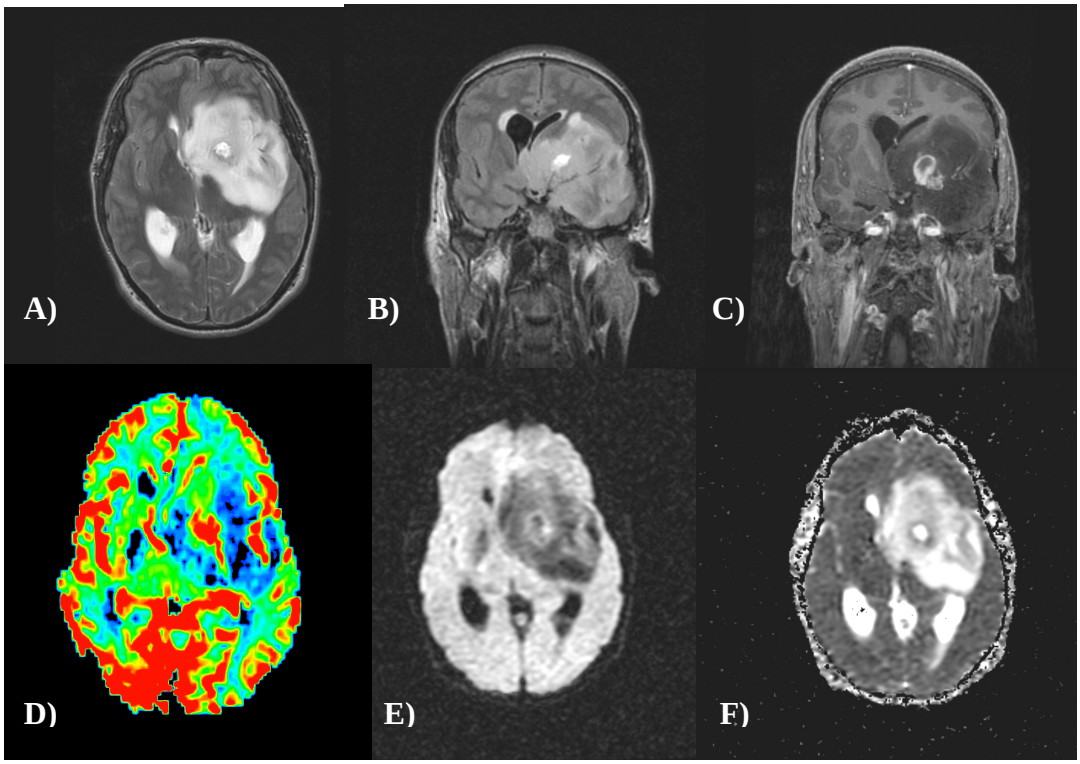

Figure 2.3. Glioblastoma multiforme. Axial T2W (A) and FLAIR (B) images show a large fronto-temporal glioma hyperintense on both sequences. It is predominately solid with central necrotic area and ring-like contrast enhancement seen on the T1W post-gadolinium show central enhancement (C). Relative CBV map (D) shows areas of high perfusion corresponding to the enhancement region. DWI (E) and ADC map (F) show an area of increased diffusion in the necrotic area and restricted diffusion around it.

2.1.2 Oligodendrogliomas

The most recent World Health Organization (WHO) classification system divides oligodendrogliomas into low-grade (Grade II) and high-grade (Grade III, anaplastic) tumours. These neoplasms account for up to 33% of all adult gliomas (Perry, 2001) and have a longer survival. Prayson et al showed a overall survival for oligodendrogliomas of 5- and 10-year of 71% and 63%, respectively (Prayson et al., 2000). The majority of the tumours occur in adults with a peak incidence of the 5th and 6th decade. They are diffusely infiltrating neoplasms which are found almost exclusively in the cerebral hemispheres, most commonly in the frontal lobes, and typically involving subcortical white matter and cortex. Both low- and high-grade oligodendroglial tumours may contain regions of increased vascular density with finely branching capillaries that have a "chicken wire" appearance (Jäger et al., 2007).

2.1.2.1. Oligodendrogliomas (WHO grade II)

They are typically located in the cerebral hemispheres and are well-differentiated, diffusely infiltrating tumours. Although oligodendrogliomas can arise in any cerebral lobe, the frontal lobe is involved in 50-65% of the patients (Kros et al., 1994).

Clinical Features

The most common signs are seizures and headache. Patients may present with a long pre-operative history of neurological sings and symptoms.

Neuroimaging

Typically on CT scan, oligodendrogliomas appear hypodense or isodense (Margain et al., 1991). On MRI the lesions appears well as a demarcated hypointensity in T1 and hyperintense in T2W images, usually located in the cortex and subcortical white matter. Peritumoural oedema is usually mild or absent; cystic changes and tumour haemorrhages may also be seen. Up to 90% of oligodendrogliomas contain visible calcification on CT, which can be central or peripheral. (Ricci, 1999) On MRI, areas of calcification may be more difficult to appreciate due to the variable appearance of calcification. Intratumoural calcification appears typically T2 hypo- and T1 hyperintense but intratumoural haemorrhage, which occurs uncommonly in oligodendrogliomas, may have a similar appearance. Contrast enhancement is variable and often heterogeneous. In general WHO grade II tumours do not infrequently exhibit some contrast enhancement whereas WHO grade III oligodendrogliomas may not enhance (White et al., 2005). However many studies have used contrast enhancement as a radiological marker of malignancy in gliomas (Daumas-Duport et al., 1997; Mihara et al., 1995; Pierallini et al., 1997). Relative CBV measurements derived from DSC MR imaging were significantly higher in low-grade oligodendrogliomas than in astrocytomas (Cha et al., 2005) (Figure 2.4).

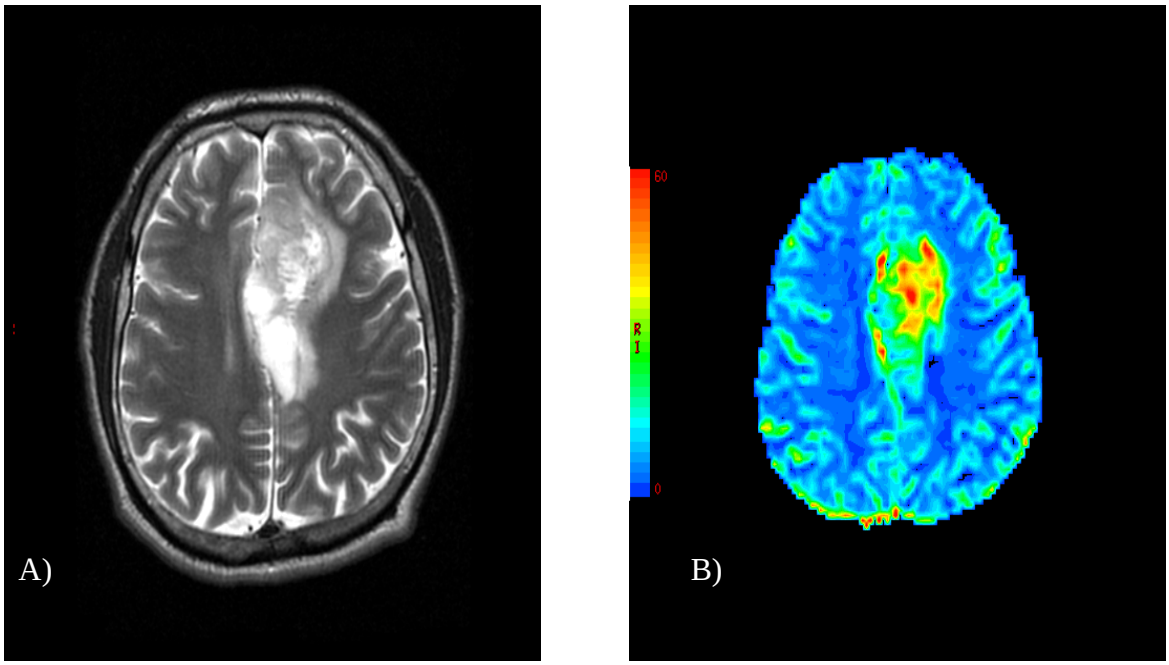

Figure 2.4. WHO grade II oligodendroglioma. Axial T2W image (A) and colour rCBV map (B) showing areas of increased rCBV (yellow and red areas) within the inhomogeneous left frontal tumour.

2.1.2.2 Anaplastic oligodendrogliomas (WHO grade III)

These tumours are defined as an oligodendroglioma with focal or diffuse histological features of malignancy and a less favourable prognosis. They manifest preferentially in adults in the 5^{th} decade.

Clinical Features

The signs are similar to those of oligodendrogliomas. However some patients may present with long standing signs suggesting a pre-existing tumour of lower grade.

Neuroimaging

Due to the presence of necrosis and cystic degeneration, intratumoural calcification and haemorrhages, these tumours may have heterogeneous patterns. Cysts appear hypointense in T1W and hyperintense in T2W images, whereas intratumoural calcification (as well as some stages of haemorrhage) appears typically T2 hypo- and T1 hyperintense. The MRI appearances of these elements are the same as for oligodendrogliomas. Contrast enhancement on CT and MRI is usual (Figure 2.5).

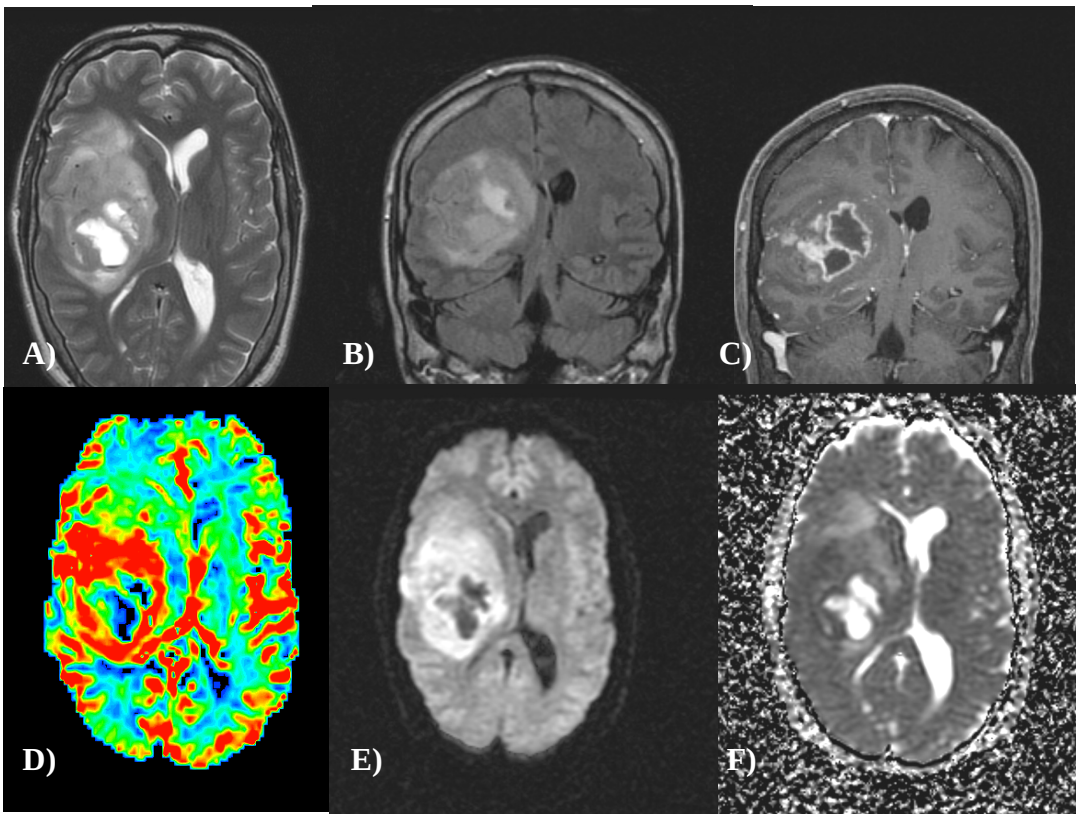

Figure 2.5. Oligodendroglioma, grade III: T2W (A) and FLAIR (B) show a large right frontal tumour that involves the cortex. It is predominantly solid with irregular enhancement, seen on the T1W after the use of contrast (C) and cystic areas, hyperintense on T2W and FLAIR and hypointense on T1W. rCBV map (D) shows areas of high perfusion on the periphery of the tumour and around the cystic areas. DWI and ADC maps (E, F, respectively) demonstrate areas of increase diffusion corresponding to the cysts and reduced diffusion around it.

2.1.3 Oligoastrocytomas

Oligoastrocytomas are heterogeneous tumours that have molecular features that overlap with either oligodendrogliomas or astrocytomas. It has been reported that at least half of the tumours that were originally classified as oligodendrogliomas would have astrocytic cells in it (Ruseell and Rubistein, 1989; Russell and Rubistein, 1989).

2.1.3.1 Oligoastrocytomas (WHO grade II)

Specific data on oligoastrocytomas are rare and difficult to interpret because of their imprecise definition, especially on the proportion of oligodendroglial and astrocytic cell population required to make their diagnosis and because in most trials, these tumours were studied together with anaplastic oligodendrogliomas or astrocytomas. Their chemosensitivity seems similar to that for anaplastic oligodendrogliomas (Kim et al., 1996).

Clinical Features

The symptoms and signs are similar to those described for astrocytomas and oligodendrogliomas, most commonly epileptic seizures.

Neuroimaging

These tumours demonstrate no special features that would allow a reliable distinction from oligodendrogliomas. On MRI the lesions appears as a hypointensity mass in T1 and hyperintense in T2W images, usually located in the cerebral hemisphere. Calcifications and contrast enhancement may be present. Figure 2.6.

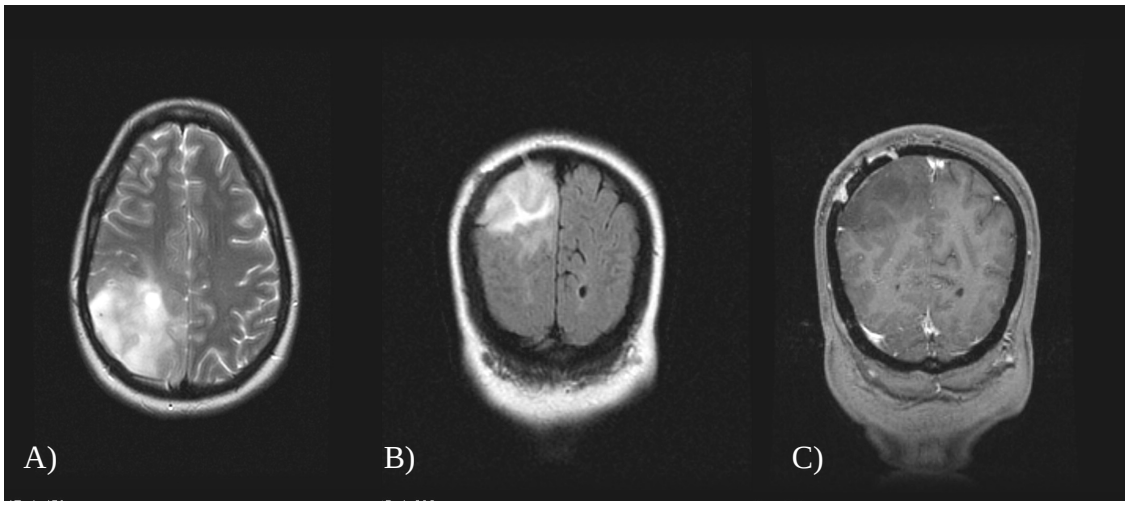

Figure 2.6. WHO grade II oligoastrocytoma. Axial T2W (A), FLAIR (B) images showing a right parietal hyperintense mass lesion.T1W post contrast (C) shows hypointense lesion without enhancement.

2.1.3.2 Anaplastic oligoastrocytomas (WHO grade III)

These tumours also have a mixture of two distinct neoplastic cell types that morphologically resembles the tumour cells in oligodendroglioma and astrocytoma. In addition they have histological features of malignancy, such as increased cellularity, nuclear atypia, pleomorphism and increased mitotic activity.

Clinical Features

In some cases, the clinical history of patients with WHO grade III may be long before diagnosis, especially with the presence of seizures, suggesting a pre-existing low-grade glioma.

Neuroimaging

On MRI the lesions appears as hypointense in T1W and hyperintense in T2W images, usually located in the cerebral hemisphere. Usually these tumours show contrast enhancement on CT and MRI. Figure 2.7.

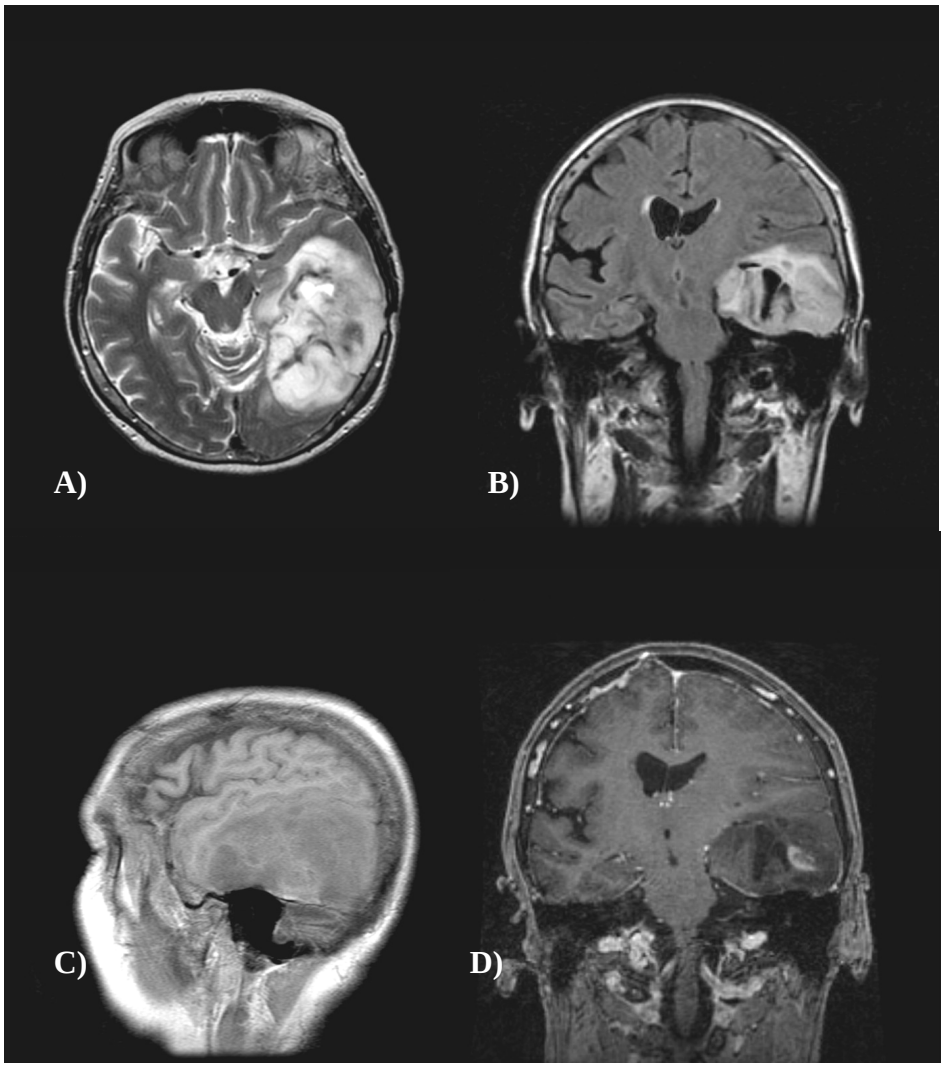

Figure 2.7. WHO grade III oligoastrocytoma. Axial T2W (A), FLAIR (B) images showing a hyperintense mass lesion in the left temporal lobe. Sagittal (C) and coronal T1W (D) shows hypointense lesion which enhances after the use of contrast (D) .

2.2 The use of advanced MR techniques in brain tumours

In this section information will be given about the new techniques used to assess brain tumours. Diffusion- and perfusion-weighted imaging were used routinely in this thesis so more details will be given to these techniques.

2.2.1 Diffusion-weighted imaging

One of the commonest applications of diffusion-weighted imaging (DWI) in the assessment of tumours is in differentiating between types of cystic lesions. It is particularly useful in distinguishing between epidermoids, where the thick content of the cyst restricts the diffusion of water, and arachnoid cysts where diffusion is free (Hakyemez et al., 2003). Similarly, the viscous content of abscesses can be differentiated from cystic tumours (Lai et al., 2002).

Both the cellularity and matrix composition of tumour will influence ADC values. Studies have shown that tumours frequently have higher ADC values compared with normal brain (Bulakbasi et al., 2003; Kono et al., 2001b). The regions with the highest ADC values are within cysts or areas of necrosis.

Sugahara et al. (Sugahara et al., 1999a) showed that tumour cellularity correlated well with the minimum ADC value of the gliomas and that diffusion-weighted MRI with EPI is a useful technique for assessing the tumour cellularity and grading of gliomas. It has been shown that there is an inverse relationship between cellularity and ADC (Kono et al., 2001b; Sugahara et al., 1999a). Significant differences have been reported between the ADC values of low- and high-grade gliomas. These differences appear to be partly related to the differences in cell density of these tumours (Guo et al., 2002; Kono et al., 2001a; Sugahara et al., 1999a). Additionally,

a substantial portion of the tumour volume is made up of extracellular matrix. One of the components of the extracellular matrix is a macromolecule called glycosaminoglycan, which have been localized to the tumour cell–associated extracellular matrix of astrocytic glial tumours in vivo (Sadeghi et al., 2003). The glycosaminoglycans are highly hydrophilic and tend to attract sodium, which is osmotically active, causing the shift of large amounts of water. Therefore, glycosaminoglycans are thought to influence the water content of the extracellular matrix and thus the value of ADC. In the same study (Sadeghi et al., 2003) the author showed that the extracellular matrix in gliomas likely contributes to differences in the ADC values between high- and low-grade glial tumours. In high-grade tumours there is also vasogenic oedema produced due to defects in the blood - brain barrier, which causes an increase in the ADC and a decrease in the DWI signal (Figure 2.8).

Several studies have sought to characterize tumour subtype and grade using ADC values. Minimum tumour ADC has been shown to distinguish histological tumour grade (Kono et al., 2001a; Tozer et al., 2007). This advanced technique provides further information which contributes towards the clinical management of brain gliomas.

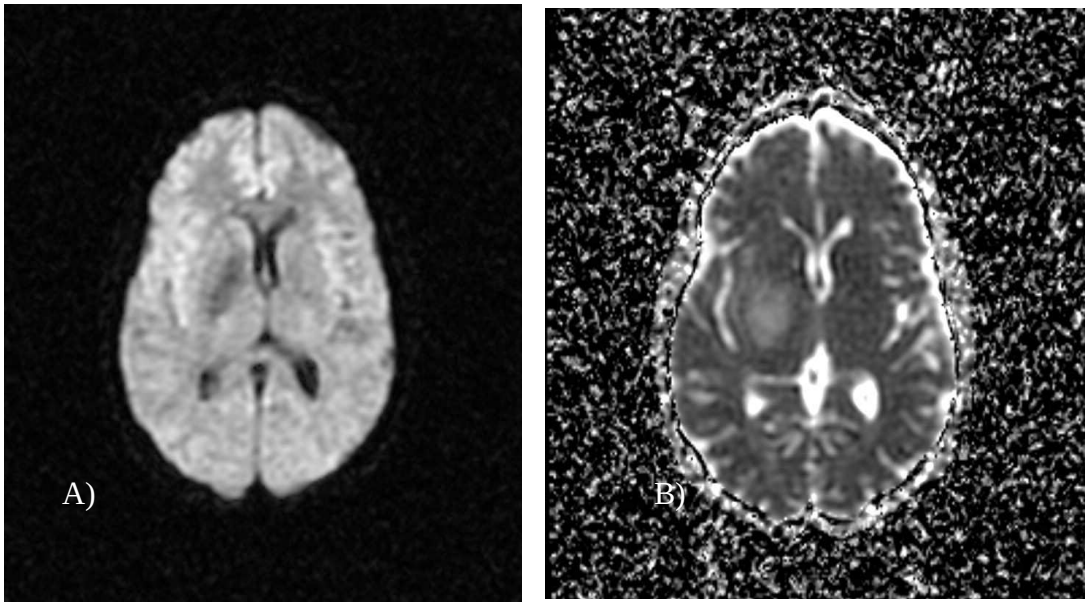

Figure 2.8: Diffusion weighted brain image (A) and ADC map (B) showing a right lesion with well defined borders with increased diffusion causing hypointensity on DWI and high signal on the ADC map in the basal ganglia.

2.2.2 Diffusion Tensor Imaging (DTI)

Diffusion tensor imaging is a modification of DWI that is sensitive to the preferential diffusion of brain water along white matter tracts (anisotropic diffusion). This technique was not included in this thesis, since it was not available at our institution at that time.

DTI can detect subtle changes in white-matter tracts in the brain (Le Bihan, 2003). In brain tumours, DTI can be used to differentiate normal white matter, oedematous brain tissue, and enhancing tumour margins (Sinha et al., 2002), provide a useful method of detecting occult white matter invasion by gliomas (Price et al., 2003) and is also able to delineate the tumour margins of gliomas (Price et al., 2006). Diffusion anisotropy is reduced in cerebral lesions due to the loss of structural organisation (Price et al., 2003). The measurement of fractional anisotropy allows prediction of histological characteristics such as cellularity, vascularity, or fibre structure in gliomas (Beppu et al., 2003). In addition, DTI may help determine if the fibres are displaced, infiltrated, or disrupted by the tumour (Witwer et al., 2002). Such knowledge could contribute to the selection of surgical indications. Ideally, DTI can be combined with functional neuroimaging methods (Krings et al., 2001) to allow mapping of individual anatomofunctional connectivity. This information would be useful for surgical planning of patients with brain glioma.

2.2.3 Perfusion-weighted imaging

In order to grow, tumours must develop networks of vascular supply. The development of neoangiogenic networks is promoted by an interaction of various pro- and antiangiogenic tissue factors. One important factor is vascular endothelial growth factor (VEGF). Its expression is promoted by nutrient-deficient states, such as tissue hypoxia or hypoglycemia, that occur as tumour cells in rapidly growing pathologic tissues expand beyond the limits of diffusion of nutrients from the native capillaries (Shweiki et al., 1992). VEGF promotes growth of new endothelial cells by stimulating cell division (Provenzale et al., 2006) and has been demonstrated to be a prognostic marker in gliomas (Abdulrauf et al., 1998). Glioma progression is strongly dependent on the development of new vascular network that occurs primarily by angiogenesis (Jouanneau, 2008). However, the new vessels formed in tumours are characteristically abnormal, having increased tortuosity (Jain et al., 2002), lack of maturity (as evidenced by decreased amounts of perivascular cells) and increased permeability to macromolecules due to the presence of large endothelial cell gaps (Hashizume et al., 2000). The result is that the neovessels often have both abnormal flow characteristics and abnormal permeability that can be exploited as potential surrogate markers for the evaluation of tumour growth. Thus, regions of high rCBV are thought to reflect areas of high capillary density, which is a reflection of tumour aggressiveness.

The use of MR perfusion is ideally suited to neuro-oncology where imaging studies of angiogenesis and tumour vasculature further our understanding of tumour biology. In gliomas, perfusion MRI has been used to characterize WHO grade (Cha et al.,

2005), tumour genotype (Jenkinson et al., 2006), guide biopsy (Cha et al., 2002) and provide prognostic information (Law et al., 2006a).

Most studies in the literature have focused on the role of perfusion MRI to determine pathology grade in mixed gliomas or astrocytomas. Values of rCBV correlate well with conventional angiographic assessment of tumour vascular density and histopathology measures of angiogenesis such as microvessel density and vascular endothelial growth factor expression, (Maia et al., 2005; Sugahara et al., 1998) which reflects the histopathological finding of increasing neovascularization with grade. Relative cerebral blood volume tends to increase with increasing tumour grade (Law et al., 2003; Lev et al., 2004). However, low-grade oligodendrogliomas can have significantly higher rCBV when compared to low-grade astrocytomas, reflecting the increased vascularity and “chicken wire” vessels seen on histology (Cha et al., 2005). In studies of mixed gliomas, the rCBV in oligodendrogliomas may render perfusion MRI-based tumour grading less accurate (Lev et al., 2004; Xu et al., 2005).

Caution should be taken with extravascular leakage of gadolinium through defective tumour vessels as it can influence rCBV measurements. The choice of the cut-off points in the analysis of the time-signal-intensity curve is important to minimize confounding effects of contrast leakage (Cha et al., 2002).

Even though perfusion has been widely used in the study of brain tumours, the choice of inclusion or exclusion of intratumoural vessels is often not explicitly stated. As this can have a confounding effect, the significance of intratumoural vessels upon rCBV measurements was investigated in chapter 3 of this thesis.

2.2.4 MR Spectroscopy

Proton MR Spectroscopy (MRS) analyses the biochemistry of a brain tumour and provides semiquantitative information about major metabolites (Law, 2004; Vlieger et al., 2004). A common pattern in brain tumours is a decrease in N-AcetylAspartate (NAA), a neuronspecific marker, and Creatine (Cr) and an increase in choline (Cho), Lactate (Lac), Lipids (L). The concentration of Cho is a reflection of the turnover of cell membranes (due to accelerated synthesis and destruction) and is more elevated in regions with a high neoplastic activity. Lactate (Lac) is the end product of nonoxidative glycolysis and a marker of hypoxia in tumour tissue. This is of increasing interest as tumour hypoxia is now recognized as a major promoter of tumour angiogenesis and invasion. Lac is probably associated with viable but hypoxic tissue, whereas mobile Lipids are thought to reflect tissue necrosis with breakdown of cell membranes.

The choice of echo time (TE) is a important technical considerations for performing MRS. It can be short (20 to 40ms), intermediate (135 to 144 ms) or long (270 to 288ms). MRS with a short TE has the advantage of demonstrating additional metabolites which may improve tumour characterisation, such as myo-Inositol, glutamate/glutamine (Glx) and lipids, but is hampered by baseline distortion and artefactual NAA peaks. Intermediate echo times have a better defined baseline and quantification of NAA and Cho is more accurate and reproducible. Long echo times lead to a decrease of signal to noise.

MRS is presently a sensitive but not very specific technique. Single voxel acquisition provides good quality spectra but is prone to sampling errors. Chemical shift imaging is technically more demanding but covers a larger volume of tissue.

MRS was not used in the work of this thesis.

2.2.5 PET

Imaging of brain tumours with ^{18}F-FDG was the first oncologic application of PET (Di Chiro et al., 1988; Patronas et al., 1982; Wong et al., 2002).^{18}F-FDG is actively transported across the BBB into the cell, where it is phosphorylated. ^{18}F-FDG uptake is generally high in high-grade tumours. The prognostic value of ^{18}F-FDG uptake is well established: High uptake in a previously known low-grade tumour establishes the diagnosis of anaplastic transformation (De Witte et al., 1996).

However, recent studies have demonstrated amino acid PET tracers are more sensitive than ^{18}F-FDG in imaging recurrent tumours and in particular recurrent low-grade tumours. They are also promising in differentiating between recurrent tumors and treatment-induced changes (Chen, 2007).

Amino acid PET tracers are important for the imaging of brain tumours because of the high uptake in tumour tissue and low uptake in normal brain tissue and it is generally increased in malignant transformation (Isselbacher, 1972). The best-studied amino acid tracer is ^{11}C-methionine (Herholz et al., 1998).

One of the main application of PET in brain tumours is to differentiate radiation necrosis and tumour re-growth (Langleben and Segall, 2000). In previously treated patients, ^{18}F-FDG PET can be helpful in differentiating recurrent tumor from radiation necrosis. Amino acid tracers are promising in that they are more sensitive in imaging brain tumors. Amino acid tracers may also be useful in distinguishing recurrent tumors from radiation necrosis, although further studies are needed (Chen, 2007).

2.2.6 Functional MRI

Blood oxygen level-dependent (BOLD) imaging detects changes in regional cerebral blood flow during various forms of brain activity. Paradigms using motor tasks, language and speech productions, and memory are able to show activation of relevant cortical areas. The main use of fMRI in tumour imaging is the pre-operative localization of eloquent cortical regions which may have been displaced, distorted or compressed by the tumour (Vlieger et al., 2004). This can improve the safety of surgery and allow for a more radical resection. If possible fMRI should be combined with DTI in order to minimise intra-operative injury to white matter tracts connected to eloquent cortical areas.

The use of fMRI was not included in this thesis.

2.3 Physiology-based MR imaging in the differential diagnosis and grading of glial tumours

2.3.1 Distinguishing between astrocytomas and oligodendrogliomas

As mentioned before, there is evidence that perfusion- and diffusion-weighted imaging can help to differentiate low-grade astrocytic from oligodendroglial tumours. WHO grade II oligodendrogliomas have significantly higher rCBV than WHO grade II astrocytomas (Cha et al., 2005) which concurs with the histological findings of increased vascular density in oligodendrogliomas. Measurement of the ADC, using a whole tumour histogram analysis, appears promising for the differentiation of astrocytomas from oligodendrogliomas. The latter have significantly lower ADC values than astrocytomas, reflecting a higher cellular density and differences in tumour matrix composition (Tozer et al., 2006).

2.3.2 Distinguishing between low-grade and high-grade gliomas

As already stated in this chapter several studies investigated the potential of advanced MR imaging to distinguish between low- and high-grade gliomas. Studies have shown (Yang et al., 2002) that mean maximum rCBV values correlated closely with histological grades. A recent study of 160 primary cerebral gliomas showed that rCBV measurements significantly increased the sensitivity and positive predictive value of conventional MR imaging in glioma grading (Law et al., 2003). Perfusion-weighted imaging had a sensitivity of 95% and positive predictive value of 87% for distinguishing low-grade from high-grade gliomas when an rCBV threshold of 1.75 was used (Law et al., 2003).

The role of DWI in differentiating high-grade from low-grade gliomas remains unclear. Initial reports were encouraging and showed lower ADC measurements in high-grade lesions (Sugahara et al., 1999a; Yang et al., 2002) but these have not been confirmed in subsequent studies (Sadeghi et al., 2003).

2.4 Controversies in the management of gliomas

The treatment of malignant gliomas is still very challenging. Despite considerable progress in the treatment of these tumours with combinations of surgery, radiotherapy, and chemotherapy, these efforts have not been curative (Dunn and Black, 2003). Brain gliomas are characterized by aggressive proliferation and expansion and tumour invasion into distant brain tissue, which makes it more difficult to find an effective treatment.

At time of presentation, most patients require treatment with corticosteroids because of peritumoral edema and resultant mass effect (Moots, 1998). Also, dexamethasone has been shown to inhibit or stimulate growth of rat 9L gliosarcoma and decrease the expression of vascular endothelial growth factor (VEGF), an important mediator of tumor-associated angiogenesis (Badruddoja et al., 2003; Maia et al., 2005). Because of the potential for long-term complications of corticosteroids, the lowest therapeutic dose should be used. In our cohort none of patients received corticosteroids.

Early studies used either whole brain radiation or regional fields. Although proven effective, these methods did increase the incidence of late radiation-induced brain injury (Vick and Paleologos, 1995). Newer technologies such as conformal fields with 3-dimentional planning and intensity-modulated radiation therapy delivers the desired dose of radiation to the target, limiting exposure to the surrounding normal brain parenchyma. The limitation of radiotherapy is that ideally it has to be administrated only at once, and finding the best timing remains a challenge in the management of these patients. However, there is also evidence for the beneficial

effect of radiosurgery on the survival of patients with high-grade gliomas (Szeifert et al., 2007).

The use of chemotherapy for the treatment of malignant brain tumours remains controversial. A study published in 2002 (Stewart, 2002) showed that the addition of chemotherapy to radiation demonstrated significant but modest improvement in survival at one year of 6 percent. The Medical Research Council (MRC) in the United Kingdom performed a large randomized trial comparing radiation therapy alone with radiation treatment followed by adjuvant treatment with PCV (procarbazine, CCNU and vincristine) (MRCBT, 2001). Despite enrolling 673 patients, no difference was detected in survival between the two groups. A more recent study showed that concurrent use of temozolomide with external beam radiation followed by adjuvant temozolomide treatment has proven to be better than radiation alone and is now the standard of care for patients with newly diagnosed GBM (Gilbert and Armstrong, 2007).

Finally there are also controversies between oncologists, neurosurgeons and pathologists in the surgical management of patients with brain glioma. The indications of resection still remain a matter of debate, especially because of the frequent location of these tumours within eloquent brain areas - thus with a risk to induce a permanent postoperative deficit (Duffau, 2006). Oncologists are often worried that a resection might damage these eloquent areas and pathologists are concern that the whole tumour might not be removed as most tumours recur within 2cm from the enhancing edge (Hochberg and Pruitt, 1980). However, all those risks can be minimezed by the use of neuronavigation with functional MRI and diffusion tensor imaging during the surgical treatment. As previously described, the main use

of intra operative fMRI is the localization of eloquent cortical regions which may have been displaced, distorted or compressed by the tumour. DTI can be used to delineate glioma margins and regions of infiltration.

Previous work has shown that surgical resection may improve outcome (Gilbert and Armstrong, 2007). The study by LaCroix evaluated 417 consecutive patients with malignant gliomas who underwent tumour resection with the pre-operative intent to perform a complete resection (Lacroix et al., 2001). After accounting for prognostic factors such as age and performance status, they found that patients who had undergone at least a 98% resection by volumetric analysis had a statistically significant improvement in overall survival.

The cohort of patients used in this thesis had a median survival of 3.76 years. This survival is much shorter than in other centres, as it will be discussed in the following chapters. Patients from our cohort only received treatment when transformation was diagnosed. Since early surgical treatment have shown to improve survival in patients with brain glioma, it would be interesting to confirm this in our centre.

2.5 Conclusion

Magnetic resonance imaging plays an important role in the detection and evaluation of brain tumours. Conventional MR imaging has principally served the role of showing the neoplasm, distinguishing tumours from other pathologic processes, and depicting basic signs of tumour response to therapy, such as change in size and degree of contrast enhancement. In the past few years, however, a number of advanced MR imaging techniques have been developed that provide new methods for the assessment of brain tumours. Diffusion- and perfusion-weighted imaging provide additional physiological information, helping to differentiate tumour subtypes and grades and may even provide prognostic information, contributing to the management of brain gliomas.

Chapter 3

Methodological Study: Implication of intratumoural vessels in glioma perfusion imaging

3.1 Introduction

As described in the previous chapters, dynamic susceptibility contrast-enhanced (DSC) MR perfusion imaging has become an important technique for studying brain tumours.

The choice of techniques for data acquisition, post-processing and analysis may influence rCBV quantification. Gradient-echo echo-planar imaging (GE-EPI) pulse-sequences are more sensitive to larger vessels than spin-echo (SE) EPI methods and provide better differentiation between histopathological tumour grades (Sugahara et al., 2001).

Wetzel et al (Wetzel et al., 2002) found inter- and intra-observer reproducibility for intratumoural rCBV was best when the highest CBV from several regions of interest was chosen, and highlighted the importance of excluding large vessels. Inclusion or exclusion of intratumoural vessels is often not explicitly stated in glioma perfusion studies, some investigators focussing on exclusion of peri-tumoural vessels (Sugahara et al., 2001). The significance of intratumoural vessels for rCBV measurements has, to our knowledge, not been formally examined.

In this short chapter we studied the influence of intratumoural vessels on rCBV characterization in three histological categories of low-grade glial tumours: astrocytomas (ACs), oligodendrogliomas (ODs) and oligoastrocytomas (OAs).

3.2 Technique and results

34 patients with low-grade gliomas, comprising 21 ACs; 8 ODs and 5 OAs had DSC imaging using gradient-echo EPI (TR =1200 ms, TE = 40 ms, flip angle 20º, 26 cm FOV, 96x128 matrix; slice thickness 5 mm) at 1.5 Tesla (GE Healthcare, Waukesha, WI) with a bolus of 0.1mmol/kg body weight gadoterate meglumine at 5 ml/sec. Colour maps of rCBV were generated with FuncTool 1.9 (GE Healthcare, Waukesha, WI) and analyzed by 2 neuroradiologists, reaching a consensus for placement of regions of interest (ROIs). At least 6 intratumoural ROI with a size of 9 pixels were placed over areas showing most elevated CBV on colour perfusion maps. Blood vessels within the tumour were identified on unprocessed perfusion images acquired between the time points of maximum arterial and venous signal drop. Slices above and below intratumoural vessels were viewed to identify potentially confounding partial volume effects from large vessels. We used 2 different methods for selecting the ROI with the maximum intra-tumoural CBV: method 1 included and method 2 excluded ROIs situated over intratumoural blood vessels and associated partial volume effects. The rCBVmax was then obtained by dividing the highest intra-tumoural CBV by the mean CBV obtained from a contra-lateral normal appearing white matter ROI. Figure 3.1.

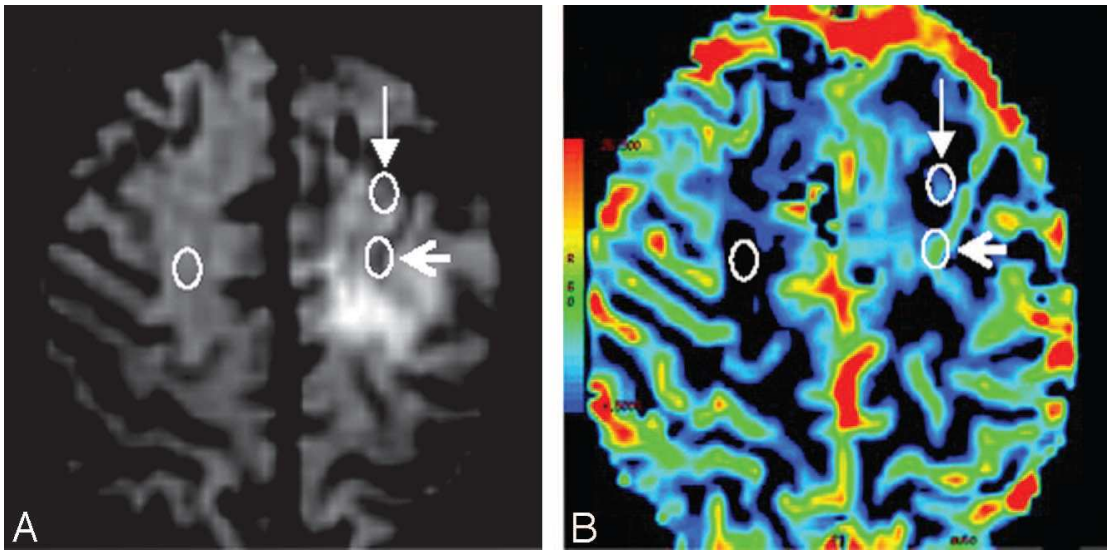

Figure 3.1. T2*-weighted image during maximum arterial signal intensity drop (*A*) and rCBV map (*B*) in low-grade OD, demonstrating the position of ROIs used to calculate rCBVmax. Method 1 (*open arrowhead*, posterior ROI in the left cerebral hemisphere, overlying an intratumoural vessel) and method 2 (*closed arrowhead*, anterior ROI in the left cerebral hemisphere, lying outside intratumoural vessels). The mean CBV from contralateral normal-appearing white matter (ROI in the right cerebral hemisphere) was used to normalize the data for each method. White circles have been superimposed on the original colour-coded ROIs generated by FuncTool. Mean rCBVmax obtained for each group with each method are shown in Table 1.1.

Table 3.1 rCBVmax obtained using methods 1 and 2 [Mean (range)].

(AC=astrocytoma, OA=oligoastrocytoma, OD=oligodendroglioma).

	ALL TUMOURS	**AC (N=21)**	**OA (N=8)**	**OD (N=5)**
Method 1	4.01 (1.54 – 6.99)	3.30 (1.54 – 6.65)	5.33 (3.07 – 6.65)	5.04 (2.74 – 6.99)
Method 2	1.63 (0.70– 3.51)*	1.44 (0.70 - 2.46)	1.53 (1.26 – 1.94)	2.21 (1.47 – 3.51)

* p <0.001 method 1 vs. method 2; Wilcoxon test

Method 1 yielded higher mean values and wider ranges than Method 2 in all 3 histological tumour types, particularly in OA and OD. For the patient group as a whole, there was a significant difference between mean rCBVmax obtained using each method ($p < 0.001$, Wilcoxon test). Ordinal regression was used to assess the relationship of rCBVmax and tumour histology, categorized in 3 groups (0: OA, 1 AC, 2 OD). Only method 2 showed a significant association between rCBVmax and the risk of being in a histological category with higher ordinate. Using method 2, the odds-ratio of being in a higher category was 4.25 (95% Confidence interval, lower**:** 1.19 and upper 15.14) for each additional unit rCBV increment (p=0.026). Method 1 did not demonstrated a significant association between rCBVmax and the risk of being in a higher category (p= 0.638).

3.3 Discussion

Several studies have demonstrated increased rCBV in high-grade gliomas compared to low-grade tumours (Cha et al., 2005; Hakyemez et al., 2005; Law et al., 2003; Lev et al., 2004; Spampinato et al., 2007; Sugahara et al., 2001; Yang et al., 2002). There is, however, considerable variation in the reported rCBV values for low- and high-grade tumours (Table 3.2). In SE-EPI DSC imaging, transverse relaxation rates peak at a vessel diameter of 1-2 μm whereas in GE-EPI DSC imaging they plateau at 3-4 μm and then remain independent of vessels size, which explains the lower rCBVs found with SE techniques (Sugahara et al., 2001). Differences may also be due to variations in the histological types of LGG examined and inclusion or exclusion of intratumoural vessels in the analysis, often not specified.

Table 3.2. rCBVmax for low-grade (LGG) and high-grade (HGG) gliomas reported in previous DSC-MR perfusion studies.

AUTHOR (REFERENCE)	**N**	**LGG MEAN RCBVMAX (RANGE)**	**HGG MEAN RCBVMAX (RANGE)**	**HISTOLOGY**	**TECHNIQUE**
Law (Law et al., 2003)	160	2.14 (0.77-9.84)	5.18 (0.96–9.80)	Histology not specified	GE-EPI
Law (Law et al., 2006a)	35	2.41 (0.37-5.96)		AC, OA, OD	GE-EPI
Sugahara (Sugahara et al., 2001)	25	1.21 (0.43-1.34) 1.22 (0.54-2.31)	4.86 (0.61-9.71) 2.90 (0.56-9.30)	AC, OD, GBM*	GE-EPI SE-EPI
Hakyemez (Hakyemez et al., 2005)	33	3.32 (1.40-8.68)	6.50 (2.39-18.60)	AC, OA, OD, GBM	GE-EPI
Yang (Yang et al., 2002)	17	1.74 (1.17-2.45)	6.10 (1.70-16.17)	AC. OA,OD, GBM	SE-EPI
Cha (Cha et al., 2005)	25	0.92 (0.48-1.34) AC 3.68 (1.29-9.24) OD		AC and OD	GE-EPI GE-EPI
Spampinato (Spampinato et al., 2007)	22	1.61	5.45	OD and OA	GE-EPI

AC: astrocytoma, OA: oligoastrocytoma, OD: oligodendroglioma, GBM: glioblastoma multiforme, GE-EPI: gradient-echo echo-planar imaging, SE- EPI: spin-echo echo-planar imaging. N: number of patients. * All low-grades were astrocytomas

We demonstrated that inclusion of large intratumoural vessels significantly increases rCBVmax values in all types of LGG. Their identification may be difficult on rCBV colour maps alone and necessitates reviewing of unprocessed perfusion data. The size of intratumoural vessels clearly identifiable on GE-EPI source data lies in millimetre range (approximating the size of peripheral leptomenigeal vessels), whereas neo-angiogenetic vessels of gliomas in animal models measure between 40-250 μm (Sugahara et al., 2001).

In concordance with previous investigators we found higher rCBVmax in tumours with oligodendral elements than in purely astrocytic tumours (Lev et al., 2004), explained by the "chicken wire" hypervascularity seen in the former. Cha et al. (Cha et al., 2005) chose intratumoural ROIs with an automated method targeting areas of maximum signal decrease during the first pass of the gadolinium-based contrast bolus. This method is likely to have incorporated intratumoural vessels and yielded mean rCBV for ODs of 3.68. Spampinato et al (Spampinato et al., 2007) presented one of the few reports specifying exclusion of large intratumoural vessels for ROI analysis. Their mean rCBV measurement for a mixed group of low-grade OA and OD (1.61) lies between our group mean rCBV measurements of OA (1.53) and OD (2.21) using Method 2. We were able to demonstrate significant association between maximum intratumoural rCBV values and histopathological classification as AC, OD, and OA, but only when using method 2. The influence of intratumoural vessels on rCBV measurements in high-grade gliomas, which are naturally subject to greater variability, was not part of this study and this could be addressed in future studies.

3.4 Conclusion

Our findings highlight the importance of using a consistent ROI placement technique, particularly if rCBV data are to be pooled in multi-centre studies. As a preferred technique we therefore recommend exclusion of intratumoural vessels when determining maximum intratumoural rCBV from GE-EPI DSC derived data. On the following chapters we use method 2 when analyzing rCBV as it proved to be a consistent and reliable technique.

Chapter 4

Relative cerebral blood volume measurements predict malignant transformation in patients with low-grade gliomas

4.1 Introduction

Adult supratentorial low-grade gliomas (WHO grade II, 2000) are a heterogeneous group of diffusely infiltrating primary brain tumours. They grow slowly for several years but, at an unpredictable time, almost all progress to high-grade (WHO grade III or IV) gliomas, which carry a poor prognosis.

The management of low-grade gliomas (LGG) remains controversial. Although some centres treat these lesions aggressively at diagnosis, large population-based studies and prospective trials have not produced evidence of improved survival following radical surgery or early radiotherapy (Johannesen et al., 2003; van den Bent et al., 2005), particularly in young patients presenting with well-controlled epilepsy.

A change in appearance on imaging frequently precedes clinical deterioration, and the development of areas of focal contrast-enhancement is the most commonly used sign of tumour progression in clinical practice; this has proved a more reliable indicator of malignancy in gliomas than border definition, mass effect, necrosis and haemorrhage (Daumas-Duport et al., 1997; Mihara et al., 1995; Pierallini et al., 1997). However, up to one third of malignant gliomas do not enhance (Scott et al., 2002) and, certain sub-types of low-grade gliomas show enhancement; typically gangliogliomas and pilocytic astrocytomas, and occasionally oligodendrogliomas (White et al., 2005).

Vascular proliferation (angiogenesis) is an important histological hallmark of malignancy in glial tumours. Pathological contrast enhancement in tumours indicates local disruption of the blood brain barrier; this is an indirect marker of angiogenesis as the walls of the new vessels may be deficient and more permeable.

As described in chapter 2, MR perfusion imaging is a sensitive marker of the microvascular density and histological grade of gliomas. Relative cerebral blood volume (rCBV) measurements correlate closely with angiographic and histological markers of tumour vascularity (Sugahara et al., 1998), and are more elevated in high-grade than in low-grade gliomas (Aronen et al., 1994; Donahue et al., 2000; Sugahara et al., 1998) (Law et al., 2003; Lev et al., 2004; Sugahara et al., 2001; Yang et al., 2002). A correlation between rCBV and the expression of vascular endothelial growth factor (VGEF) has been demonstrated, using immunohistochemical staining of surgical specimens (Maia et al., 2005). A recent study of patients referred for preoperative assessment of low-grade gliomas showed that baseline rCBV measurements made prior to surgery correlated inversely with the time to subsequent tumour progression (Law et al., 2006a).

Thus, the purpose of this chapter was to analyze longitudinal MR perfusion imaging of conservatively treated low-grade gliomas to determine whether rCBV is a predictor of malignant transformation.

4.2 Methods

4.2.1 Patients

Thirty five patients were recruited sequentially from the neuro-oncology clinic of the National Hospital of Neurology and Neurosurgery, in London. The inclusion criteria were: (i) histologically confirmed WHO grade II gliomas (Kleihues P, 2000); (ii) no previous treatment except biopsy (surgery, radiotherapy or chemotherapy) and (iii) age $\geq$ 18 years. Patients underwent conventional and perfusion imaging at study entry, 6 months and 12 months later. For the remainder of the study they were

assessed clinically and conventional MR imaging was performed every six months. The study was approved by the local research ethics committee and all patients provided informed consent.

4.2.2 MRI protocol

All MR data were acquired with a clinical 1.5 T system (Signa LX, GE Medical Systems, Milwaukee, WI, USA). The following images were acquired:

1) 3D Coronal Spoiled gradient echo (SPGR) sequence [parameters: TE=6.4ms; TR=14.4ms; TI=650ms; flip angle 15º; 256 x 256 matrix; 24cm x 18cm FOV (3/4 phase FOV); slice thickness 1.5 mm, contiguous sections], pre- and post-contrast (0.2mmol/kg of gadoterate meglumine (Dotarem ®)).
2) 2D Coronal oblique fast spin echo (FSE) fluid-attenuated inversion recovery (FLAIR) [TE=161ms; TR=8774ms; TI=2192ms; 256x192 (reconstructed to 256x256) matrix; 24cm x 24cm FOV; slice thickness 5mm and gap 1.5mm].

3) Axial Dynamic susceptibility-weighted perfusion contrast-enhanced images using a T2*-weighted gradient-echo echo-planar sequence were acquired during the first pass of a 0.1mmol/kg bolus of gadoterate meglumine (Dotarem ®), injected at a rate of 5 ml/sec [TE = 40 ms; TR =1200 ms; flip angle 90º; 128 x 92 matrix; 26cm x 26cm FOV; slice thickness 5 mm, contiguous sections]. These images were acquired before the post-contrast T1 weighted images from sequence 1.

4.2.3 MRI analysis

1) Pre- and post-contrast spoiled gradient echo (SPGR) images were analyzed by visual inspection in order to assess whether tumour enhancement was present and/or different from that visible on the images acquired at the previous time point, using Agfa IMPAX PACS system.

2) Dynamic susceptibility-weighted perfusion images were processed off-line on Advantage Workstation commercial processing software (Functool, General Electric Medical Systems, WI, USA). The beginning and end of the first pass bolus was determined by inspection of time-signal intensity curves, and care was taken to exclude any recirculation-related signal. For rCBV calculations, only the area under the curve of the first pass bolus was considered. Colour-coded rCBV maps were generated. For each slice, one region of interest (ROI) of 9 pixels was placed within the tumour, on the area showing the most elevated CBV on colour perfusion maps, and one more ROI was positioned in the contralateral normal white matter. Attention was given not to include intra-tumoural or peri-tumoural arteries and veins in a ROI, as described elsewhere (Brasil Caseiras et al., 2008). The maximum CBV value of all intra-tumoural ROIs and the mean CBV of the contralateral ROIs were calculated (Figure 4.1). The rCBV values were then expressed as a ratio of the maximum intra-tumour CBV and the mean CBV in the contralateral normal appearing white matter. This approach has been shown to provide the best inter-observer and intra-observer reproducibility (Law et al., 2003; Wetzel et al., 2002).

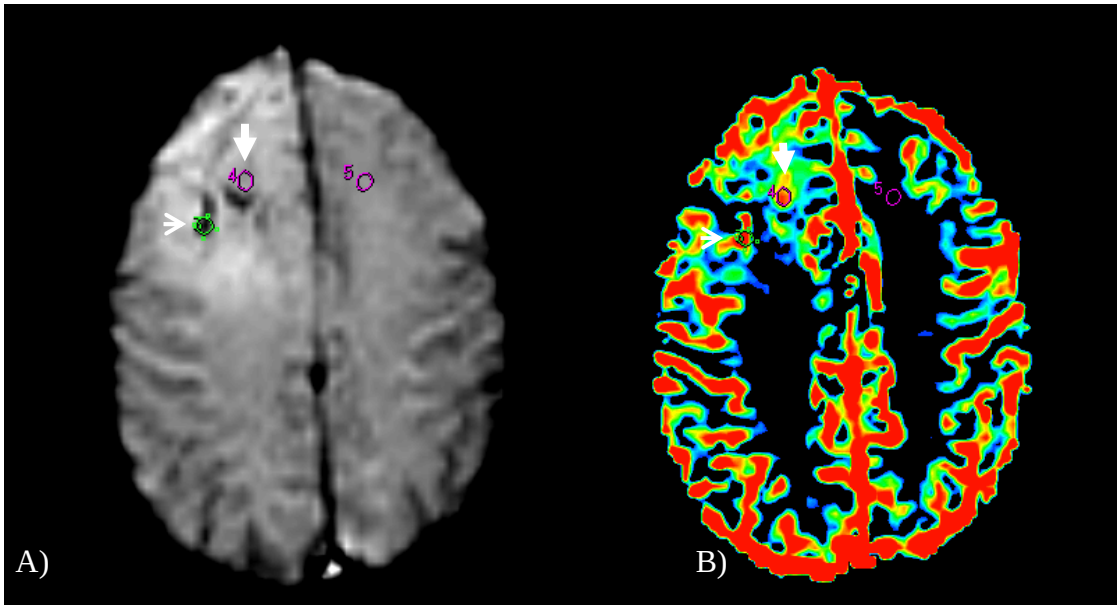

Figure 4.1: T2*-weighted image during maximum arterial contrast signal intensity drop (A), and rCBV map (B). Note that for the calculation of maximum rCBV value, intra- or peri-tumoural vessels were not included (open arrow). An ROI was placed on the area showing the most elevated CBV (closed arrow) and also on the contralateral white mater. The maximum CBV value of the intra-tumoural ROIs and the mean CBV of the contralateral ROIs were calculated.

4.2.4 Statistical analysis

Analysis was performed using Stata 9 (Stata Corporation, College Station, TX USA) and $p<0.05$ was considered to be significant.

At the last individual available follow-up visit, patients were classified into three categories of roughly equal sizes: 1) Stable: patients without radiological evidence of malignant transformation. These patients' MRI studies showed either no enhancement or stable enhancement of the tumour compared to study entry (n=11), 2) Progressive: patients with radiological evidence of malignant transformation showing one or more new areas of contrast enhancement or increase of previously stable enhancement (n=13), and 3) Death (n=11).

1. Changes in rCBV over time

The Friedman test was used to analyze the distribution of rCBV at study entry, 6 months and 12 months, and to assess whether there were significant changes of the mean values between these three time points and also between the changes of rCBV within 6 and 12 months.

2. Differences between groups

The Mann-Whitney test was used to determine whether there was a significant difference in the median of rCBV values between two groups. The Kruskal-Wallis test was used when more than two independent groups were involved.

a) Histological groups

Relative CBV at each time point were used as dependent variables. Firstly, tumour histology was used as the grouping variable and was divided into two groups: the

first included tumours with oligodendroglial elements (oligodendrogliomas and oligoastrocytomas; total number=13); the second group included pure astrocytomas (total number=22). Secondly, tumour histology was used again as a grouping variable, but it was divided into three groups: i) oligodendrogliomas (n=8), ii) astrocytomas (n=22) and iii) oligoastrocytomas (n=5).

b) Outcome groups

Relative CBV at each time point were used as dependent variables. Outcome (used as the grouping variable) was divided into two groups: those patients without adverse event (stable patients, n=11) and those who presented an adverse event (transformation and death, n= 24).

3. Association with transformation

To investigate if rCBV at study entry, 6 and 12 months was associated with transformation, independently from histology, age and gender, an ordinal logistic multiple regression analysis was repeated for each time points (i.e. study entry, 6 and 12 months). Additionally the ordinal logistic analysis was also applied to investigate whether changes of rCBV in 6 months or in 12 months were associated with transformation. Firstly, rCBV was modelled individually. Then the rCBV parameters that remained significant were modelled together with histology (using 2 tumour subtypes and 3 tumour subtypes), age and gender.

The dependable variable was classified in two groups, patients that transformed and those who did not. The covariate was rCBV and its changes at each time point.

4. Time to transformation analysis

A Cox regression curve was used to investigate the best predictor of time to transformation. Time was measured as years from study entry to transformation. Stable patients were censored at last follow-up. The covariates at each time point were: rCBV values, histology (first using 2 tumour subtypes and then 3 tumour subtypes), age and gender. The same analysis was repeated using changes of rCBV between study entry and 6 months and also between study entry and 12 months.

The same analysis was performed in a subgroup including pure astrocytomas and another one including oligodendrogliomas and oligoastrocytomas.

Kaplan Meier curve for the strongest predictor

A Kaplan Meier curve was produced for the strongest predictor of time to transformation.

A receiver operating characteristic (ROC) analysis was applied to assess which variable cut-off at study entry was able to allow the differentiation between patients who progressed to high-grade gliomas and those who did not.

4.3 Results

Patients

Demographic data are shown on table 4.1.

Thirty-five patients (mean age: 42; standard deviation (SD) 13.05 ; 24 males and 11 females) with histology proven WHO grade II gliomas (22 astrocytomas, 8 oligodendrogliomas and 5 oligoastrocytomas) were studied for a median total follow-up length of 2.9 years (range 0.4 – 5.6). All 35 patients had MRI studies at 6 months after study entry, while 4 (11%) patients failed to attend the 12 months scan

(1 patient died, 1 patient went abroad for treatment, and 2 patients clinically progressed and dropped out). Of the patients who had these MRI studies, perfusion imaging was not available in 1 patient at study entry, 2 patients at 6 months and 4 patients at 12 months, due to technical problems.

Eleven out of 35 patients (31.4%) remained stable during the follow-up, while 13 patients (37.1%) progressed and 11 (31.4%) died. All deaths were related to tumour progression. The median length of follow-up was 2.4 years for the stable (range: 0.5 – 5.3 years) and 2.0 years for the progressive group of patients (range: 0.5 – 5.5 years). Patients who died were radiologically followed-up for a median of 2.0 years (range: 0.5 – 3 years), but were clinically studied for longer (median 3.9 years; range 1- 4.8).

Stable patients only received palliative treatment (mainly anti-epileptic medication) during the study. Patients did not receive any aggressive treatment until progression to a high-grade glioma had occurred. Twenty-two out of 35 patients (68.5%) were treated after transformation, which included surgery in 9 patients, radiotherapy in 16 patients and chemotherapy in 8 cases. The median time from study entry to treatment was 2.4 years (range: 0.6 – 5.5). Only two patients received treatment within the first year of the study, but both cases were treatment-free at study entry and 6 months; no further MRI data were available after the first 6 months in these two cases.

Table 4.1: Demographic data and rCBV values at study entry, 6 months and 12 months and its changes within 6 and 12 months.

Pat ID	Histology	Age	Gender	rCBV at study entry	rCBV at 6m	rCBV Changes in 6 months	rCBV at 12m	rCBV Changes in 12m
1	O	30	F	2.02	3.01	0.99	3.44	0.43
2	A	51	M	2.46	2.82	0.36	-	-
3	A	30	M	2.00	3.74	1.74	na	na
4	O	57	M	1.94	2.07	0.13	3.29	1.22
5	OA	25	M	1.28	1.77	0.49	1.86	0.09
6	A	37	M	0.99	1.78	0.79	na	na
7	A	30	M	0.94	1.94	1.00	-	-
8	O	56	M	2.53	2.86	0.33	3.15	0.29
9	A	38	M	na	1.66	1.66	1.51	-0.15
10	OA	48	M	1.26	2.23	0.97	-	-
11	A	56	M	1.04	2.66	1.62	2.25	-0.41
12	OA	42	F	1.91	2.54	0.63	3.32	0.78
13	A	58	M	2.24	na	na	na	na
14	A	29	F	2.38	na	na	na	na
15	A	41	M	1.04	1.24	0.20	1.72	0.48
16	A	34	M	1.56	2.03	0.47	2.3	0.27
17	A	47	F	1.09	1.35	0.26	1.59	0.24
18	O	28	F	2.81	4.62	1.81	4.16	-0.46
19	A	35	M	0.91	1.76	0.85	1.37	-0.39
20	OA	65	F	1.28	1.57	0.29	1.52	-0.05
21	A	30	M	1.91	2.17	0.26	2.5	0.33
22	O	24	M	1.59	2.14	0.55	2.15	0.01
23	A	52	M	1.37	1.94	0.57	2.43	0.49
24	O	53	F	1.84	2	0.16	2.01	0.01
25	O	63	F	1.47	1.96	0.49	1.98	0.02
26	O	36	M	3.51	4.24	0.73	7.9	3.66
27	A	60	F	1.14	1.53	0.39	2.7	1.17
28	A	38	M	0.80	1.43	0.63	1.54	0.11
29	OA	69	M	1.94	2.35	0.41	2.35	0
30	A	29	F	1.18	1.73	0.55	1.31	-0.42
31	A	32	M	1.61	2.66	1.05	2.91	0.25
32	A	57	F	1.49	2.34	0.85	2.17	-0.17
33	A	32	M	1.42	1.5	0.08	2.17	0.67
34	A	39	M	1.79	2.23	0.44	-	-
35	A	29	M	0.70	1.51	0.81	1.68	0.17

F: female, M: male, A: astrocytoma, O: oligodendroglioma, OA: oligoastrocytoma, na: not available due to technical problems, (-): patient failed to attend follow up. S: stable, P: progressive, D: death.

1. Changes in rCBV over time

There were significant changes in the mean values of rCBV between study entry, 6 and 12 months. (all p values were < 0.001) and also between the changes of rCBV within 6 and 12 months (p=0.03).

The median, mean values, standard deviation and range of rCBV for each time point and the change of these parameters within the first 6 and 12 months after study entry are given in Table 4.2.

Table 4.2. Mean, median, standard deviation and range of rCBV at each time point and of rCBV changes in 6 and 12 months.

Time point	**Mean**	**Median**	**Minimum**	**Maximum**	**Std Deviation**
Study Entry rCBV	1.63	1.53	.70	3.51	.63
6m rCBV	2.22	2.03	1.24	4.62	.79
12m rCBV	2.49	2.17	1.31	7.90	1.30
Changes of rCBV between SE and 6 months	.68	.55	.08	1.81	.47
Changes of rCBV between SE and 12 months	.89	.71	-.94	4.39	.87

Std: Standard deviation

2. Differences between groups

a) Histological groups

At study entry, there was a significant difference (p=0.01) in the median values of rCBV between patients with tumours with oligodendroglial elements and those with pure astrocytomas. There was also a significant difference between these two groups at 6 (p=0.02) and 12 months (p=0.04).

Similarly there was a significant difference (p=0.01) in the median values of rCBV at study entry between patients with oligodendrogliomas, astrocytomas and oligoastrocytomas. There was also a significant difference between these three groups at 6 (p=0.04) and 12 months (p=0.05).

Astrocytomas had the lowest rCBV values whereas oligodendrogliomas had the highest rCBV values and the rCBV of oligoastrocytomas lay in between. Table 4.3.

Table 4.3. Mean, median, standard deviation, and range of rCBV values for patients with pathologically proved low-grade gliomas in each histological category.

Histology	Time point	N	Mean	Median	Minimum	Maximum	Std Deviation
OD	Study Entry rCBV	8	2.21	1.98	1.47	3.51	.69
	6m rCBV	8	2.86	2.50	1.96	4.62	1.05
	12m rCBV	8	3.51	3.22	1.98	7.90	1.94
AC	Study Entry rCBV	22	1.43	1.37	.70	2.46	.53
	6m rCBV	22	2.00	1.86	1.24	3.74	.61
	12m rCBV	22	2.01	2.17	1.31	2.91	.51
OA	Study Entry rCBV	5	1.53	1.28	1.26	1.94	.36
	6m rCBV	5	2.09	2.23	1.57	2.54	.41
	12m rCBV	5	2.26	2.11	1.52	3.32	.78

AC: astrocytomas OD: Oligodendrogliomas, OA: oligoastrocytomas, N: number of cases, Std: standard.

b) Outcome groups

There is a borderline significant difference (p=0.55) in the median values of rCBV at study entry between patients who had an adverse event (transformation or death) and those who did not. Relative CBV values at 6 or 12 months were not able to differentiate patients between these two groups.

Table 4.4 shows the mean, median, standard deviation, and range of rCBV values for patients in each clinical-radiological category.

Table 4.4. Mean, median, standard deviation, and range of rCBV values for patients with pathologically proved low-grade gliomas in each clinical-radiological category.

Radiological-Clinical Outcome	Time Point	N	Mean	Median	Minimum	Maximum	Std Deviation
Stable	Study Entry rCBV	11	1.32	1.42	.70	1.94	.40
	6m rCBV	11	1.93	1.94	1.43	2.66	.42
	12m rCBV	11	2.09	2.17	1.31	2.91	.53
Progressive	Study Entry rCBV	13	1.99	1.89	.99	3.51	.72
	6m rCBV	13	2.52	2.07	1.57	4.62	.97
	12m rCBV	13	3.08	2.43	1.51	7.90	1.80
Dead	Study Entry rCBV	11	1.55	1.28	.91	2.38	.54
	6m rCBV	11	2.16	2.17	1.24	3.74	.77
	12m rCBV	11	2.09	1.86	1.37	3.32	.67

Std: standard; N: number of cases

3. Association with transformation

Relative CBV at study entry significantly predicted transformation (p= 0.05), with an odds ration of being a transformer of 2.82 for each SD of rCBV [Standard deviation (SD): 0.62, 95% Confidence Interval (CI): 0.98 – 7.96]. However it did not survive when histology, age and gender were added to the model.

Relative CBV at 6 and 12 months were not able to predict transformation (p values= 0.14 and 0.27, respectively), neither did the changes of rCBV between study entry and 6 months (p=0.48) nor the rCBV changes between study entry and 12 months (p = 0.22).

4. Time to transformation analysis

a) Using variable at study entry

a.1) When astrocytomas and oligodendroglial tumours were analyzed together

We found that rCBV at study entry was a predictor of time to transformation. The risk of becoming a progressive during the study was 1.57 higher per each additional SD of rCBV at study entry (p value = 0.026, SD: 0.62, 95% CI: 1.05 – 2.33). These results were independent of the other covariates in the model: histology, age and gender. Table 4.5.

a.2) When only astrocytomas were analysed

Relative CBV at study entry was a predictor of time to transformation. The risk of becoming a progressive during the study was 2.09 higher per each additional SD of rCBV at study entry (p value = 0.01, SD: 0.52, 95% CI: 1.13 – 3.88). These results were independent of age and gender. Table 4.6.

a.3)When only oligodendrogliomas and oligoastrocytomas were analysed

Relative CBV at study entry was not a predictor of time to transformation (p=0.33).

b) Using variable at 6 months

b.1) When astrocytomas and oligodendroglial tumours were analyzed together

Relative CBV at 6 months follow up predicted time to transformation. The risk of becoming a progressive during the study was 1.62 higher per each additional SD of rCBV at 6 months follow-up (p value = 0.028, SD: 0.78, 95% CI: 1.05 – 2.50). However it did not survive when other variables were considerate in the model. Table 4.5.

Changes of rCBV between study entry and 6 months did not predict time to transformation (p=0.5).

b.2) When only astrocytomas were analysed

Neither rCBV at 6 months follow up or changes of rCBV between study entry and 6 months predicted time to transformation (p=0.23 and p =0.94, respectively).

b.3) When only oligodendrogliomas and oligoastrocytomas were analysed

Relative CBV at 6 months follow up did not predict time to transformation (p=0.07).

Changes of rCBV between study entry and 6 months did predict time to transformation. The risk of becoming a progressive during the study was 2.65 higher per each additional SD of changes of rCBV within 6 months (p value = 0.02, SD: 0.44, 95% CI: 1.14 – 6.14). However it did not survive when age was considerate in the model. Table 4.7.

c) Using variables at 12 months

c.1) When astrocytomas and oligodendroglial tumours were analyzed together

Relative CBV at 12 months follow up predicted time to transformation. The risk of becoming a progressive during the study was 1.51 higher per each additional SD of rCBV at 12 months follow-up (p value = 0.03, SD: 1.29, 95% CI: 1.02 – 2.22). However it did not survive when other variables were considerate in the model. Table 4.5.

Changes of rCBV between study entry and 12 months did not predict time to transformation (p=0.3).

c.2) When only astrocytomas were analysed

Relative CBV at 12 months did not predict time to transformation (p=0.37)

Changes of rCBV between study entry and 12 months did not predict time to transformation (p=0.49).

c.3) When only oligodendrogliomas and oligoastrocytomas were analysed

Relative CBV at 12 months follow up predicted time to transformation. The risk of becoming a progressive during the study was 2.08 higher per each additional SD of rCBV at 12 months follow-up (p value = 0.04, SD: 1.71, 95% CI: 1.00 – 4.11). However it did not survive when other variables were considerate in the model. Table 4.7.

Changes of rCBV between study entry and 12 months did predict time to transformation. The risk of becoming a progressive during the study was 2.06 higher per each additional SD of changes of rCBV within 12 months (p value = 0.04, SD: 1.14, 95% CI: 1.03 – 4.13). However it did not survive when other variables were added in the model. Table 4.7.

Table 4.5. Odds ratio, standard deviation, confidence interval and p values of predictors of time to transformation at each time point. All tumour subtypes included

PREDICTOR	ODDS RATIO	STANDARD DEVIATION	CONFIDENCE INTERVAL	P VALUE
rCBV at SE	1.57	0.62	1.05 – 2.33	0.026
rCBV at 6months*	1.62	0.78	1.05 – 2.50	0.028
rCBV at 12 months*	1.51	1.29	1.02 – 2.22	0.03

SE: study entry. * Results did not survive when other variables were added in the model.

Table 4.6. Odds ratio, standard deviation, confidence interval and p values of the only predictor of time to transformation for patients with low-grade astrocytomas.

PREDICTOR	ODDS RATIO	STANDARD DEVIATION	CONFIDENCE INTERVAL	P VALUE
rCBV at SE	2.09	0.52	1.13 – 3.88	0.01

SE: study entry.

Table 4.7. Odds ratio, standard deviation, confidence interval and p values of the predictors of time to transformation for patients with low-grade oligodendrogliomas and oligoastrocytomas.

PREDICTOR	ODDS RATIO	STANDARD DEVIATION	CONFIDENCE INTERVAL	P VALUE
Changes of rCBV between SE and 6 months*	2.65	0.44	1.14 – 6.14	0.02
rCBV at 12 months*	2.08	1.71	1.00 – 4.11	0.04
Changes of rCBV between SE and 12 months *	2.06	1.14	1.03-4.13	0.04

SE: study entry. * Results did not survive when other variables were added in the model.

Kaplan Meier curve for the strongest predictor

When all tumour subtypes were included rCBV at study entry showed to be the strongest predictor of time to transformation among other time points. It was then entered in the analysis with the ROC curve. The analysis showed that the rCBV value at study entry associated with the highest specificity was 1.84. This cut off was based on high specificity. At 90% specificity on the ROC curve, we get three thresholds (1.84, 1.91 and 1.94), but 1.84 was chosen because a similar number was previously used in the literature (Law et al., 2006a).

When the entire cohort was analysed using this value as a threshold, we found a borderline significance difference in time to transformation between patients with rCBV smaller than 1.84 and those with rCBV equal or above this cut-off ($p = 0.06$) (Figure 4.2.A). Median time to transformation was 2.63 years (95% CI: 1.22 – 4.03) for patients with rCBV at study entry less than 1.84, compared with 1.58 years (95% CI: .99 – 2.16) for patients with rCBV greater than or equal to 1.84.

When only astrocytomas were included in the analysis we found a significant difference in time to transformation between patients with rCBV smaller than 1.84 and those with rCBV equal or above this cut-off ($p = 0.03$) (Figure 4.2.B). Median time to transformation was 2.63 years (95% CI: 1.44 – 3.81) for patients with rCBV at study entry less than 1.84, compared with 0.99 years (95% CI: 0.07 – 1.91) for patients with rCBV greater than or equal to 1.84.

When only oligodendrogliomas were analysed there was no significant difference in the time to transformation between groups with low and high rCBV ($p=0.8$).

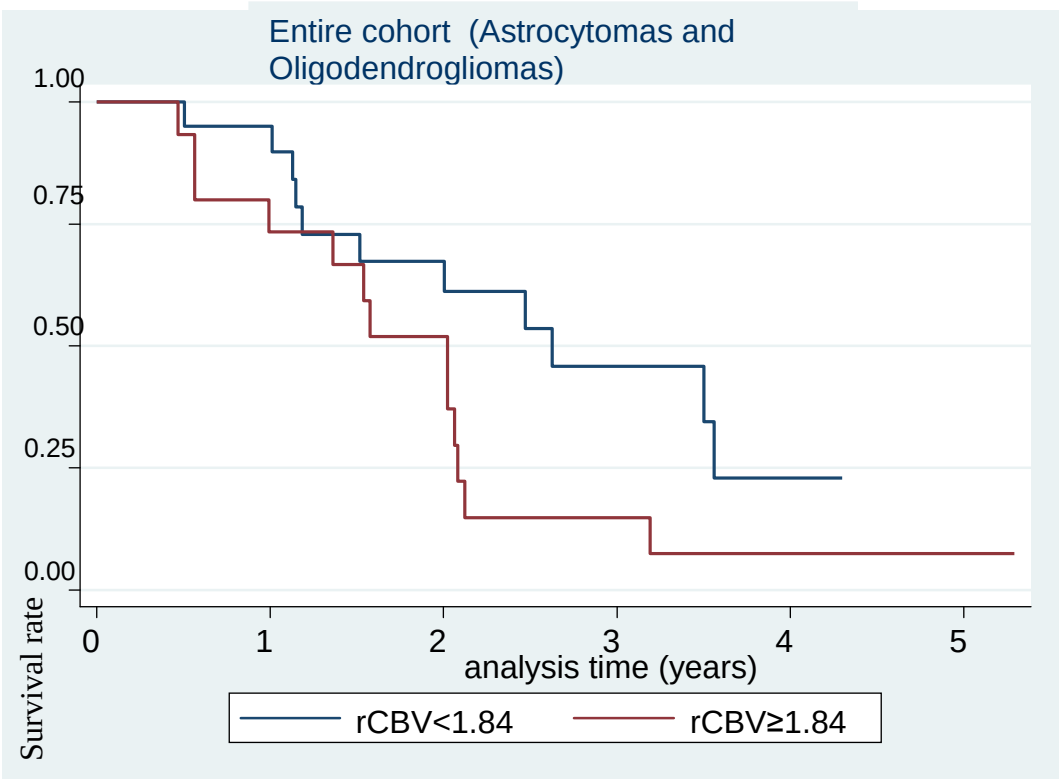

. Figure 4.2 A.

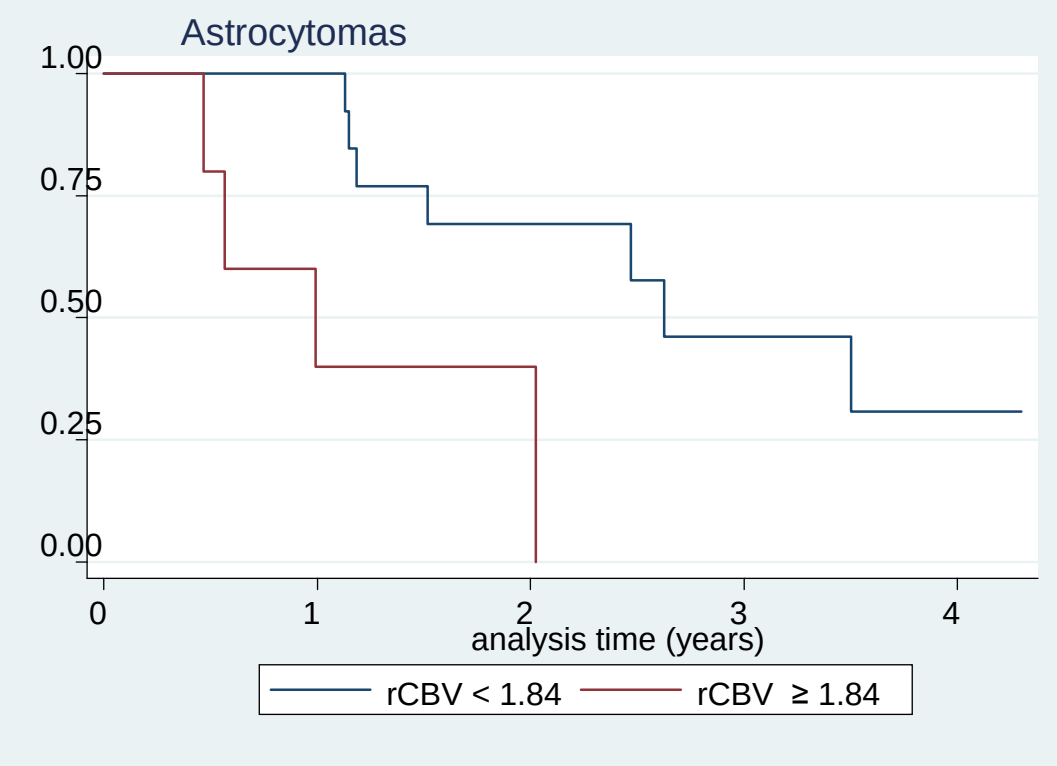

Figure 4.2 B.

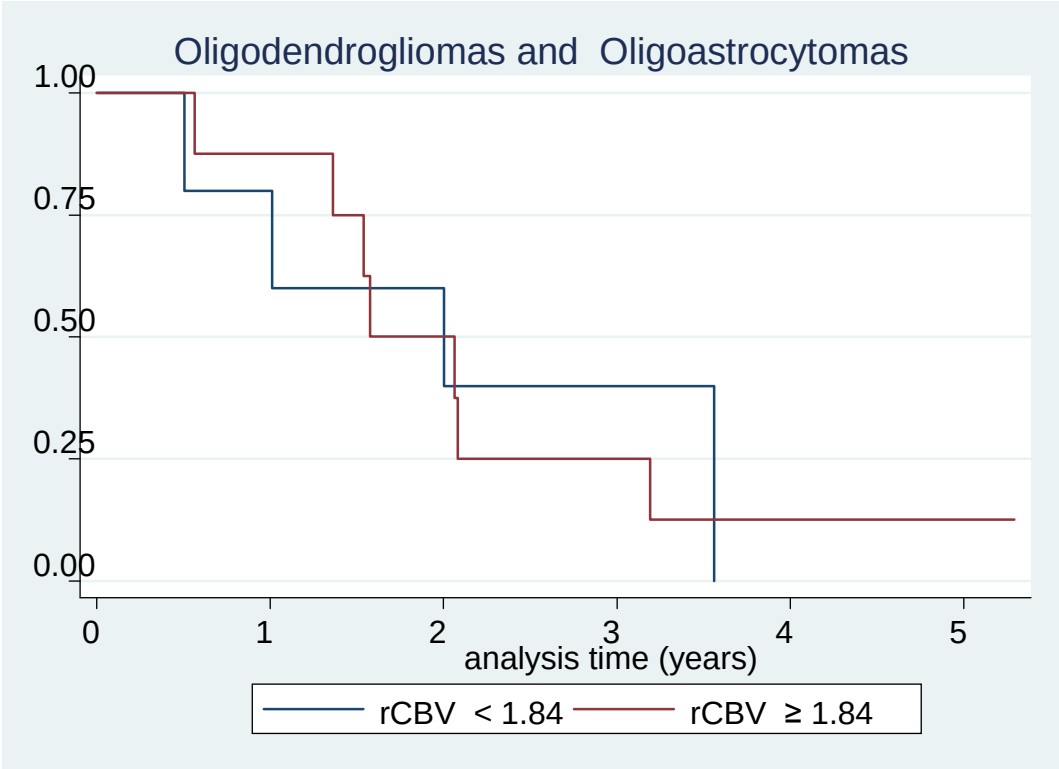

Figure 4.2.C.

Figure 4.2: A) Analysis using entire cohort. Kaplan-Meier survival curve for time to transformation within groups with low (<1.84) and high (≥1.84) rCBV. Patients with low-grade gliomas with low rCBV had a median time to progression of 2.63 years. Patients with low-grade gliomas with high rCBV had a median time to progression of 1.58 years.

B) Analysis using subgroup of astrocytomas. Kaplan-Meier survival curve for time to transformation within groups with low (<1.84) and high (≥1.84) rCBV. Patients with low-grade astrocytomas with low rCBV had a median time to progression of 2.63 years. Patients with low-grade gliomas with high rCBV had a median time to progression of 0.99 years.

C) Analysis using subgroup of oligoastrocytomas and oligodendrogliomas. There was no significant difference in the time to transformation between groups with low (<1.84) and high (≥1.84) rCBV.

4.4 Discussion

Perfusion MRI in gliomas has mostly been used to predict the histological grade (Cha et al., 2005; Law et al., 2003; Sugahara et al., 1998) and more recently tumour genotype (Jenkinson et al., 2006). Law et al (Law et al., 2006a) used baseline rCBV measurement in patients with low-grade gliomas, who underwent aggressive treatment, to obtain prognostic information about survival and tumour progression.

In this chapter we used serial perfusion MR imaging over a one year period in a cohort of patients with conservatively treated gliomas to assess whether serial rCBV measurements and its changes between time points can predict outcome.

We found significant differences in rCBV between time points. This could be explained by the fact that values of rCBV correlate well with vascular endothelial growth factor (VEGF) (Maia et al., 2005). The expression of VGEF is promoted by nutrient-deficient states, such as tissue hypoxia or hypoglycemia, that occur as tumour cells in rapidly growing pathologic tissues expand beyond the limits of diffusion of nutrients from the native capillaries (Shweiki et al., 1992). This hypothesis is corroborated by a previous study of longitudinal rCBV measurements in a smaller cohort of patients with low-grade glioma that showed a dramatic rCBV increase closer to the point of transformation to a high-grade tumour (Danchaivijitr et al., 2008).

In our cohort, rCBV at study entry, 6 and 12 months follow up was not only able to differentiate tumours with oligodendroglial elements and those with pure astrocytomas but also between oligodendrogliomas, astrocytomas and oligoastrocytomas. This is in keeping with the literature where maximum tumour rCBV measurements derived from DSC MR imaging were significantly higher in low-grade oligodendrogliomas than in astrocytomas (Cha et al., 2005). In addition we demonstrated significantly higher rCBV values in oligoastrocytomas compared to pure astrocytomas. The findings of our cohort and available

literature suggest that rCBV can be used to distinguish low-grade gliomas subtypes. However, no previous publications have studied the association of rCBV with tumour subtype at different time points. Interestingly, in our study the significance is higher at study entry than at other time points. This could be due to the overall raise in rCBV over time, which we found in all subtypes, as the tumour grows and angiogenesis increases. Histological classification and the influence of longitudinal rCBV changes on the ability to predict low-grade gliomas subtypes would have to be clarified in a bigger cohort.

Law et al (Law et al., 2006a) have shown that rCBV was also able to differentiate patients that had an adverse event (transformation or death) from those who did not. In that study patients that transformed or died had a higher rCBV. Even though we used a different definition for transformation, we showed a borderline difference in the study entry rCBV values between patients that presented an adverse event from those who did not.

Finally we have showed that rCBV at study entry significantly predicted time to transformation, independent of histology, age and gender. At time points 6 and 12 months rCBV is still predictive, but loses its significance when compared to the other variables in the model. When only astrocytomas were analyzed rCBV at study entry was the only predictor of time to transformation. Interestingly, changes of rCBV between study entry and 6 and study entry and 12 months did not predict transformation when all tumour subtypes were included. However it did predict transformation when only oligodendroglial tumours were analyzed. This subgroup analysis suggests that values at study entry are most useful in astrocytic tumours, whereas changes in rCBV over a short period of time may be more helpful in tumours with oligodendroglial elements, which have generally a wider range of rCBV values.

In a previous study it has been shown that rCBV was a significant predictor of adverse outcome (transformation or death) (Law et al., 2006b) and in a different publication the same author showed that low rCBV values were associated with longer time to progression (Law et

al., 2006a). None of the previous publications has tested if rCBV measurements at different time points were also able to predict time to transformation. The same author used an rCBV threshold of 1.75 to compare the group with high rCBV and the group with low rCBV in terms of time to progression/death (Law et al., 2006a). Lesions with rCBVs that were more than 1.75 had a median time to progression/death of 245 days, whereas lesions with rCBVs less than 1.75 had a median time to progression/death of 4620 days. In our cohort there was a significant difference in time to transformation between patients with rCBV smaller and greater than 1.84. Median progression time was 1.58 years for patients with rCBV greater than or equal to 1.84 compared with 2.63 years for patients with rCBV at study entry less than 1.84. When only astrocytomas where analysed we also found a significant difference in time to transformation between patients with rCBV smaller and greater than 1.84. Median progression time was 0.99 years for patients with rCBV greater than or equal to 1.84 compared with 2.63 years for patients with rCBV at study entry less than 1.84. When only oligodendroglial elements were analysed, there was not a significant difference between these two groups. This in keeping with our previous results, as rCBV at study entry did not predict time to transformation in this subgroup. It is important to note that on our analysis we used transformation as end point whereas Law et all used transformation/death as end point. This could already explain differences in time to transformation and time to transformation/death between the groups. The former group demonstrated a shorter time to progression/death in patients with high rCBV when compared with our study. This could also be explained by the fact that we used different definitions of time to transformation. Law et al (Law et al., 2006a) used decline in neurologic status or Karnofsky score or increase in tumour size by more than 25% at MR imaging. When relying on clinical signs one can assume that transformation is detected at a later stage, as changes in imaging appearance precede clinical deterioration. Focal contrast-enhancement has proved to be a more reliable indicator of malignancy in

gliomas than border definition, mass effect, necrosis and haemorrhage (Daumas-Duport et al., 1997; Mihara et al., 1995; Pierallini et al., 1997). We therefore selected contrast enhancement as criterion for the classification of malignant transformation.

In our cohort few patients presented decline in neurologic status after being classified as transformers. In contrast, our cohort shows a shorter time to progression in patients with low rCBV when compared to the former group. This could be explained because the former study also included paediatric patients, which have a longer survival time and that low-grade gliomas receive aggressive treatment (i.e. surgery, chemotherapy or radiotherapy) prolonging their survival, whereas in our cohort we only recruited adults and these patients are conservatively treated until a transformation to a higher grade occurs. Moreover on the former study the average follow up was 4.2 years, whereas on ours it was 2.9 years.

4.5 Conclusion

In this chapter we have shown that rCBV is an important variable when assessing brain gliomas. It contributes towards the understanding of the natural history of brain gliomas, and helps to differentiate between tumour subtypes and also much needed prognostic information on these patients. Relative rCBV can be used to distinguish between patients that had an adverse event from those who did not, but more importantly it can be used to predict time to transformation, which it is important when planning treatment. It would be very useful to assess if these results could be replicated in other institutions, which will be assessed in following chapter.

Chapter 5

Relative cerebral blood volume measurements predict malignant transformation in patients with low-grade gliomas, in a two-institution setting

5.1 Introduction

Low-grade gliomas (LGG) account for approximately 20% of central nervous system glial tumours and, in the United States, approximately 1800 new cases of LGG are reported each year. As outlined in chapter 4 most of these tumours transform into more aggressive phenotypes at some point in their natural history, however this malignant transformation has been difficult to predict so far.

Multiple studies have assessed factors present at diagnosis that may predict tumour behaviour (Bauman et al., 1999; Medbery et al., 1988; Pignatti et al., 2002). In a multi-institutional study of 401 patients, aged less than 40 years, with epilepsy as the presenting symptom, and absence of contrast enhancement on CT, all were associated with improved survival (Bauman et al., 1999).

Histopathology remains currently the standard reference for determining the glioma biology. Primary brain tumours are classified according to their predominant cell type and graded based upon the presence or absence of standard pathologic features, such as necrosis, mitotic figures, nuclear atypia, and endothelial cell proliferation. Low-grade astrocytomas have increased cellularity and atypia; but no mitoses, endothelial proliferation, or necrosis. Although there is an established system of classifying and subclassifying these low-grade tumours, the prognostic value of defining subcategories of gliomas is based upon mitotic activity, proliferation and/or necrosis is still controversial. One study evaluated the utility of the WHO classification of childhood supratentorial astrocytic tumours in 340 children and found that the presence or absence of endothelial proliferation, necrosis, and mitosis but not other histologic features was inadequate to classify these neoplasms into prognostically homogenous groups (Gilles et al., 2000).

Central nervous system histopathology is limited by sampling error, in which case the most aggressive portion of the tumour may be missed, by inter- and intraobserver variability (Coons et al., 1997; Prayson et al., 2000) and by the dynamic nature of gliomas, whereby tumours can de-differentiate into more aggressive phenotypes (Jackson et al., 2001). In the later study it was shown a discrepancy between the diagnosis made from small biopsy samples and the diagnosis from resected specimens. It would be greatly beneficial to clinical teams to have an additional method of predicting the behaviour of gliomas which can overcome some of these limitations of histopathology and is also reproducible and reliable.

Measurement of rCBV has been shown to predict time to transformation in our cohort (chapter 4) and in another study (Law et al., 2006a). The aim of this chapter is to assess whether rCBV measurements can be used to predict patient outcome in a multi-institution setting.

5.2 Methods

5.2.1 Patients

69 consecutive patients with low-grade glioma met the inclusion criteria for this study. Inclusion criteria were (i) histologically confirmed brain gliomas, (ii) patients who were referred for preoperative assessment for intracranial tumours and (iii) patients who did not show evidence of systemic malignancy or immune suppression.

Patients underwent conventional and perfusion imaging every 6 months at the Institute of Neurology (ION) and every 3 months at the New York University Medical Centre (NYUMC). At these time points, clinical assessment was also performed.

The study was approved by the institutional review board and local research ethics committee and all patients provided informed consent.

5.2.2 MRI protocol

At the ION, studies were acquired with a 1.5 T system (Signa LX, GE Medical Systems, Milwaukee, WI). The following sequences were acquired: pre- and post-contrast (0.2mmol/kg) coronal spoiled gradient echo (SPGR) sequence with TR/TE 14.4/6.4 (repetition time msec/echo time msec), Coronal FLAIR with 8774/161/2192 (repetition time msec/echo time msec/inversion msec) and T2-weighted (6000/102).

At the NYUMC, imaging was also performed at 1.5 T (Siemens Vision or Symphony; Siemens, Erlangen, Germany). The following sequences were obtained: pre- and post-contrast (0.2mmol/kg) transverse T1-weighted spin echo, with 600/14; transverse fluid-attenuated inversion recovery (FLAIR), with 9000/110/2500; and T2-weighted (3400/119) MR imaging.

At both centres, dynamic susceptibility-weighted perfusion contrast-enhanced MR images were acquired with a gradient-echo echo-planar imaging sequence during the first pass of a standard-dose (0.1 mmol/kg) bolus at a rate of 5ml/sec, except for the 5 patients in the 0–16 year age group, in whom the injection rate was reduced to 3 ml/sec. The contrast used was gadoterate meglumine (Dotarem ®) at the ION and gadopentetate dimeglumine (Magnevist; Berlex Laboratories, Wayne, NJ) at NYUMC. Six to 10 sections were positioned to cover the tumour based on T2-weighted and FLAIR images. At the ION the imaging parameters were: 1200/40; field of view, 260 x 260 mm; section thickness, 5 mm, contiguous sections; matrix, 128 x 92; flip angle, 90°. For the NYUMC, imaging parameters were as follows: 1000/54; field of view, 230 x 230 mm; section thickness, 5 mm; matrix, 128 x 128; in-plane voxel size, 1.8 x 1.8 mm; intersection gap, flip angle, 30°.

Contrast-enhanced T1-weighted MR imaging was also performed at both centres after the acquisition of dynamic susceptibility-weighted perfusion contrast-enhanced imaging data.

5.2.3 MRI analysis

1) Relative cerebral blood volume measurements

The procedure used to calculate relative cerebral blood volume (rCBV) from the dynamic susceptibility-weighted perfusion contrast-enhanced MR imaging data was based on standard algorithms that have been previously described (Rosen et al., 1991; Rosen et al., 1990). A summary of the analysis was published elsewhere (Law et al., 2006a).

At the ION data processing was performed off-line using Advantage Workstation commercial processing software (Functool, General Electric Medical Systems). At the NYUMC, it was performed at a workstation (Unix; The Open Group, San Francisco, Calif) with programs developed in house in the C and Interactive Data Language programming languages. In each case colour overlay maps of rCBV were produced. To improve the signal-to-noise ratio the rCBV measurements used in this study were calculated from ROIs of 15-20 pixels placed in regions of highest rCBV on colour overlay maps. At least four separate ROI measurements were made, and the maximum rCBV value of these was recorded. This method had been shown to provide the highest intra- and interobserver reproducibility of rCBV measurements (Wetzel et al., 2002). Large peri- or intratumoural vessels were avoided when placing the ROIs, as they can be an important confounding factor (Brasil Caseiras et al., 2008).

5.2.4 Statistical Analysis

Analysis was performed in Stata 9 (Stata Corporation, College Station, TX USA) and $p<0.05$ was considered to be significant.

At the last individual follow-up visit patients were classified into four categories: 1) Complete response: MR image with no visible tumour and no new neurologic deficit; 2) Stable: no change in the neurologic examination or Karnofsky score, a change in tumour size of less than 25% at MR imaging; 3) Progressive: was defined as a decline in neurologic status or Karnofsky score, an increase in tumour size of more than 25% 4) Death. This classification was based in part on the method described by Levin et al (Levin et al., 2003). The mean, standard deviation, and median of the rCBV measurements were obtained for patients in each clinical-radiological response category.

1. Differences between clinical-radiological outcome groups

The Mann-Whitney test was used to determine whether there was a significant difference in the median of rCBV values between patients that presented a complete response and the ones that remained stable. The same analysis was repeated between progressive patients who died.

2. Differences between groups with adverse and non adverse event

The Mann-Whitney test was used to determine whether there was a significant difference in the median of rCBV values between two independent groups. The grouping variable was the presence of adverse event (progressive disease or death) and non adverse event (complete response and stable).

3. Association of rCBV with adverse event

To investigate if rCBV at study entry was associated with adverse event, a logistic regression analysis was performed. Firstly, rCBV was modelled individually. Then it was modelled together with histology, age and gender. Centre was also added in to the model to assess if the results were significantly independent of the institution (i.e. ION or NYUMC). The dependable variable was adverse or non adverse event. The covariate was rCBV at study entry.

4. Association of rCBV with time to progression

Kaplan-Meier survival curves and log-rank test were used to characterize and compare the group with high ($\geq$ 1.75) and low rCBV ($<$ 1.75) in terms of time to progression. This threshold value had previously been found to give the optimal sensitivity and specificity for differentiating low-grade from high-grade gliomas (Law et al., 2003). Time to progression was defined as the time from the study entry or initial surgical diagnosis until progression was reached. Data for those patients with complete response and stable disease at the time of most recent follow-up were appropriately censored. Kaplan Meier survival curves and log-rank test were then applied to compare the time to transformation in the two groups of patients defined by the cut-off. Differences between the two groups defined were tested using the log-rank test.

5.3 Results

Patients

Sixty-nine patients (23 female and 46 male patients; median age, 40 years; range, 4-80 years) were studied for a median total length of 396 days (range from 63 to 2009). Five patients were in the 0 – 16 years age group. The pathologic diagnoses were: 34 low-grade astrocytomas, 20 low-grade oligodendrogliomas, 9 low-grade mixed oligo-astrocytomas, 1 ganglioglioma, and 5 with indeterminate histology. Thirty-five patients were followed up at the Department of Radiology, NYUMC, whereas 34 were followed up at the ION.

Four out of 69 patients (5.7%) were defined as complete response, 32 (46.3%) as stable while 13 (18.8%) were progressive during the follow-up and 17 (24.6%) died. In 3 cases the clinical outcome was not known because the patients dropped out of the study and went abroad. These patients were excluded from the analysis because of lack of clinical information. Thirty-four out of 69 patients were classified as stable or progressive using only the clinical criteria whereas the remaining used both radiological and clinical, as described previously.

At the ION the low-grade gliomas were treated conservatively until there was clinical or radiological evidence of disease progression. Following this, 22 patients received treatment (surgery: 10; radiotherapy: 14 and chemotherapy: 8 patients). At the NYUMC cohort 29 patients received treatment during the study, which included surgery in 27 patients, radiotherapy in 20 and chemotherapy in 19 patients.

The median, mean, and standard deviation for study entry rCBV in each of the four clinical response categories are represented in Table 5.1.

Table 5.1. Mean and median relative CBVs for patients with pathologically proven low-grade glioma in each clinical response category.

Outcome	**Mean rCBV ± SD**	**Median rCBV**
Complete Response (n=4)	1.41 ± 0.13	1.44
Stable (n=32)	1.75 ± 0.91	1.53
No Adverse Event (n=36)	1.71 ± 0.86	1.49
Progressive (n=13)	3.21 ± 1.81	3.09
Death (n=17)	2.06 ± 1.06	1.79
Adverse Event (n=30)	2.56 ± 1.52	2.38

N=number of subjects. SD: standard deviation

1. Differences between clinical-radiological outcome groups

Thirty-six patients demonstrated no adverse event, whereas 30 patients had an adverse event. There was no significant difference between the median rCBV of patients with complete response (n=4) and those with stable disease (n=32) (Figures 5.1 and 5.2). However, a significant difference was found between those with progressive disease (n=13) and those who died of disease (n=17) (p value = 0.03).

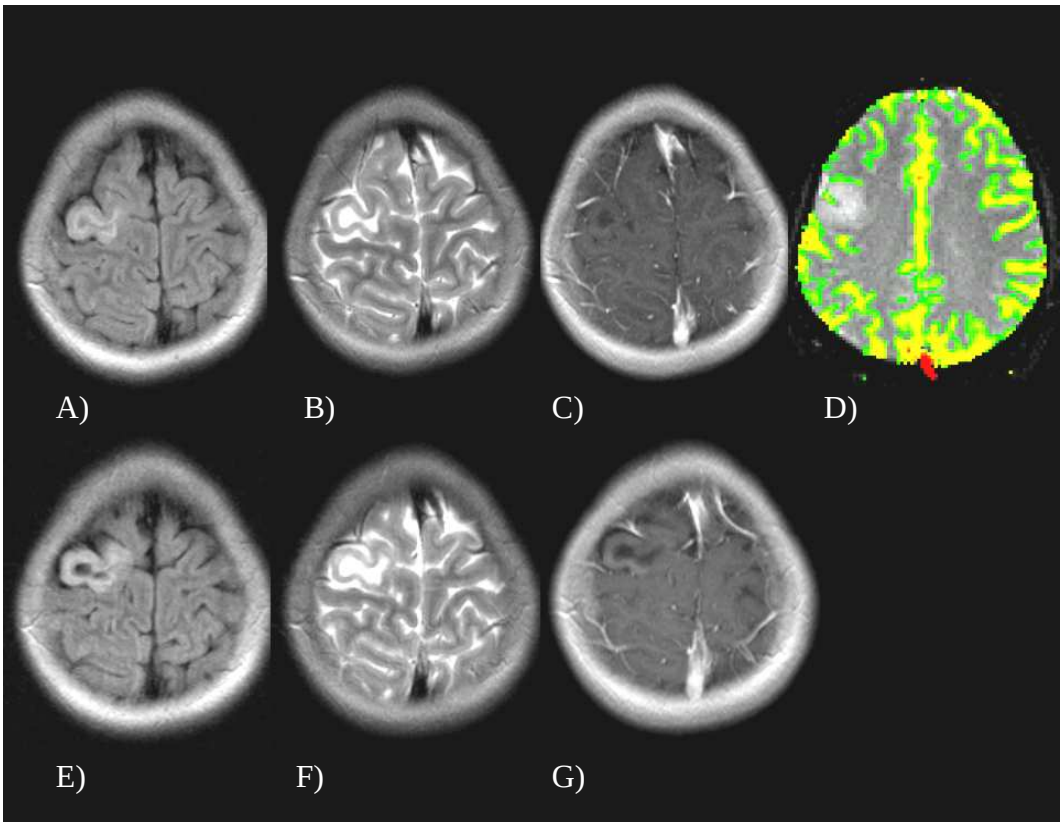

Figure 5.1. 26-year-old male with pathology proven low-grade astrocytoma with a low baseline rCBV (1.24), which remained stable.

Top Row : A, Axial FLAIR image; B, Axial T2*-weighted image shows increased signal within the middle frontal gyrus on the right side. C, Contrast-enhanced axial T1-weighted image demonstrates no appreciable enhancement compatible with an imaging and pathologic diagnosis of LGG. D, Gradient-echo axial DSC MRI image with rCBV colour overlay map, shows a lesion with low initial perfusion with an rCBV of 1.24 more in keeping with a LGG.

Bottom Row: E, Axial FLAIR image at 376 days follow up. F, Axial T2-weighted image shows a stable appearance to the right frontal LGG. G, Contrast-enhanced axial T1-weighted image demonstrates no change in the appearance of the glioma with no enhancement to suggest malignant transformation.

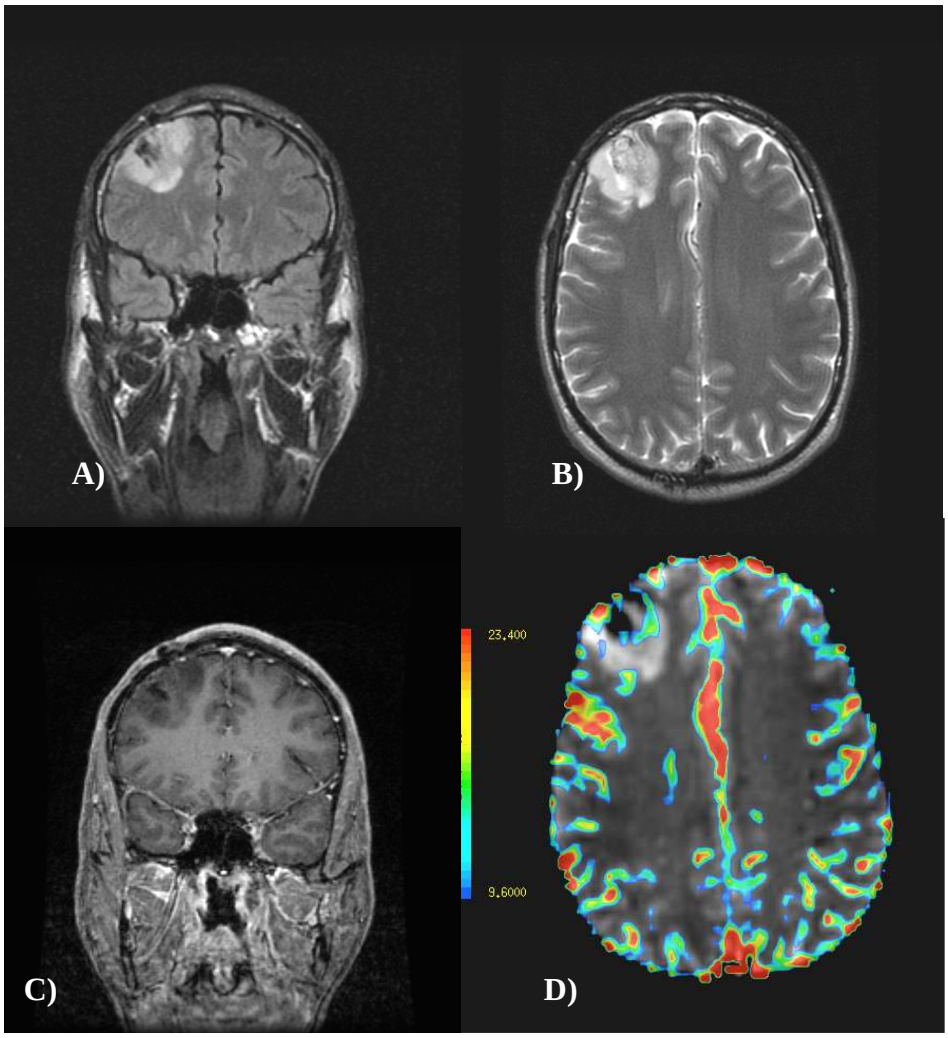

Figure 5.2: 32-year-old male with pathology proven right frontal low-grade astrocytoma, which remained stable. Coronal FLAIR image (A) and Axial T2-weighted image (B) shows increased signal in the right frontal lobe. C) Contrast-enhanced coronal T1-weighted image demonstrates no appreciable enhancement compatible with an imaging and pathologic diagnosis of LGG. D) Gradient-echo axial DSC MRI image with rCBV colour overlay map, shows areas of highest perfusion within the tumour. rCBV at study entry was 1.61.

2. Differences between groups with adverse and non adverse event

There is a significant difference in the median rCBV values between patients that had an adverse event from those who did not (p=0.01), the latter having lower rCBV values than the former.

3. Association of rCBV with adverse event

Relative CBV at study entry was significantly associated with an adverse event, independently from age, gender or centre (p = 0.0134). The odds ratio of detecting an adverse event was 2.19 (standard deviation: 1.24; 95% confidence interval: 1.15 – 4.16) for each per standard deviation of rCBV at study entry. (Figure 5.3).

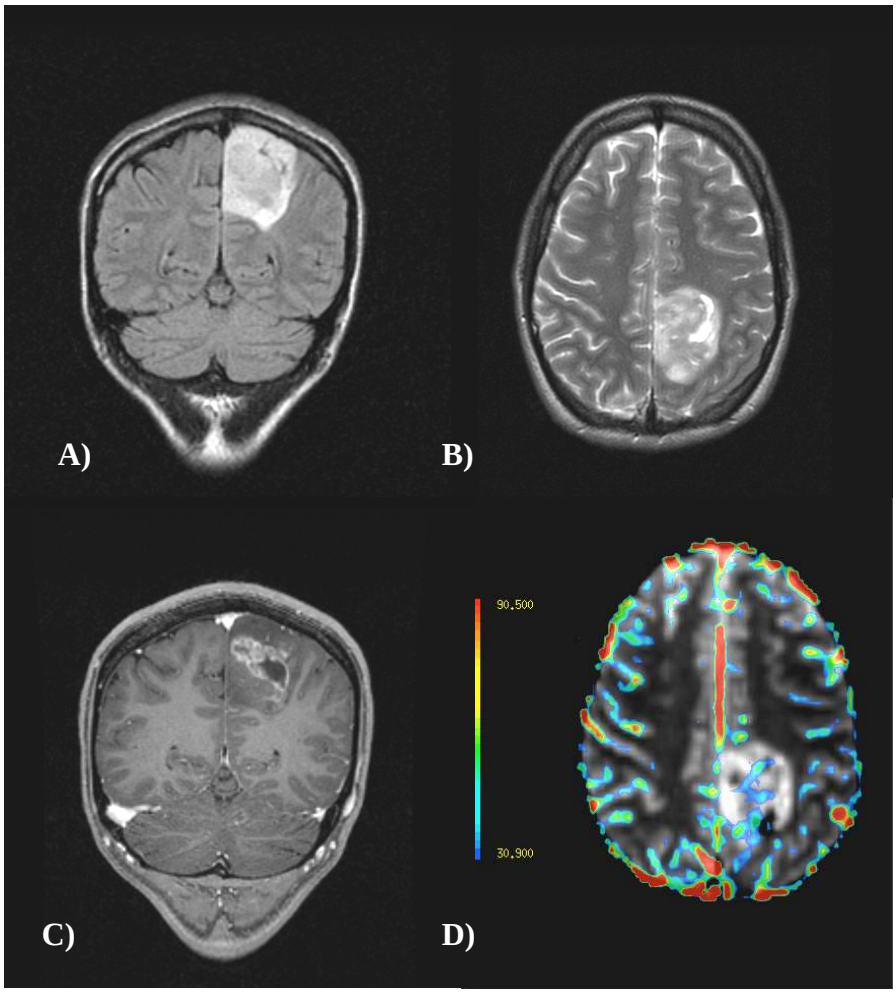

Figure 5.3: 28-year-old female with pathology proven left frontal low-grade oligodendroglioma, which presented an adverse event. Coronal FLAIR image (A) and Axial T2-weighted image (B) shows increased signal in the left frontal lobe. C) Contrast-enhanced coronal T1-weighted image demonstrates enhancement. D) rCBV map shows areas of highest perfusion within the tumour. rCBV at study entry was 2.81.

4. Association of rCBV with time to progression

Thirty-six patients showed a baseline rCBV < 1.75, compared to 30 with a baseline rCBV ≥ 1.75. Relative CBV was significantly negatively associated with time to progression or death (p=0.0059, 0.0057 for numeric and binary representations, respectively). The median time to progression among subjects with rCBV > 1.75 was 365 days, 95% confidence interval: 355 to 742 days, while the median time to progression among subjects with rCBV < 1.75 could not be estimated (since more than 50% of these subjects were progression-free at time of last observation). However, there is 95% confidence that the median in this cohort was at least 889 days (Figure 5.4).

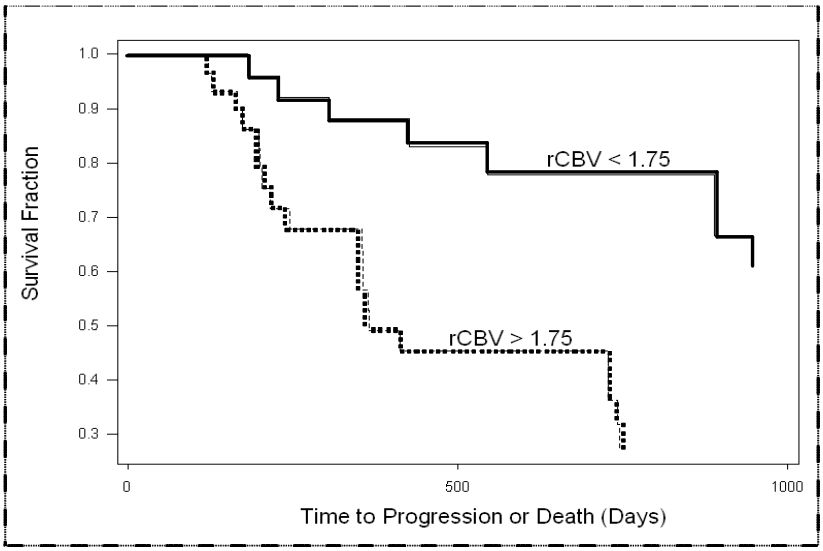

Figure 5.4. Kaplan-Meier survival curves for time to progression within groups with low (< 1.75) and high (rCBV > 1.75) at both institutions. Patients with low-grade glioma with low rCBV at baseline had a probable median time to progression of 889 days, whereas the median time to progression among subjects with high rCBV was 365 days.

5.4 Discussion

In this multi-institution study we demonstrated a significant difference in mean rCBV values between patients with progressive disease and those who died, and were also able to detect the presence of an adverse event using rCBV at study entry, independently from histology, gender, age or centre.

Previous studies have also shown that patients with an adverse event had a significantly higher rCBV than did patients who did not have an adverse event and also that rCBV was significantly negative associated with survival (Law et al., 2006a). Aronen et al (Aronen et al., 1994) demonstrated that patients with brain gliomas with rCBV> 1.5 were more likely to develop into high-grade gliomas. Similarly, Tzika et al (Tzika et al., 2004) demonstrated that blood volume measurements could be used to distinguish between progressive and stable tumours in paediatric patients. These higher rCBV values in certain patients with low-grade glioma could be explained by the fact that they might already have high-grade components at the time of the histopathologic assessment or that rCBV is possibly higher in patients that are undergoing malignant transformation. Whatever the reason, it appears that LGGs with higher rCBV are more likely to behave as high-grade tumours, whereas LGGs with lower rCBV values are more likely to behave as a true low-grade glioma (Law et al., 2006a).

An important finding was the significant negative association of rCBV with time to progression. Patients with low-grade gliomas and high rCBV (> 1.75) had a median time to progression of 365 days, whereas in patients with low rCBV (< 1.75) there was a 95% confidence that the median time was 889 days. Although caution should be taken when adopting a threshold value, this cut-off has previously been found to give the optimal sensitivity and specificity for differentiating low- from high-grade gliomas at a single institution (Law et al., 2003).

Other studies have shown similar results. Lev et al (Lev et al., 2004) demonstrated a mean survival time of 24 months for patients with rCBV > 1.75 and Law et al (Law et al., 2006a) presented a median survival time of 8 months for patients with rCBV > 1.75. However Leighton et al (Leighton et al., 1997) reviewed the outcome of patients with pathologically confirmed low-grade glioma and showed a median time of survival for patients with low-grade glioma of 10.5 years and a median progression-free survival of 4.9 years. This difference could be explained by the fact that changes in rCBV might be an indicator of imminent or occurring malignant transformation; alternatively it may reflect histological sampling error and inter- or intrapathologist variability leading to erroneous classification of a high-grade glioma as a low-grade tumour.

One limitation of a multi centre study is the use of different MR systems in each centre. However in this study the MR sequences used in both centres for Dynamic Susceptibility-weighted Perfusion Contrast-enhanced MR Imaging were highly comparable, with both using a gradient echo technique. This is an important consideration as DSC MRI using spin-echo techniques generally yields lower rCBV values (Sugahara et al., 2001).

Another important factor for successful multi-centre study is to standardize the post processing methods. In this study it was agreed to use the highest rCBV value of several ROI placements, as previously described by Wetzel (Wetzel et al., 2002) and to exclude large intra- and peri-tumoural vessels from the rCBV measurements (Brasil Caseiras et al., 2008).

There were differences in the definition criterion for malignant transformation. The current clinical practice at the ION is to use contrast enhancement as a criteria for transformation, which has been shown to be a more reliable indicator of malignancy in gliomas (Daumas-Duport et al., 1997; Mihara et al., 1995; Pierallini et al., 1997). At the NYUMC transformation is defined by clinical criteria and by an increase in tumour volume, but enhancement is not included as a radiological sign. For the purpose of this multi-centre study,

it was decided by senior ION and NYUMC members to adopt the NYUMC criteria of transformation. One of the reasons to exclude enhancement as an additional criterion for malignant transformation was that many of the NYUMC patients had extensive surgery at an early stage and that post operative enhancement could have been a confounding factor.

In this chapter the time to event analysis uses transformation or death as the end point, whereas in other chapters, where only data from the ION was used, time to transformation and death are analyzed separately. Despite using different criteria and end points, the results were independent from the centres and chapters 4 and 5 show consistent results regarding the potential of rCBV for differentiating patients that had an adverse from those who did not. Both chapters showed that rCBV at study entry is able to predict time to transformation or time to transformation/death.

Finally, there were differences in the treatment protocols between the two cohorts. At the NYUMC patients received either stereotactic resection or biopsy, with or without radiation therapy, as initial treatment. At the ION patients had a biopsy at study entry but only received aggressive treatment after radiological evidence of malignant transformation was diagnosed, using the enhancement criteria described above. This means that all 34 ION patients were initially treatment-free. Nevertheless, in both groups the majority patients received treatment at some point during the study (22 patients received treatment during the study at the ION and 29 patients at the NYUMC). Despite these differences in the timing of more aggressive forms of treatment, rCBV proved to be a significant and independent predictor of patient outcome in the combined data of the two centres.

The current standard reference for glioma grading is histopathology diagnosis. As mentioned before, there are several limitations, including sampling error. The triage, treatment and survival statistics of low-grade gliomas based of histopathology alone therefore, remain a challenge. Measurement of rCBV are less subject to sampling error as the entire tumour can

be assessed by DSC MRI using appropriate slice positioning. Measurements of rCBV correlate with regional tumour vascularity and expression of vascular endothelial growth factor (VGEF) (Maia et al., 2005), which represent important biological aspects that influence tumour behaviour.

The fact that rCBV measurements correlated well with time to progression or death, and that these findings can be replicated between institutions, provides an argument for the more widespread use of rCBV measurements as an adjunct to the pathology. We anticipate that DSC MRI will play an increasing role in assessing the risk of transformation in individual patients and may contribute towards a tailored approach to low-grade glioma management and treatment strategies.

5.5 Conclusion

Despite differences in the MRI equipment and therapeutic approaches between the two institutions rCBV at study entry has proved to be a useful predictor for time to transformation or death. This demonstrates the potential use for rCBV measurements in larger scale multi-centre study for low-grade gliomas. Such studies would also allow looking at the outcome of astrocytomas and oligodendrogliomas separately. In the following chapter, we will test the predictive value of rCBV measurements against other imaging parameters such as ADC and tumour volume and growth.

Chapter 6

Tumour volume and tumour growth predict outcome in patients with brain gliomas better than rCBV and ADC

6.1 Introduction

As described in chapter 4 the management of LGG remains controversial. However in a more recent study (Smith et al., 2008) it has been demonstrated that patients with low-grade glioma who underwent a at least 90% extent of resection had 5- and 8-year overall survival rates of 97% and 91% respectively. Similarly Claus et al (Claus et al., 2005) demonstrated that the 5-year age-adjusted and histologic-adjusted death rate for patients who underwent surgical resection using intraoperative MRI guidance was 17.6%. A randomised multi-centre trial [European Organization for Research and Treatment of Cancer (EORTC)] showed that early radiotherapy in adult LGG increases the median transformation-free survival but not the overall survival when compared with delayed radiotherapy (van den Bent et al., 2005).

In view of the morbidity associated with surgery and radiotherapy some centres, including ours, adopt a "watch and wait" policy in neurologically intact patients, especially with tumours in eloquent locations, and instigate aggressive therapy at the time of malignant transformation.

Magnetic Resonance Imaging (MRI) plays an important role in diagnosing malignant transformation in gliomas and imaging changes often precede clinical deterioration. On conventional MR imaging the development of areas of focal contrast-enhancement is the most commonly used sign of transformation to a high-grade glioma, in clinical practice (Mihara et al., 1995; Pierallini et al., 1997).

Conventional MRI images are also used to quantify changes in tumour size, which are most commonly obtained using linear measurements (Levin et al., 2003). A serial study of untreated oligodendrogliomas and mixed gliomas measured mean tumour diameters and demonstrated a constant growth of these tumours during the "premalignant" phase (Mandonnet et al., 2003). The same group subsequently analysed growth rates of WHO

Grade II gliomas, based on tumour diameter, and found an inverse relationship between individual growth rates and survival (Pallud et al., 2006).

As discussed in previous chapters, perfusion-weighted MR imaging has been successfully used in the investigation of brain tumours. Measurements of rCBV correlate well with histological measurements of tumour vascularity (Sugahara et al., 1999b) and presence of vascular endothelial growth factor (VGEF) (Maia et al., 2005). DSC perfusion MRI significantly improves on the specificity and sensitivity of conventional MRI in differentiating between high and low-grade gliomas (Law et al., 2003) . In chapters 4 and 5 it was demonstrated rCBV is a useful predictor of time to transformation.

Apparent diffusion coefficient (ADC) measurements have been used for glioma grading, with conflicting results (Cha, 2006). Two recent studies found pre-treatment ADC measurement in high-grade astrocytomas (WHO grade III and IV) a useful predictor of patient survival (Higano et al., 2006; Murakami et al., 2007).

The purpose of this chapter was to identify radiological markers of tumour behaviour and to determine the best predictor of patient outcome. We surmise that this will help to stratify the risk of early transformation and contribute to clinical decision making, particularly with respect to timing of aggressive forms of therapy. Therefore we compared the tumour volume, rCBV and ADC in a cohort of patients with conservatively-treated low-grade glioma as predictors of the overall patient outcome and the time to malignant transformation and to death.

6.2 Methods

6.2.1 Patients

All patients were recruited sequentially from the neuro-oncology clinic of the National Hospital for Neurology and Neurosurgery, in London. The inclusion criteria were: (i) histologically confirmed WHO grade II gliomas (Kleihues P, 2000); (ii) no previous treatment except biopsy (surgery, radiotherapy or chemotherapy) and (iii) age $\geq$ 18 years. Patients underwent conventional, perfusion and diffusion imaging at study entry, 6 months and 12 months. For the remainder of the study patients were clinically assessed and MR imaging was performed at six monthly intervals. The study was approved by the local research ethics committee and all patients provided informed consent.

6.2.2 MRI protocol

All MR data were acquired with a clinical 1.5 T system (Signa LX, GE Medical Systems, Milwaukee, WI, USA). The following images were acquired:

1) 3D Coronal Spoiled gradient echo (SPGR) sequence, as mentioned on chapter 4.

2) 2D Coronal oblique FSE fluid-attenuated inversion recovery (FLAIR) as mentioned on chapter 4.

3) Axial Dynamic susceptibility-weighted perfusion sequence, as mentioned on chapter 4.

4) Axial Diffusion-weighted images (DWI) using a single shot spin-echo EPI sequence [TE=99.5ms; TR=10000ms; 128 x 96 matrix; 26cm x 26cm FOV; slice thickness 5mm, contiguous sections]. Images were acquired at b=0 and b=1000 s mm^2 by applying the

diffusion gradients along three orthogonal axes to produce three diffusion-weighted images which were then co-added.

6.2.3 MRI analysis

1) The analyses of the pre- and post-contrast SPGR images was previously described on chapter 4.

2) FLAIR images were analysed, blinded to clinical details, on a Sun workstation (Sunblade 150, Sun Microsystems, Mountain View, CA, USA) using DispImage v. 4.9 software (Plummer, 1992). Semi-automated contouring technique was used to calculate tumour volume at each time point (Figure 6.1). The intra-rate correlation calculated on two separate measurements in 57 tumours was 0.98 (95% CI: 0.97-0.98).

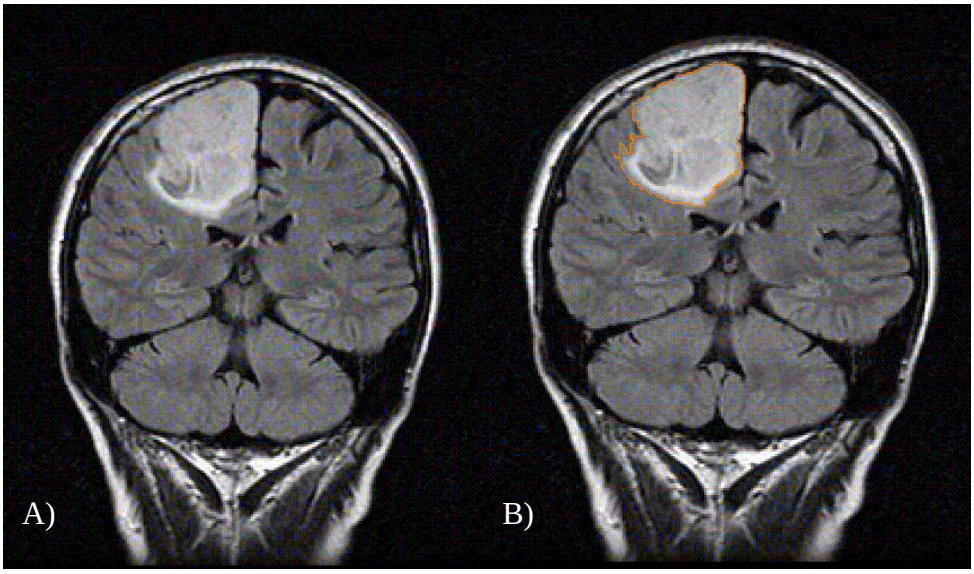

Figure 6.1: A) Coronal FLAIR image showing right frontal lobe low-grade astrocytoma. B) Semi automatic contour on DispImage for determination of tumour volume. The volume at entry study of this patient was 93.30ml.

3) The analyses of dynamic susceptibility-weighted perfusion images was previously described on chapter 4. Figure 6.2.

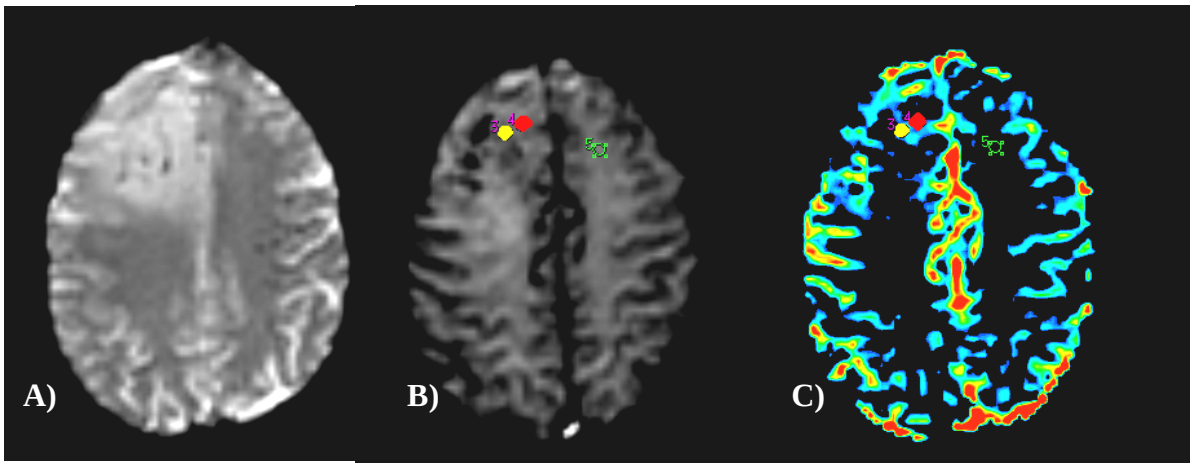

Figure 6.2: A) T2-weighted image showing a left frontal low-grade oligodendroglioma. B) T2*-weighed image during the maximum arterial and venous contrast concentration. C) rCBV map demonstrating the position of a ROI yielding maximum CBVs within the tumour (red ROI). Note that intra-tumoural vessels (yellow ROI) were avoided while placing the ROI. The mean CBV from contra-lateral white mater was used to normalize the data.

4) ADC maps were generated using commercial image processing software (Functool 1.9, General Electric Medical Systems). The tumour was contoured on each slice of the b=0 images and the saved regions were applied to the ADC map using DispImage v 4.9 software. Whole tumour ADC histograms were generated using DispImage following transfer of ADC maps onto a Sun Workstation. This method has been described in detail elsewhere (Tozer et al., 2007) (Figure 6.3). The histograms were normalized for the total number of tumour pixels and bin width. The following histogram parameters were extracted and used in the statistical analysis: peak height (PH), peak location (PL), mean value, 10th, 25th, 50th, 75th and 90th centile points.

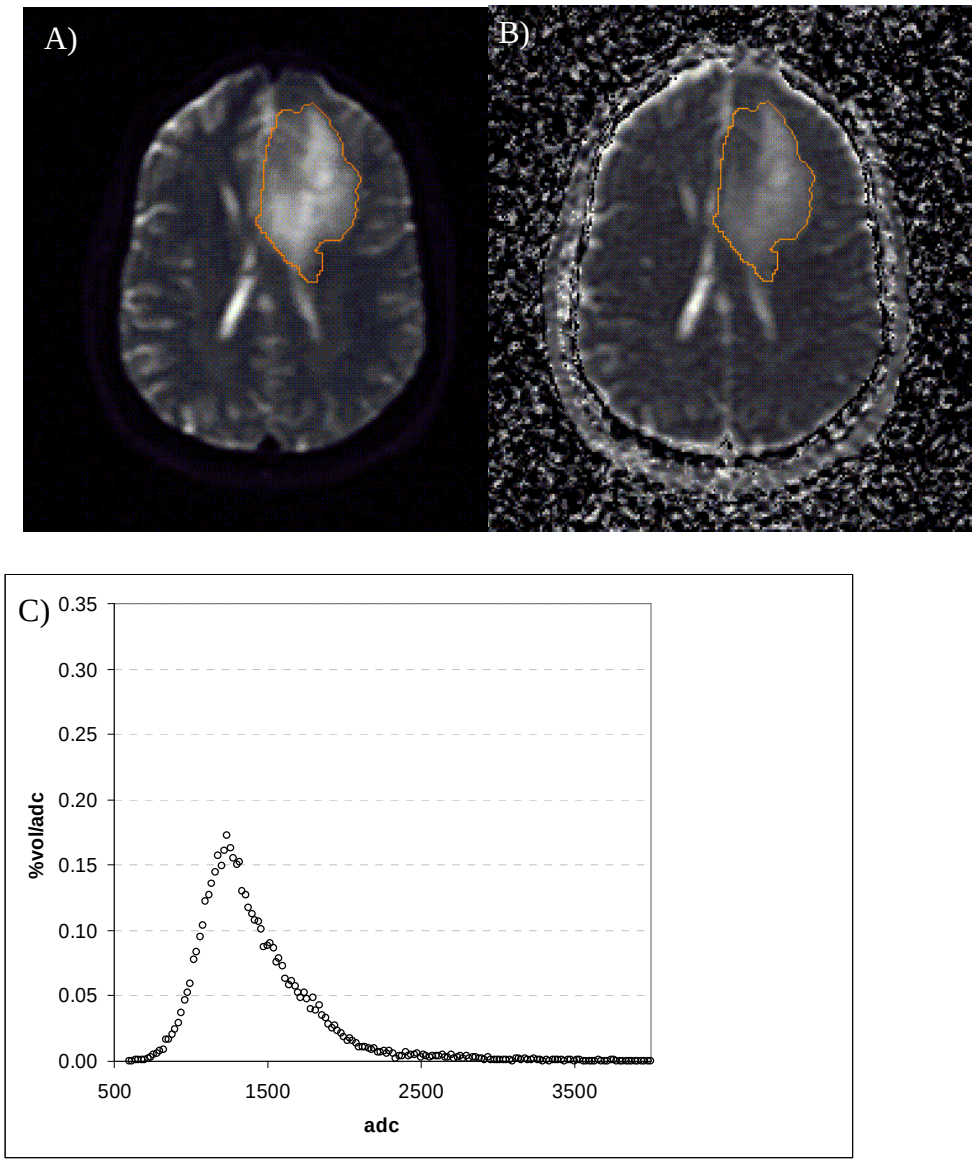

Figure 6.3. Determination of ADC histogram. Each tumour was contoured on all slices of the b=0 sequence (A) and copied into the ADC map (B). A whole tumour ADC histogram was generated from all pixels within the tumour contours (C).

6.2.4 Statistical analysis

Analysis was performed in Stata 9 (Stata Corporation, College Station, TX USA) and $p<0.05$ was considered to be significant.

1. Changes in MRI parameters over time

The Friedman test was used to analyze the distribution of tumour volume, rCBV and ADC values at study entry, 6 months and 12 months, and to assess whether there were significant changes of the mean values between these three time points.

2. Ordinal logistic regression analysis

To investigate which MRI measure (tumour volume, rCBV and ADC histogram parameters) at study entry, 6 months and 12 months was associated with patient outcome, independently from the others, and from histology, age and gender, an ordinal logistic multiple regression analysis was repeated for each time point. Firstly, predictors were modelled individually. Secondly, the significant radiological predictors were modelled together to determine the set of independent significant predictors.

The dependent variable was "patient outcome", which was classified at the last individual available follow-up visit into three categories of roughly equal sizes: 1) Stable: patients without radiological evidence of malignant transformation. These patients' MRI studies showed either no enhancement or stable enhancement of the tumour since study entry (n=12), 2) Progressive: patients with radiological evidence of malignant transformation showing one or more new areas of contrast enhancement or increase in previously stable enhancement (n=13), and 3) Death (n=11). As mentioned in previous chapters, contrast enhancement was used as criterion for transformation.

This ordinal variable was used as outcome in a multiple ordinal logistic regression in order to determine independent predictors. The following covariates were used: tumour volume, tumour rCBV, diffusion histograms parameters, histology, age and gender. Tumour histology was first divided into two groups: the first group included tumours with oligodendroglial elements (oligodendrogliomas and oligoastrocytomas; total number=14); the second group included pure astrocytomas (total number=22). Then tumour histology was also divided into three different groups: i) oligodendrogliomas (n=8), ii) astrocytomas (n=22) and iii) oligoastrocytomas (n=6).

The same analysis was then repeated to determine whether changes in tumour volume, rCBV and ADC histogram parameters between 6 months and study entry and 12 months and study entry were associated with patient outcome, independently from the other MRI changes, histology, age and gender.

3. Time to event analysis

To complete the analysis of the association between MRI parameters and outcome, we also investigated the best independent predictors of time to transformation and time to death. This analysis allowed us to check whether the predictors found to be significant in the ordinal logistic regression analysis were also predictors of time to transformation and time to death.

(i)Predictors of time to transformation

A Cox regression was used with time measured as years from study entry to transformation. Stable patients were censored at last follow-up. The covariates at each time point were: histology (including 2 tumour subtypes and 3 tumour subtypes), gender, age, tumour volume, rCBV, ADC parameters and changes of these parameters in 6 and 12 months. Firstly, predictors were modelled individually. Secondly, the significant radiological predictors were

modelled together to determine the set of independent significant predictors. Treatment was not added to the model because patients were treatment free until transformation was reached. We performed a subgroup analysis using only astrocytic tumours which represent 61% of our cohort and of tumours with oligodendroglial elements, which represent 39% of our cohort.

(ii)Predictors of time to death

The same analyses were repeated with time as years from study entry to death. However on this analysis, the presence of treatment was added to the model as a covariate. Patients alive at the time of latest follow-up were censored at that time.

Kaplan Meier curves for the strongest predictors

Kaplan Meier curves were produced for the strongest predictors of time to transformation and of time to death.

A receiver operating characteristic (ROC) analysis was applied to assess which variable cut-off at study entry and at short-term changes had the highest accuracy of prediction to allow the differentiation between patients who progressed to high-grade gliomas and those who did not, and between alive and dead patients, respectively. Kaplan Meier survival curves and log-rank test were then applied to compare the time to transformation and time to death in the two groups of patients defined by the cut-off. Differences between the two groups defined were tested using the log-rank test.

6.3 Results

Patients

Demographic data are shown in Table 6.1.

Thirty-six patients (mean age: 42; SD 12.8 ; 24 males and 12 females) with histology proven WHO grade II gliomas (22 astrocytomas, 8 oligodendrogliomas and 6 oligoastrocytomas) were studied for a median total follow-up length of 2.9 years (range 0.4 – 5.5). All 36 patients had MRI studies at 6 months after study entry, while 4 (11%) patients failed to attend the 12 months scan (1 patient died, 1 patient went abroad for treatment, and 2 patients clinically progressed and dropped out).

Twelve out of 36 patients (33.3%) remained stable during the follow-up, while 13 patients (36.1%) progressed and 11 (30.5%) died. All deaths were related to tumour progression. The median length of follow-up was 2.4 years for the stable (range: 0.4 – 5.3 years) and 2.0 years for the progressive group of patients (range: 0.5 – 5.5 years). Patients who died were radiologically followed-up for a median of 2.0 years (range: 0.5 – 3 years), but were clinically studied for longer (median 3.9 years; range 1- 4.8).

Patients did not receive any treatment until malignant transformation. Twenty-two out of 36 patients (61%) received treatment during the study, which included surgery in 9 patients, radiotherapy in 16 patients and chemotherapy in 8 cases. The median time from study entry to treatment was 2.4 years (range: 0.6 – 5.5). Only 2 patients received treatment within the first year of the study, but both cases were treatment-free at study entry and 6 months; no further MRI data were available after the first 6 months in these 2 cases.

Table 6.1. Demographic data and MRI parameters at study entry for all patients

PATIENT ID, AGE AND GENDER			HISTOLOGY	VOLUME IN ML AT SE	RCBV	MEDIAN ADC	OUTCOME	YEARS OF FOLLOW UP
1	30	F	O	45.6	2.02	1131.5	P	3.1
2	51	M	A	93.3	2.46	1215.5	P	0.5
3	30	M	A	83.4	2.00	1480.5	D	4.8
4	57	M	O	132.2	1.94	1205.5	P	3.6
5	25	M	OA	84.6	1.28	1149.5	D	1.6
6	37	M	A	77.1	0.99	1289.5	P	5.6
7	30	M	A	77.0	0.94	1749.5	S	0.4
8	56	M	O	72.0	2.53	1229.5	P	4.6
9	38	M	A	73.9	na	1400.5	P	3.8
10	48	M	OA	83.1	1.26	1450.5	D	3.0
11	56	M	A	84.2	1.04	1169.5	D	2.9
12	42	F	OA	101.0	1.91	1342.5	D	3.8
13	58	M	A	169.3	2.24	1122.5	D	1.0
14	29	F	A	59.0	2.38	1674.5	D	4.2
15	41	M	A	136.9	1.04	2013.5	D	2.2
16	34	M	A	58.7	1.56	1643.5	P	1.9
17	47	F	A	75.0	1.09	1466.5	D	4.8
18	28	F	O	24.4	2.81	978.5	P	1.2
19	35	M	A	64.8	0.91	1669.5	D	4.2
20	65	F	OA	92.3	1.28	1649.5	P	4.0
21	30	M	A	106.7	1.91	1504.5	D	4.1
22	24	M	O	44.6	1.59	1241.5	P	2.0
23	52	M	A	40.4	1.37	1151.5	P	1.7
24	53	F	O	94.9	1.84	1569.5	P	2.1
25	37	F	OA	105.4	na	1369.5	S	1.5
26	63	F	O	38.9	1.47	1322.5	S	3.5
27	36	M	O	71.6	3.51	1291.5	P	1.3
28	60	F	A	47.5	1.14	1307.5	S	1.1
29	38	M	A	79.1	0.80	1491.5	S	2.0
30	69	M	OA	37.4	1.94	1169.5	S	5.3
31	29	F	A	43.8	1.18	1767.5	S	2.7
32	32	M	A	20.1	1.61	1256.5	S	2.4
33	57	F	A	72.3	1.49	1275.5	S	4.3
34	32	M	A	42.9	1.42	1843.5	S	1.6
35	39	M	A	30.8	1.79	1364.5	S	0.6
36	29	M	A	66.0	0.70	1724.5	S	3.7

SE: study entry, F: female, M: male, A: astrocytoma, O: oligodendroglioma, OA: oligoastrocytoma, na: not available due to technical problems, S: stable, P: progressive, D: death.

1. Changes in MRI parameters over time

There were significant changes in the mean values of the tumour volume between study entry, 6 months and 12 months and in the mean values of rCBV between these time points (all p values were < 0.001). There were significant changes in the mean values of tumour growth in 6 and 12 months ($p<0.001$) and in the mean values of changes in rCBV in 6 and 12 months ($p=0.034$). The whole tumour ADC histogram parameters did not show any significant change between time points.

The mean values and standard deviation of tumour volume, rCBV and ADC for each time point and the change of these parameters within the first 6 and 12 months after study entry are given in Table 6.2. The mean values and standard deviation of ADC parameters for each time point and the change of these parameters within the first 6 and 12 months after study entry are given in Table 6.3.

Table 6.2. Mean, standard deviation, median and range values of tumour volume, maximum rCBV and ADC 50th centile, at each time point and of tumour growth within the first 6 and 12 months.

TIME POINT / CHANGES BETWEEN TIME POINTS	**VOLUME MEAN (SD)**	**VOLUME MEDIAN (RANGE)**	**MAX. RCBV MEAN (SD)**	**MAX. RCBV MEDIAN (RANGE)**	**ADC 50TH ($X10^{-6}$ MM^2S^{-1}) CENTILE MEAN (SD)**	**ADC 50TH ($X10^{-6}$ MM^2S^{-1}) CENTILE MEDIAN (RANGE)**
At study entry (SE)	73.06 (32.32)	73.11 (20.11-169.31)	1.63 (0.63)	1.53 (0.70-3.51)	1407.86 (240.72)	1353.50 (978.50-2013.50)
At 6 months	81.82 (35.15)	81.94 (21.96-186.77)	2.22 (0.79)	2.03 (1.24-4.62)	1387.44 (258.94)	1319.50 (978.50-2013.50)
Change between SE and 6 months	8.76 (7.06)	9.18 (-11.88-23.36)	0.47 (0.36)	0.34 (0.08-1.81)	-5.47 (74.67)	00 (-246-180)
Change between SE and 12 months	2.69 (3.68)	1.62 (00-19.56)	0.89 (0.87)	0.71 (-0.94 -4.39)	-0.84 (80.63)	00 (-221 – 257)

SE: study entry; SD: standard deviation; N: number of subjects

Mean and median values of volume are given in millilitres.

Table 6.3: Mean, standard deviation, median and range values of ADC parameters, at each time point.

ADC parameters at each time point	Mean	Std Deviation	Median	Minimum	Maximum
Study entry ph	.04	.01	.04	.02	.06
Study entry pl	1327.31	429.09	1334.00	9.50	2113.50
Study entry mean*	1401.77	212.03	1370.47	1016.45	1885.33
Study entry 10^{th} centile*	1051.19	170.32	1045.00	689.50	1384.50
Study entry 25^{th} centile*	1216.75	202.53	1171.50	818.50	1673.50
Study entry 50^{th} centile*	1407.86	240.72	1353.50	978.50	2013.50
Study entry 75^{th} centile*	1593.97	256.58	1596.00	1158.50	2173.50
Study entry 90^{th} centile*	1798.42	308.75	1778.00	1318.50	2629.50
6 months ph	.04	.01	.04	.02	.06
6 months pl	1388.62	305.53	1297.50	995.50	2113.50
6 months mean*	1394.73	227.63	1355.17	1016.45	1882.92
6 months 10^{th} centile*	1052.15	180.70	1003.00	718.50	1529.50
6 months 25^{th} centile*	1209.79	223.78	1154.00	818.50	1749.50
6 months 50^{th} centile*	1387.44	258.94	1319.50	978.50	2013.50
6 months 75^{th} centile*	1561.56	262.99	1536.00	1155.50	2173.50
6 months 90^{th} centile*	1740.38	265.40	1733.50	1318.50	2333.50
12 months ph	.036	.010	.035	.021	.068
12 months pl	1384.88	307.63	1366.00	879.50	2113.50
12 months mean*	1411.08	214.87	1391.89	1003.23	1885.33
12 months 10^{th} centile*	1051.75	155.81	1035.00	709.50	1386.50
12 months 25^{th} centile*	1214.88	205.09	1174.00	829.50	1673.50
12 months 50^{th} centile*	1402.38	249.55	1344.00	989.50	2013.50
12 months 75^{th} centile*	1589.25	256.77	1571.00	1149.50	2173.50
12 months 90^{th} centile*	1778.63	252.19	1782.50	1309.50	2333.50

* ($x10^{-6}$ mm^2s^{-1}); ph: peak height; pl: peak location.

2. Ordinal logistic regression analysis

Tumour volume obtained at study entry, 6 months and 12 months significantly predicted patient outcome, better than, and independently from, rCBV, ADC values, histology, age and gender. In particular, the tumour volume showed a significant association with patient outcome, with an odds ratio of being in a more severe outcome category of 3.15 [Standard Deviation (SD): 32.32, 95% Confidence Interval (CI) (1.42 - 7.00), p=0.005] at study entry (Figure 5.4), 4.47 (SD: 35.14, 95% CI: 1.77 – 11.24, p=0.001) at six months and 9.48 (SD: 58.39, 95% CI: 2.00 – 44.93, p=0.005) at twelve months, for each additional SD of tumour volume (Table 6.4). In contrast, neither rCBV nor ADC values were associated with outcome at any time point (all p values > 0.05).

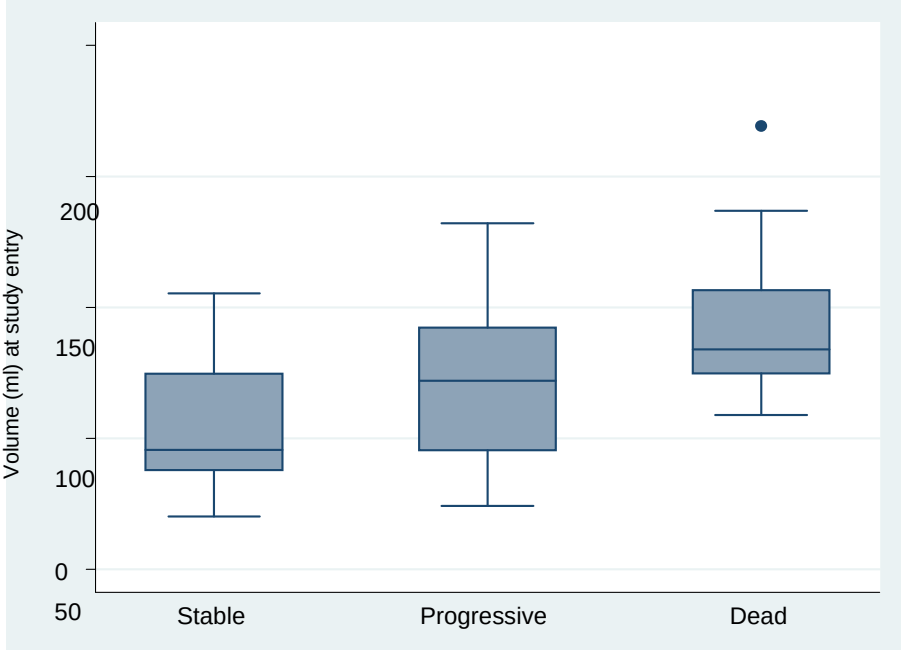

Figure 6.4. Graph showing association between tumour volume at study entry (ml) and outcome categories.

Changes in tumour volume between study entry and 6 months and between study entry and 12 months were also significantly associated with patient outcome, independent of short-term changes in rCBV and, of histology, age and gender ($p=0.001$ and $p=0.004$ respectively). The odds ratio of being in a more severe outcome category was 6.68 (SD: 7.05, 95% CI: 2.26-19.70) for each SD of tumour growth over the first 6 months and 93.24 (SD: 3.67, 95% CI: 4.13-2101.05) for each SD of tumour growth over the first 12 months. Table 6.4.

Changes in rCBV and ADC during the first 6 and 12 months did not predict patient outcome.

Table 6.4: Results from the ordinal logistic regression showing the ability of tumour volume in predicting patients' outcome at each time point.

TIME POINT	ODDS RATIO	SD	CONFIDENCE INTERVAL	P VALUE
Volume at Study Entry	3.15	32.32	1.42-7.00	0.005
Volume at 6 Months	4.47	35.14	1.77-11.24	0.001
Volume at 12 Months	9.48	58.39	2.00 – 44.93	0.005
Changes in volume within 6 months	6.68	7.05	2.26 – 19.70	0.001
Changes in volume within 12 months	93.24	3.67	4.13 – 2101.05	0.004

SD: standard deviation; n: number of subjects

3. Time to event analysis

(i) Predictors of time to transformation

a) Using variables at study entry

We found that tumour volume and rCBV were both independent predictors of time to transformation at study entry. The risk of transforming during follow up was 2.39 higher per each additional SD of tumour volume at study entry (95% CI 1.36-4.20, p = 0.002, SD: 32.32) and 1.66 higher per each additional SD of rCBV at study entry (95% CI: 1.06 – 2.61, p = 0.02, SD: 0.62). (Table 6.5).These results were independent of the other covariates in the model: histology, gender, and age. ADC histogram measures were not significantly associated with time to transformation.

Even when only astrocytomas were analyzed, tumour volume and rCBV at study entry were still predictors of time to transformation. The risk of transforming during follow up was 2.48 higher per additional SD of tumour volume at study entry (95% CI 1.29 – 4.76, p= 0.006, SD: 33.64) and 4.23 higher per each additional SD of rCBV at study entry (95% CI 1.67-10.72, p = 0.002, SD: 0.52).

b) Using variables at 6 months

A Cox regression analysis using all parameters available at 6 months (including the study entry data) showed that changes in tumour volume over 6 months was the only independent predictor of time to transformation: the risk of transforming during the study was 3.25 higher per each additional SD of tumour growth within 6 months (95% CI: 1.62 – 6.49, p value = 0.001, SD: 7.05).

c) Using variables at 12 months

Tumour volume and changes in tumour volume between study entry and 12 months were the only independent predictors of time to transformation at 12 months follow up. The risk of transforming during the study was 4.73 higher per each additional SD of tumour volume at 12 months (95% CI: 1.15 – 19.41, p = 0.03, SD: 58.39). The risk of transforming during the study was 2.48 higher per each additional SD of tumour growth within 12 months (95% CI: 1.35 – 4.56, p = 0.03, SD: 3.67) (Table 6.5.).

Table 6.5: Predictors of time to transformation

TIME POINT	PREDICTOR	ODDS RATIO	SD	CI	P VALUE
Study entry	Tumour volume	2.39	32.32	1.36 - 4.20	0.002
	rCBV	1.66	0.62	1.06 - 2.61	0.02
6 months*	Changes in tumour volume	3.25	7.05	1.62 - 6.49	0.01
12 months	Tumour volume	4.73	58.39	1.15 - 19.41	0.03
	Changes in tumour volume	2.48	3.67	1.35 - 4.56	0.03

SD: standard deviation; CI: confidence interval; n: number of subjects when all parameters are present.

* A Cox regression analysis using all parameters available at 6 months (including the study entry data) showed that changes in tumour volume within 6 months, rather than volume and rCBV at study entry, was the only independent predictor of time to transformation.

(ii) Predictors of time to death

a) Using variables at study entry

Tumour volume at study entry was the only independent predictor of time to death: the risk of dying at any time of the study was 5.54 per each additional SD of tumour volume at study entry (95% CI: 1.79 – 17.12, p value = 0.003, SD: 32.32) (Table 6.6).

b) Using variables at 6 months

Tumour volume and changes in tumour volume between study entry and 6 months were the only independent predictors of time to death at 6 months follow up. The risk of dying at any time of the study was 4.31 per each additional SD of tumour volume at study entry (95% CI: 1.75 – 10.59), p value = 0.001, SD: 32.32. The risk of dying at any time of the study was 2.46 per each additional SD of tumour growth within 6 months (95% CI: 1.11 – 5.42, p value = 0.02, SD: 7.05) (Table 6.6).

c) Using variables at 12 months

Tumour volume and changes in tumour volume between study entry and 12 months were the only independent predictors of time to death at 12 months follow up. The risk of dying at any time of the study was 6.81 per each additional SD of tumour volume at study entry (95% CI: 2.08 – 22.62, p value = 0.002, SD: 58.39). The risk of dying at any time of the study was 2.80 per each additional SD of tumour growth within 12 months (95% CI: 1.35-5.79, p value = 0.005, SD: 3.67) (Table 6.6).

Table 6.6. Predictors of time to death

TIME POINT	PREDICTOR	ODDS RATIO	SD	CI	P VALUE
Study Entry	Tumour volume	4.31	32.32	1.75 – 10.59	0.001
6 months	Tumour volume	4.51	35.14	1.81 – 11.22	0.002
	Changes in tumour volume	2.46	7.05	1.11-5.42	0.02
12 months	Tumour volume	6.81	58.39	2.08 – 22.62	0.002
	Changes in tumour volume	2.80	3.67	1.35 – 5.79	0.005

SD: standard deviation; CI: confidence interval.

Kaplan Meier curves for the strongest predictors

As tumour growth within the first 6 months and tumour volume at study entry were the best independent predictors of time to transformation and to death, respectively, they were entered in the analysis with the ROC curve.

a) Strongest predictor of time to transformation

This analysis showed that the tumour growth in the first 6 months was associated with the highest accuracy of prediction of time to transformation was 6.21ml (sensitivity: 83.3%; specificity: 83.3%; correctly classified: 83.3%). Using this value as a cut-off, we found a significant difference in time to transformation between patients with tumour growth smaller than 6.21ml and those with tumour volume equal or above this cut-off ($p = 0.003$) (Figure 6.5). Mean time to transformation was 3.91 years (95% CI: 2.81 - 5.02) for patients with tumour growth within 6 months less than 6.21 ml compared with 1.84 years (95% CI: 1.44 – 2.24) for patients with tumour growth greater than or equal to 6.21 ml.

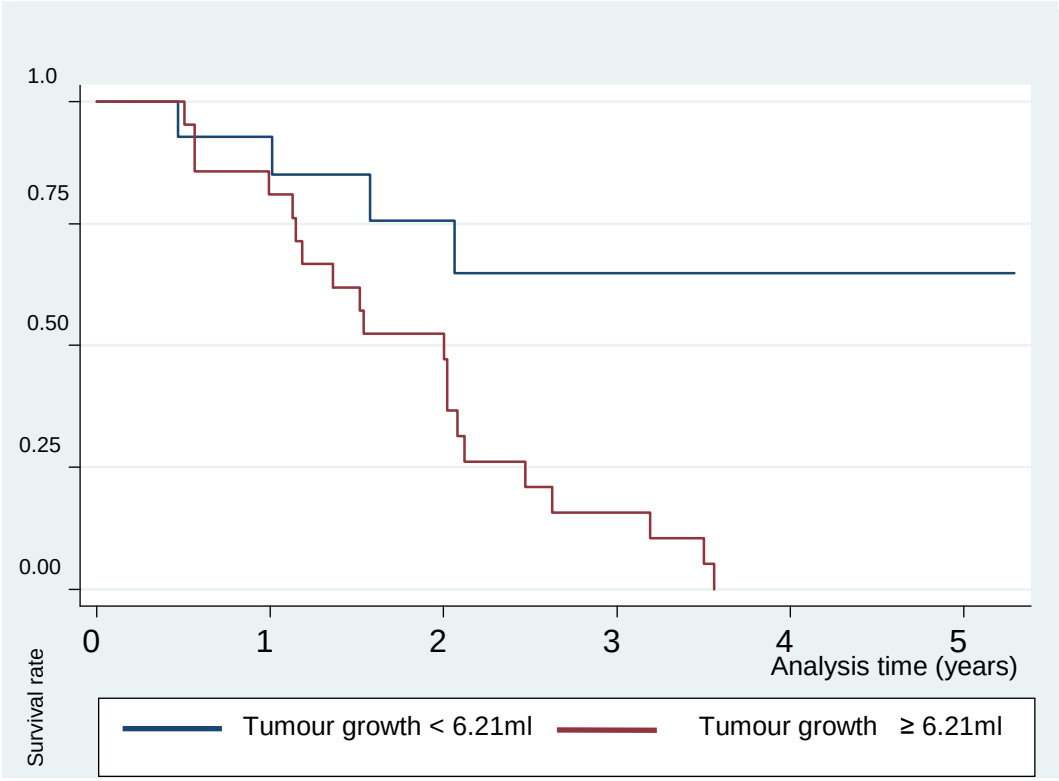

Figure 6.5. Graph showing comparison of time to progression between groups with small (< 6.21 ml) and large (≥ 6.21 ml) tumour growth within 6 months. Patients with small tumour growth mean time to progression of 3.91 years (blue curve), whereas patients with large tumour growth had a mean time to progression of 1.84 years (red curve). Note that, after 3 years of follow up, all patients with large tumour growth had transformed, whereas almost 60% of patients with small tumour growth did not transform.

b) Strongest predictor of time to death

A ROC curve showed that the tumour volume associated with the highest accuracy of prediction of time to death was 83.14ml (sensitivity: 66.67%; specificity: 79.17%; correctly classified: 75%). Using this value as a cut-off, we found a significant difference in survival between patients with tumour volume smaller than 83.14ml and those with tumour volume equal or above this cut-off ($p = 0.0016$) (Figure 6.6). Mean survival time was 5 years (95% CI: 4.52 – 5.48) for patients with tumour volumes at study entry less than 83.14 ml compared with 3.27 years (95% CI: 2.49 - 4.05) for patients with tumour volumes greater than or equal to 83.14 ml.

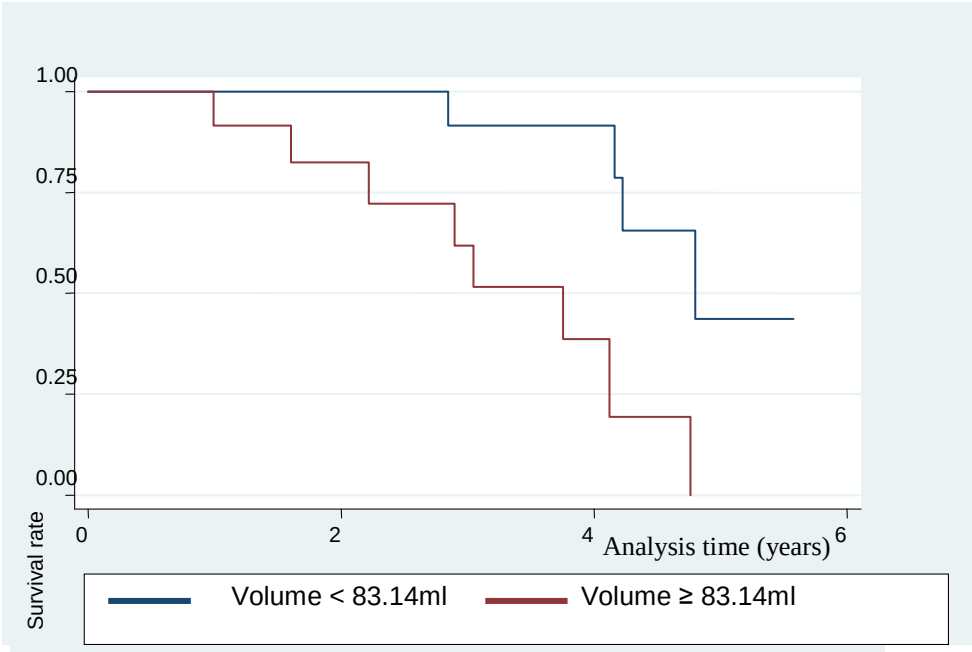

Figure 6.6. Graph showing comparison of survival between groups with small (< 83.14ml) and large (≥ 83.14ml) tumour volumes at study entry. Patients with small tumour volumes had a median survival time of 5 years (blue curve), whereas patients with large tumour volume had a median survival time of 3.27 years (red curve). Note that, after almost 5 years of follow up, all patients with large tumour volume would probably be dead, whereas more than 40% of patients with small tumour volume would still be alive.

6.4 Discussion

We have, for the first time, investigated tumour volume, rCBV and ADC histogram parameters in a longitudinal study of patients with conservatively treated low-grade gliomas to determine the best MRI predictor of outcome. Previous retrospective studies have explored tumour volume (Mariani et al., 2004) and tumour growth (Dempsey et al., 2005; Mariani et al., 2004; Pallud et al., 2006) as individual predictors of outcome and/or survival in patients with brain gliomas. However, the novelty of the work presented in this chapter lies in the prospective comparison of several MR variables as predictors of outcome.

We found that tumour volume at study entry and tumour growth were the strongest predictors of patient outcome, which was assessed using 3 categories (i.e. stable, progression and death). These parameters remained significant when adjusting for the other MRI variables, histology, age, gender and treatment. Furthermore when performing a time to event analysis, tumour growth in the first 6 months was the best independent predictor of time to transformation and tumour volume at study entry was the only independent predictor of time to death.

Our results are broadly in keeping with previous studies investigating tumour volume and growth in low-grade gliomas. Mariani (Mariani et al., 2004) performed a retrospective study of tumour volume over a 9-year-period and found preoperative tumour volume to be the strongest predictor of overall survival. They also stated that tumour volume was the only predictor of malignant transformation. However oligodendrogliomas were not included and all patients were treated surgically prior to malignant transformation.

Pallud et al (Pallud et al., 2006) found an inverse correlation between individual growth rates of low-grade gliomas and patient survival. Tumours with a median growth rate below 8mm/year had a much better prognosis than tumours with higher growth rates. This was a large study (143 patients), but was retrospective, spanning a 12-year-period, with a large

variation of the time interval between successive MRI studies ranging from 3 to 219.3 months (mean, 33.4 months). In contrast to our study, there was a heavy bias towards oligodendrogliomas, which accounted for two thirds of tumours studied, perhaps reflecting local differences in neuropathological criteria. In addition, measurements were based on maximum tumour diameters in three planes rather than true volumetric calculations and some patients had surgery before malignant transformation.

Based on our time to death analysis, it can be predicted that patients with a tumour volume exceeding 83.14 ml are likely to die within 5 years of presentation. Other studies have shown different survival rates. The EORTC work (van den Bent et al., 2005) demonstrated that the median survival for patients who received radiotherapy was 7.4 years compared with 7.2 years for patients who did not receive radiotherapy. It has also been demonstrated that WHO grade II gliomas survival rate is around 8 years (Claus et al., 2005; Smith et al., 2008). This could be attributed to the fact that in all these studies patients with low grade glioma received surgery after the diagnosis, whereas our patients were treatment free until they progressed to high-grade gliomas and only 25% underwent surgery during the study.

Despite the fact that oligodendrogliomas have been reported to have a better outcome than astrocytomas (van den Bent, 2007), we found that predictors of patient outcome, time to transformation and time to death were independent not only from gender and age but also from histology. One explanation could be the small number of pure oligodendrogliomas in our cohort (n=8). However if *all tumours* with oligodendroglial elements are taken into account, they represent 39% of the cohort, making the group roughly balanced with pure astrocytomas.

As mentioned in previous chapters, parameters derived from physiological MR imaging such as rCBV and ADC measurements provide additional information about tumour behaviour,

which goes beyond morphological aspects. In this chapter, we found that rCBV at study entry is a predictor of time to transformation, but not as strong as tumour growth.

In our cohort 9 of 12 stable patients had low-grade astrocytomas. As it is known that this tumour subtype have lower rCBV compared to oligodendrogliomas (Cha et al., 2005), another Cox regression was used to investigate if rCBV remained a predictor of time to transformation when only astrocytomas were considered. The results confirmed the potential of rCBV in predicting time to transformation in the subgroup of purely astrocytic tumours.

As it was discussed in chapter 4, Law and colleagues (Law et al., 2006a) demonstrated a significant negative correlation between rCBV and time to progression in a patient cohort which differed from ours in several respects, previously mentioned. Law et al did, however, not compare rCBV with ADC and tumour growth or tumour volume at study entry. Using a Cox regression survival model we were able to demonstrate that tumour growth within 6 months was in fact a stronger predictor for time to progression than rCBV. In addition, rCBV was not a predictor of time to death or of patient outcome in the ordinal logistic multiple regression analysis, when compared with other variables. In an earlier study Lev et al showed a correlation of normalized CBV with survival, but this became non-significant once age and histological grade were added to the model (Lev et al., 2004).

A recent MR perfusion study of low-grade gliomas, showed that rCBV increases significantly within 12 months prior to malignant transformation (Danchaivijitr et al., 2008), which might reflect neo-angiogenesis in low-grade gliomas that are evolving to a higher grade. It may be that the predictive value of rCBV measurements for patient outcome increases nearer the time of transformation, but this will have to be confirmed with further studies.

With respect to the ADC measurements, we did not find significant changes over time within one year. This is not entirely unexpected as measurement of ADC has been, on the whole, less promising than rCBV measurements (Cha, 2006) in differentiating between low- and

high-grade tumours. ADC parameters at each time point and changes in ADC between study entry and 6 months and between study entry and 12 months did not predict patient outcome neither time to transformation or time to death. This is in contrast with a retrospective study (Higano et al., 2006). The author showed that pre-operative ADC measurements were able to predict the prognosis of anaplastic astrocytomas and glioblastomas. Tumours with a minimum ADC above 0.90 x 10^{-3} mm^2 sec^{-1} had a better prognosis than those with lower ADC values. However, this study used manual ROI placement over solid tumour portions to identify the lowest intratumoural ADC values, which is more operator-dependent than the histogram analysis we used. It also included paediatric patients, who usually have a better prognosis (Chandler et al., 1993; Devaux BC, 1993; Salcman et al., 1994).

Methodological considerations

In this thesis, tumour volume was calculated, rather than using linear measurements of tumour size. Dempsey et al (Dempsey et al., 2005) had compared volumetric, bidimensional, and unidimensional measurements of tumour size in 70 patients with recurrent malignant glioma and showed that only the volumetric measurement was found to be predictive of survival in patients with brain gliomas. Additionally other studies which compared linear tumour measurements with clinical outcome yielded inconsistent findings (Chow et al., 2000; Reeves and Marks, 1979; Wood et al., 1988).

We have chosen to outline the tumour volume on FLAIR images, as these have been demonstrated to be more sensitive to subtle glioma tumour volume change than T2 WI (Connor et al., 2004). For our volume measurements, we used the coronal FLAIR images with an interslice gap of 1.5mm. Although this might lead to less precise measurements than

contiguous slices, the tumour volumes were big enough to consider the possible effect of partial volume to be negligible.

In accordance with our current clinical practise, we used contrast enhancement as radiological criterion for transformation since it had proved to be a more reliable indicator of malignancy in gliomas than border definition, mass effect, necrosis and haemorrhage (Daumas-Duport et al., 1997; Mihara et al., 1995; Pierallini et al., 1997).

Our patient cohort included a mixture of low-grade astrocytomas, oligoastrocytomas and oligodendrogliomas, which is representative of the typical mix of histological subtypes seen in neuro-oncological practice. The documented differences in rCBV and ADC values between low-grade oligodendrogliomas and low-grade astrocytic tumours may be a confounding factor when analyzing the predictive value of these parameters in a mixed group. Low-grade oligodendrogliomas tend to have higher rCBV values (Cha et al., 2005) and lower ADC values (Tozer et al., 2007) than low-grade astrocytic tumours. However when only low-grade astrocytomas were analyzed, we demonstrated that rCBV at study entry proved to be a predictor of time to transformation. It may be useful in future to look at the predictive value of rCBV and ADC in astrocytomas and oligodendrogliomas separately in a larger patient cohort.

Of the statistical methods used, the time to transformation and death analysis are more powerful at detecting associations between early predictor variables and outcome than the logistic regression. The logistic regression analysis provides information about the likelihood of patient status after a fixed time interval: although this is a simpler form of analysis, it can be easier to interpret and apply in a clinical setting, when a likely outcome may be more important than its timing. Another statistical consideration regards the determination of the

thresholds for our time-to-event analyses (time to progression and time-to death). The thresholds of tumour volume and tumour growth were obtained with the ROC analysis and were based on the highest accuracy of prediction. However, a confidence interval was not available, as is usually the case when working with ROC analysis. Although the cut-off acquired was the most successful threshold in our cohort, it is worth cautioning that the exact optimal threshold determined from the ROC analysis for our dataset may not be generalized to a different population. Whilst we would expect comparable datasets to show similar prediction, slightly different cut-off thresholds are likely to be obtained. Further studies are required to investigate an optimal binary threshold which may be used in daily clinical practice.

6.5 Conclusion

This chapter shows the result of an original prospective study which compares tumour volume with other variables presented in previous chapters (rCBV and ADC) in order to find the best predictor of outcome in patients with low-grade glioma. After using different statistics tests, tumour volume was not only associated with outcome, but also tumour growth within 6 months was the best independent predictor of time to transformation and tumour volume at study entry was the only independent predictor of time to death. Acquisition and calculation of tumour volumes can easily performed with standard MRI equipment. The incorporation of tumour volume measurements into the diagnostic work-up of patients with brain gliomas may prove a useful adjunct in clinical decision making and could influence the timing of aggressive treatment.

Conclusions

The aim of this thesis was to apply conventional, perfusion- and diffusion-weighted MR imaging in patients with histology proven low-grade gliomas in order to provide further insights into the biological behaviour these brain tumours, which could influence their clinical management.

After comprehensive work using the analysis of rCBV, ADC and conventional MRI in a unique cohort, I have been able to show how these techniques can contribute to the understanding of the natural history of low-grade gliomas.

Although ADC is able to differentiate oligodendrogliomas from astrocytomas (Tozer et al., 2007) and is useful in the grading of gliomas (Sugahara et al., 1999a), ADC histogram parameters were not able to demonstrate an association with patient outcome or with time transformation or death. Further studies with bigger cohorts will be needed to verify the utility of ADC as a predictor of outcome.

However, rCBV proved to be an important tool in the study of gliomas. Relative CBV is not only associated with transformation but it is also able to predict time to malignant transformation in our centre and also in a multi-centre cohort.

When ADC, rCBV and tumour growth and volume were compared in order to find the best MR predictor of patient outcome in patients with low-grade glioma, tumour volume and tumour growth at different time points were stronger predictors than rCBV and ADC and also independent of age, gender, histology and treatment. When a time to event analysis was used comparing tumour volume, tumour growth, rCBV and ADC, tumour growth proved to be the best independent predictor of time to transformation and tumour volume was the only independent predictor of time to death.

These original results make an important contribution for the management of patients with brain gliomas and provide additional information which may help early decision making in clinical practice.

In the National Hospital for Neurology and Neurosurgery patients with low-grade glioma are only treated once malignant transformation is diagnosed. However our survival and time to transformation is much shorter than the ones described in the literature. This work lead clinicians in this institution to question whether or not patients with brain glioma that had tumours volume at study entry bigger than 83.14ml and / or a tumour growth of 6.21ml in the first 6 months should be regarded as high grade tumours. It may be appropriate that these patients are managed more aggressively.

Future directions

Previous chapters demonstrated the importance of MRI parameters in understanding the natural history and predicting prognosis in patients with brain gliomas. There is scope for further work, whereby rCBV and ADC may be used to improve the diagnosis and treatment of these patients.

The acquisition of rCBV using DSC MRI remains somewhat subjective with inter and intra observer variability. Young and al (Young et al., 2007) also demonstrated that histogram analysis of perfusion MR provides prediction of glioma grade. Law et al (Law et al., 2007) showed that rCBV acquired using histogram analysis is as effective as rCBVmax in the correlation of glioma grade. The histogram method simplifies the analysis and may allow inexperienced operators to obtain reproducible data. It would be interesting to implement this method for future acquisitions of rCBV.

There is a need to provide imaging markers for treatment response in patients with brain gliomas. Chenevert et al (Chenevert et al., 2000) showed that increased diffusion values could be detected in human brain tumours shortly after treatment initiation. Another study has demonstrated that regions within the 80% isodose of radiotherapy showed a reduction in rCBV over a 3 month period (Price et al., 2007). Perfusion-weighted MRI allows in vivo imaging of the overall tumour vascularity and an indirect assessment of tumour angiogenesis, which is an essential indicator for tumour classification and determination of biological aggressiveness (Cha et al., 2002). Additionally, diffusion-weighted MRI reflects pathologic features, such as changes in cellularity (Provenzale et al., 2006), which is present as the tumour progresses. In summary rCBV and ADC could be used as potential markers for treatment response. Changes in treatments could be made if certain imaging markers have not

changed over a period of time. It would be reassuring to know that effective treatment is mirrored by significant changes in MRI markers.

Another important application of these techniques is differentiation of radiation necrosis from tumour recurrence in patients with primary and secondary brain tumours.

Differentiation between tumour recurrence and treatment-related brain injury is often difficult with conventional MRI. It is unclear whether a previously reported increase of contrast material uptake in patients with irradiated primary and secondary tumours are transient due to the radiation itself or is due to tumour progression or necrosis. Diffusion-weighted imaging appears helpful because water diffusion is greater in necrotic tumours than in tumour tissues in recurrence. It has been demonstrated that there are significant differences in the maximal ADC values between radiation necrosis and tumour recurrence (Asao et al., 2005). It has also been shown that there is a dose-related reduction in rCBV in normal brain after radiotherapy (Price et al., 2007) and that rCBV is able to predict patient outcome and monitor radiation-induced effects (Fuss et al., 2001; Fuss et al., 2000). However the best marker for differentiating radiation necrosis from tumour progression remains unclear. A long radiological follow up would be needed as patients with a single brain metastasis have a median survival in the range of 10–18 months (Melisko et al., 2008) and that treated low-grade glioma have 5-year survival rate of 97% (Smith et al., 2008) .

Finally, the use of diffusion tensor imaging (DTI) would be extremely beneficial to plan surgical treatment in these patients. DTI is able to identify subtle white matter disruptions (Price et al., 2003) and also delineate margins in glioma (Price et al., 2006). Such techniques can improve the delineation of surgery resection and also in planning radiotherapy treatment. Ideally this sequence would be used in the neuronavigation system improving the respectability of brain tumours.

References

Abdulrauf SI, Edvardsen K, Ho KL, Yang XY, Rock JP, Rosenblum ML. Vascular endothelial growth factor expression and vascular density as prognostic markers of survival in patients with low-grade astrocytoma. J Neurosurg 1998; 88: 513-20.

Aronen HJ, Gazit IA, Louis DN, Buchbinder BR, Pardoe FS, Weisskoff RM, et al. Cerebral blood volume maps of gliomas: comparison with tumour grade and histologic findings. Radiology 1994; 191: 41-45.

Asao C, Korogi Y, Kitajima M, Hirai T, Baba Y, Makino K, et al. Diffusion-weighted imaging of radiation-induced brain injury for differentiation from tumor recurrence. AJNR Am J Neuroradiol 2005; 26: 1455-60.

Badruddoja MA, Krouwer HG, Rand SD, Rebro KJ, Pathak AP, Schmainda KM. Antiangiogenic effects of dexamethasone in 9L gliosarcoma assessed by MRI cerebral blood volume maps. Neuro Oncol 2003; 5: 235-43.

Bartoli CR, Okabe K, Akiyama I, Coull B, Godleski JJ. Repeat microsphere delivery for serial measurement of regional blood perfusion in the chronically instrumented, conscious canine. J Surg Res 2008; 145: 135-41.

Bauman G, Pahapill P, Macdonald P, Fisher B, Leighton C, Cairncross G. Low grade glioma: a measuring radiographic response to radiotherapy. Can J Neurol Sci 1999; 26: 18-22.

Behin A, Hoang-Xuan K, Carpetier AF, Delattre JY. Primary brain tumours in adults. Lancet 2003; 361: 323-331.

Beppu T, Inoue T, Shibata Y, Kurose A, Arai H, Ogasawara K, et al. Measurement of fractional anisotropy using diffusion tensor MRI in supratentorial astrocytic tumors. J Neurooncol 2003; 63: 109-16.

Brasil Caseiras G, Thornton JS, Yousry T, Benton C, Rees J, Waldman AD, et al. Inclusion or Exclusion of Intratumoral Vessels in Relative Cerebral Blood Volume Characterization in Low-Grade Gliomas: Does It Make a Difference? AJNR Am J Neuroradiol 2008.

Bulakbasi N, Kocaoglu M, Ors F, Tayfun C, Ucoz T. Combination of single-voxel proton MR spectroscopy and apparent diffusion coefficient calculation in the evaluation of common brain tumors. AJNR Am J Neuroradiol 2003; 24: 225-33.

Burger PC, Bigner SH. Practical approaches to the diagnosis of central nervous system tumors. Mod Pathol 1988; 1: 493-511.

Calamante F, Thomas DL, Pell GS, Wiersma J, Turner R. Measuring cerebral blood flow using magnetic resonance techniques. J Cereb blood flow metab 1999; 19: 701-735.

Cha S. Perfusion MR imaging of brain tumors. Top Magn Reson Imaging 2004; 15: 279-89.

Cha S. Update on brain tumor imaging: from anatomy to physiology. AJNR Am J Neuroradiol 2006; 27: 475-87.

Cha S, Knopp EA, Johnson G, Wetzel SG, Litt AW, Zagzag D. Intracranial mass lesions: dynamic contrast- enhanced susceptibility- weighted echo- planar perfusion MR imaging. Radiology 2002; 223: 11-29.

Cha S, Tihan T, Crawford F, Fischbein NJ, Chang S, Bollen A, et al. Differentiation of low-grade oligodendrogliomas from low-grade astrocytomas by using quantitative blood-volume measurements derived from dynamic susceptibility contrast-enhanced MR imaging. AJNR Am J Neuroradiol 2005; 26: 266-73.

Chandler KL, Prados MD, Malec M, Wilson CB. Long-term survival in patients with glioblastoma multiforme. Neurosurgery 1993; 32: 716-20; discussion 720.

Chaskis C, Stadnik T, Michotte A, Van Rompaey K, D'Haens J. Prognostic value of perfusion-weighted imaging in brain glioma: a prospective study. Acta Neurochir (Wien) 2006; 148: 277-85; discussion 285.

Chen W. Clinical applications of PET in brain tumors. J Nucl Med 2007; 48: 1468-81.

Chenevert TL, Stegman LD, Taylor JM, Robertson PL, Greenberg HS, Rehemtulla A, et al. Diffusion magnetic resonance imaging: an early surrogate marker of therapeutic efficacy in brain tumors. J Natl Cancer Inst 2000; 92: 2029-36.

Chow KL, Gobin YP, Cloughesy T, Sayre JW, Villablanca JP, Vinuela F. Prognostic factors in recurrent glioblastoma multiforme and anaplastic astrocytoma treated with selective intra-arterial chemotherapy. AJNR Am J Neuroradiol 2000; 21: 471-8.

Claus EB, Horlacher A, Hsu L, Schwartz RB, Dello-Iacono D, Talos F, et al. Survival rates in patients with low-grade glioma after intraoperative magnetic resonance image guidance. Cancer 2005; 103: 1227-33.

Connor SE, Gunny R, Hampton T, O'Gorman R. Magnetic resonance image registration and subtraction in the assessment of minor changes in low grade glioma volume. Eur Radiol 2004; 14: 2061-6.

Coons SW, Johnson PC, Pearl DK. The prognostic significance of Ki-67 labeling indices for oligodendrogliomas. Neurosurgery 1997; 41: 878-84; discussion 884-5.

Danchaivijitr N, Waldman AD, Tozer DJ, Benton CE, Brasil Caseiras G, Tofts PS, et al. Low-grade gliomas: do changes in rCBV measurements at longitudinal perfusion-weighted MR imaging predict malignant transformation? Radiology 2008; 247: 170-8.

Daumas-Duport C, Tucker ML, Kolles H, Cervera P, Beuvon F, Varlet P, et al. Oligodendrogliomas. Part II: A new grading system based on morphological and imaging criteria. J Neurooncol 1997; 34: 61-78.

De Witte O, Levivier M, Violon P, Salmon I, Damhaut P, Wikler D, Jr., et al. Prognostic value positron emission tomography with [18F]fluoro-2-deoxy-D-glucose in the low-grade glioma. Neurosurgery 1996; 39: 470-6; discussion 476-7.

Dempsey MF, Condon BR, Hadley DM. Measurement of tumor "size" in recurrent malignant glioma: 1D, 2D, or 3D? AJNR Am J Neuroradiol 2005; 26: 770-6.

Devaux BC OFJ, Kelly PJ. . Resection, biopsy, and survival in malignant glial neoplasms: a retrospective study of clinical parameters, therapy, and outcome. J Neurosurg 1993: 767-775.

Di Chiro G, Oldfield E, Wright DC, De Michele D, Katz DA, Patronas NJ, et al. Cerebral necrosis after radiotherapy and/or intraarterial chemotherapy for brain tumors: PET and neuropathologic studies. AJR Am J Roentgenol 1988; 150: 189-97.

Dixon AK, Adam AN, Allison DJ, Grainger RG. Grainger and Allison's Diagnostic Radiology. 2007.

Donahue KM, Krouwer HG, Rand SD, Pathak AP, Marszalkowski CS, Censky SC, et al. Utility of simultaneously acquired gradient-echo and spin-echo cerebral blood volume and morphology maps in brain tumor patients. Magn Reson Med 2000; 43: 845-53.

Duffau H. New concepts in surgery of WHO grade II gliomas: functional brain mapping, connectionism and plasticity--a review. J Neurooncol 2006; 79: 77-115.

Dunn IF, Black PM. The neurosurgeon as local oncologist: cellular and molecular neurosurgery in malignant glioma therapy. Neurosurgery 2003; 52: 1411-22; discussion 1422-4.

Earnest Ft, Kelly PJ, Scheithauer BW, Kall BA, Cascino TL, Ehman RL, et al. Cerebral astrocytomas: histopathologic correlation of MR and CT contrast enhancement with stereotactic biopsy. Radiology 1988; 166: 823-7.

Eastwood JD, Lev MH, Wintermark M, Fitzek C, Barboriak DP, Delong DM, et al. Correlation of early dynamic CT perfusion imaging with whole-brain MR diffusion and perfusion imaging in acute hemispheric stroke. AJNR Am J Neuroradiol 2003; 24: 1869-75.

Ellika SK, Jain R, Patel SC, Scarpace L, Schultz LR, Rock JP, et al. Role of perfusion CT in glioma grading and comparison with conventional MR imaging features. AJNR Am J Neuroradiol 2007; 28: 1981-7.

Fuss M, Wenz F, Essig M, Muenter M, Debus J, Herman TS, et al. Tumor angiogenesis of low-grade astrocytomas measured by dynamic susceptibility contrast-enhanced MRI (DSC-MRI) is predictive of local tumor control after radiation therapy. Int J Radiat Oncol Biol Phys 2001; 51: 478-82.

Fuss M, Wenz F, Scholdei R, Essig M, Debus J, Knopp MV, et al. Radiation-induced regional cerebral blood volume (rCBV) changes in normal brain and low-grade astrocytomas: quantification and time and dose-dependent occurrence. Int J Radiat Oncol Biol Phys 2000; 48: 53-8.

Gilbert MR, Armstrong TS. Management of patients with newly diagnosed malignant primary brain tumors with a focus on the evolving role of temozolomide. Ther Clin Risk Manag 2007; 3: 1027-33.

Gilles FH, Brown WD, Leviton A, Tavare CJ, Adelman L, Rorke LB, et al. Limitations of the World Health Organization classification of childhood supratentorial astrocytic tumors. Children Brain Tumor Consortium. Cancer 2000; 88: 1477-83.

Grabb PA, Albright AL, Pang D. Dissemination of supratentorial malignant gliomas via the cerebrospinal fluid in children. Neurosurgery 1992; 30: 64-71.

Guo AC, Cummings TJ, Dash RC, Provenzale JM. Lymphomas and high- grade astrocytomas: comparison of water diffusibility and histologic characteristics. Radiology 2002; 224: 177-183.

Hakyemez B, Erdogan C, Ercan I, Ergin N, Uysal S, Atahan S. High-grade and low-grade gliomas: differentiation by using perfusion MR imaging. Clin Radiol 2005; 60: 493-502.

Hakyemez B, Yildiz H, Ergin N, Uysal S, Parlak M. [Flair and diffusion weighted MR imaging in differentiating epidermoid cysts from arachnoid cysts]. Tani Girisim Radyol 2003; 9: 418-26.

Hale SL, Alker KJ, Kloner RA. Evaluation of nonradioactive, colored microspheres for measurement of regional myocardial blood flow in dogs. Circulation 1988; 78: 428-34.

Hashizume H, Baluk P, Morikawa S, McLean JW, Thurston G, Roberge S, et al. Openings between defective endothelial cells explain tumor vessel leakiness. Am J Pathol 2000; 156: 1363-80.

Herholz K, Holzer T, Bauer B, Schroder R, Voges J, Ernestus RI, et al. 11C-methionine PET for differential diagnosis of low-grade gliomas. Neurology 1998; 50: 1316-22.

Higano S, Yun X, Kumabe T, Watanabe M, Mugikura S, Umetsu A, et al. Malignant astrocytic tumors: clinical importance of apparent diffusion coefficient in prediction of grade and prognosis. Radiology 2006; 241: 839-46.

Hochberg FH, Pruitt A. Assumptions in the radiotherapy of glioblastoma. Neurology 1980; 30: 907-11.

Hoffmann JN, Steinhagen S, Kast C, Scheuber HP, Jochum M, Gippner-Steppert C, et al. Chronic left heart catheterization for microvascular blood flow determination in the

rabbit: a minimally invasive technique using specially designed port devices. J Surg Res 2002; 102: 119-25.

Isselbacher KJ. Sugar and amino acid transport by cells in culture--differences between normal and malignant cells. N Engl J Med 1972; 286: 929-33.

Jackson RJ, Fuller GN, Abi-Said D, Lang FF, Gokaslan ZL, Shi WM, et al. Limitations of stereotactic biopsy in the initial management of gliomas. Neuro Oncol 2001; 3: 193-200.

Jäger HR, Caseiras GB, Rich PM. Grainger and Allison's Diagnostic Radiology, Chapter 56. 2007; 2: 1271-1294.

Jain RK, Munn LL, Fukumura D. Dissecting tumour pathophysiology using intravital microscopy. Nat Rev Cancer 2002; 2: 266-76.

Jenkinson MD, Du Plessis DG, Walker C, Smith TS. Advanced MRI in the management of adult gliomas. Br J Neurosurg 2007; 21: 550-61.

Jenkinson MD, Smith TS, Joyce KA, Fildes D, Broome J, du Plessis DG, et al. Cerebral blood volume, genotype and chemosensitivity in oligodendroglial tumours. Neuroradiology 2006; 48: 703-13.

Johannesen T, Langmark F, Lote K. Progress in long-term survival in adult patients with supratentorial low-grade gliomas: a population-based study of 993 patients in whom tumours were diagnosed between 1970 and 1993.

. J Neurosurg 2003: 854-862.

Jouanneau E. Angiogenesis and gliomas: current issues and development of surrogate markers. Neurosurgery 2008; 62: 31-50; discussion 50-2.

Kim L, Hochberg FH, Thornton AF, Harsh GRt, Patel H, Finkelstein D, et al. Procarbazine, lomustine, and vincristine (PCV) chemotherapy for grade III and grade IV oligoastrocytomas. J Neurosurg 1996; 85: 602-7.

Kleihues P, Burger P, BScheithaur. The new WHO classification of brain tumours. Brain Pathol 1993; 3: 255-268.

Kleihues P CW, eds. World Health Organisation Classification of Tumours: Pathology and genetics of tumours of the nervous system

Lyon: IRAC Press, 2000.

Kono K, Inoue Y, Nakayama K, Shakudo M, Morino M, Ohata K, et al. The role of diffusion-weighted imaging in patients with brain tumors. AJNR Am J Neuroradiol 2001a; 22: 1081-8.

Kono K, Inoue Y, Nakayama K, Shakudo M, Morino M, Ohata K, et al. The role of diffusion-weighted imaging in patients with brain tumors. AJNR Am J Neuroradiol 2001b; 22: 1081-8.

Krings T, Reinges MH, Thiex R, Gilsbach JM, Thron A. Functional and diffusion-weighted magnetic resonance images of space-occupying lesions affecting the motor system: imaging the motor cortex and pyramidal tracts. J Neurosurg 2001; 95: 816-24.

Kros JM, Pieterman H, van Eden CG, Avezaat CJ. Oligodendroglioma: the Rotterdam-Dijkzigt experience. Neurosurgery 1994; 34: 959-66; discussion 966.

Lacroix M, Abi-Said D, Fourney DR, Gokaslan ZL, Shi W, DeMonte F, et al. A multivariate analysis of 416 patients with glioblastoma multiforme: prognosis, extent of resection, and survival. J Neurosurg 2001; 95: 190-8.

Lai PH, Ho JT, Chen WL, Hsu SS, Wang JS, Pan HB, et al. Brain abscess and necrotic brain tumor: discrimination with proton MR spectroscopy and diffusion-weighted imaging. AJNR Am J Neuroradiol 2002; 23: 1369-77.

Langleben DD, Segall GM. PET in differentiation of recurrent brain tumor from radiation injury. J Nucl Med 2000; 41: 1861-7.

Law M. MR spectroscopy of brain tumors. Top Magn Reson Imaging 2004; 15: 291-313.

Law M, Oh S, Babb JS, Wang E, Inglese M, Zagzag D, et al. Low-grade gliomas: dynamic susceptibility-weighted contrast-enhanced perfusion MR imaging--prediction of patient clinical response. Radiology 2006a; 238: 658-67.

Law M, Oh S, Johnson G, Babb JS, Zagzag D, Golfinos J, et al. Perfusion magnetic resonance imaging predicts patient outcome as an adjunct to histopathology: a second reference standard in the surgical and nonsurgical treatment of low-grade gliomas. Neurosurgery 2006b; 58: 1099-107; discussion 1099-107.

Law M, Yang S, Wang H, Babb JS, Johnson G, Cha S, et al. Glioma grading: sensitivity, specificity, and predictive values of perfusion MR imaging and proton MR spectroscopic imaging compared with conventional MR imaging. AJNR Am J Neuroradiol 2003; 24: 1989-98.

Law M, Young R, Babb J, Pollack E, Johnson G. Histogram analysis versus region of interest analysis of dynamic susceptibility contrast perfusion MR imaging data in the grading of cerebral gliomas. AJNR Am J Neuroradiol 2007; 28: 761-6.

Le Bihan D. Looking into the functional architecture of the brain with diffusion MRI. Nat Rev Neurosci 2003; 4: 469-80.

Le Bihan D, Turner R, Douek P, Patronas N. Diffusion MR imaging: clinical applications. AJR Am J Roentgenol 1992; 159: 591-9.

Lee YC, Liu RS, Liao YC, Sun CM, Wang PS, Wang PN, et al. Statistical parametric mapping of brain SPECT perfusion abnormalities in patients with Alzheimer's disease. Eur Neurol 2003; 49: 142-5.

Leighton C, Fisher B, Bauman G, Depiero S, Stitt L, MacDonald D, et al. Supratentorial low-grade glioma in adults: an analysis of prognostic factors and timing of radiation. J Clin Oncol 1997; 15: 1294-301.

Lev MH, Ozsunar Y, Henson JW, Rasheed AA, Barest GD, Harsh GRt, et al. Glial tumor grading and outcome prediction using dynamic spin-echo MR susceptibility mapping compared with conventional contrast-enhanced MR: confounding effect of elevated rCBV of oligodendrogliomas [corrected]. AJNR Am J Neuroradiol 2004; 25: 214-21.

Levin VA, Hess KR, Choucair A, Flynn PJ, Jaeckle KA, Kyritsis AP, et al. Phase III randomized study of postradiotherapy chemotherapy with combination alpha-difluoromethylornithine-PCV versus PCV for anaplastic gliomas. Clin Cancer Res 2003; 9: 981-90.

Louis DN, Ohgaki H, Wiestler OD, Cavenee WK, Burger PC, Jouvet A, et al. The 2007 WHO classification of tumours of the central nervous system. Acta Neuropathol 2007; 114: 97-109.

Maia AC, Jr., Malheiros SM, da Rocha AJ, da Silva CJ, Gabbai AA, Ferraz FA, et al. MR cerebral blood volume maps correlated with vascular endothelial growth factor expression and tumor grade in nonenhancing gliomas. AJNR Am J Neuroradiol 2005; 26: 777-83.

Makowski EL, Meschia G, Droegemueller W, Battaglia FC. Measurement of umbilical arterial blood flow to the sheep placenta and fetus in utero. Distribution to cotyledons and the intercotyledonary chorion. Circ Res 1968; 23: 623-31.

Mandonnet E, Delattre JY, Tanguy ML, Swanson KR, Carpentier AF, Duffau H, et al. Continuous growth of mean tumor diameter in a subset of grade II gliomas. Ann Neurol 2003; 53: 524-8.

Margain D, Peretti-Viton P, Perez-Castillo AM, Martini P, Salamon G. Oligodendrogliomas. J Neuroradiol 1991; 18: 153-60.

Mariani L, Siegenthaler P, Guzman R, Friedrich D, Fathi AR, Ozdoba C, et al. The impact of tumour volume and surgery on the outcome of adults with supratentorial WHO grade II astrocytomas and oligoastrocytomas. Acta Neurochir (Wien) 2004; 146: 441-8.

McRobbie D, Moore E, Graves M, Prince M. MRI from Picture to Proton. 2005.

Medbery CA, 3rd, Straus KL, Steinberg SM, Cotelingam JD, Fisher WS. Low-grade astrocytomas: treatment results and prognostic variables. Int J Radiat Oncol Biol Phys 1988; 15: 837-41.

Melisko ME, Moore DH, Sneed PK, De Franco J, Rugo HS. Brain metastases in breast cancer: clinical and pathologic characteristics associated with improvements in survival. J Neurooncol 2008.

Merlet P, Mazoyer B, Hittinger L, Valette H, Saal JP, Bendriem B, et al. Assessment of coronary reserve in man: comparison between positron emission tomography with oxygen-15-labeled water and intracoronary Doppler technique. J Nucl Med 1993; 34: 1899-904.

Mihara F, Numaguchi Y, Rothman M, Sato S, Fiandaca MS. MR imaging of adult supratentorial astrocytomas: an attempt of semi-automatic grading. Radiat Med 1995; 13: 5-9.

Miles KA. Perfusion imaging with computed tomography: brain and beyond. Eur Radiol 2006; 16 Suppl 7: M37-43.

Moots PL. Pitfalls in the management of patients with malignant gliomas. Semin Neurol 1998; 18: 257-65.

MRCBT. Randomized trial of procarbazine, lomustine, and vincristine in the adjuvant treatment of high-grade astrocytoma: a Medical Research Council trial. J Clin Oncol. 2001; 19: 509–18.

Murakami R, Sugahara T, Nakamura H, Hirai T, Kitajima M, Hayashida Y, et al. Malignant supratentorial astrocytoma treated with postoperative radiation therapy: prognostic value of pretreatment quantitative diffusion-weighted MR imaging. Radiology 2007; 243: 493-9.

Nabavi DG, Cenic A, Craen RA, Gelb AW, Bennett JD, Kozak R, et al. CT assessment of cerebral perfusion: experimental validation and initial clinical experience. Radiology 1999; 213: 141-9.

Nelson SJ, Cha S. Imaging glioblastoma multiforme. Cancer J 2003; 9: 134-45.

Nitrini R, Buchpiguel CA, Caramelli P, Bahia VS, Mathias SC, Nascimento CM, et al. SPECT in Alzheimer's disease: features associated with bilateral parietotemporal hypoperfusion. Acta Neurol Scand 2000; 101: 172-6.

Osborn A. Diagnostic Neuroradiology. Vol 1. St Louis: Mosby- Year book, Inc, 1994.

Pallud J, Mandonnet E, Duffau H, Kujas M, Guillevin R, Galanaud D, et al. Prognostic value of initial magnetic resonance imaging growth rates for World Health Organization grade II gliomas. Ann Neurol 2006; 60: 380-3.

Patronas NJ, Di Chiro G, Brooks RA, DeLaPaz RL, Kornblith PL, Smith BH, et al. Work in progress: [18F] fluorodeoxyglucose and positron emission tomography in the evaluation of radiation necrosis of the brain. Radiology 1982; 144: 885-9.

Perry A. Oligodendroglial neoplasms: current concepts, misconceptions, and folklore. Adv Anat Pathol 2001 183-99.

Pierallini A, Bonamini M, Bozzao A, Pantano P, Stefano DD, Ferone E, et al. Supratentorial diffuse astrocytic tumours: proposal of an MRI classification. Eur Radiol 1997; 7: 395-9.

Pignatti F, van den Bent M, Curran D, Debruyne C, Sylvester R, Therasse P, et al. Prognostic factors for survival in adult patients with cerebral low-grade glioma. J Clin Oncol 2002; 20: 2076-84.

Plummer D. Dispimage: a display and analysis tool for medical images.

. Rev Neuroradiol 1992; 5

489-95.

.

Prayson RA, Mohan DS, Song P, Suh JH. Clinicopathologic study of forty-four histologically pure supratentorial oligodendrogliomas. Ann Diagn Pathol 2000; 4: 218-27.

Price SJ. The role of advanced MR imaging in understanding brain tumour pathology. Br J Neurosurg 2007; 21: 562-75.

Price SJ, Burnet NG, Donovan T, Green HA, Pena A, Antoun NM, et al. Diffusion tensor imaging of brain tumours at 3T: a potential tool for assessing white matter tract invasion? Clin Radiol 2003; 58: 455-62.

Price SJ, Jena R, Burnet NG, Hutchinson PJ, Dean AF, Pena A, et al. Improved delineation of glioma margins and regions of infiltration with the use of diffusion tensor imaging: an image-guided biopsy study. AJNR Am J Neuroradiol 2006; 27: 1969-74.

Price SJ, Jena R, Green HA, Kirkby NF, Lynch AG, Coles CE, et al. Early radiotherapy dose response and lack of hypersensitivity effect in normal brain tissue: a sequential dynamic susceptibility imaging study of cerebral perfusion. Clin Oncol (R Coll Radiol) 2007; 19: 577-87.

Provenzale JM, Mukundan S, Barboriak DP. Diffusion-weighted and perfusion MR imaging for brain tumor characterization and assessment of treatment response. Radiology 2006; 239: 632-49.

Reeves GI, Marks JE. Prognostic significance of lesion size for glioblastoma multiforme. Radiology 1979; 132: 469-71.

Ricci P. Imaging of adult brain tumors. Neuroimaging Clin North Am 1999; 9: 651-669.

Rosen BR, Belliveau JW, Buchbinder BB, McKinstry RC, Porkka LM, Kennedy DN, et al. Contrast agents and cerebral hemodynamics. Magn Reson Med 1991; 19: 285-292.

Rosen BR, Belliveau JW, Vevea JM, Brady TJ. Perfusion imaging with NMR contrast agents. Magn Reson Med 1990; 14: 249-265.

Rudolph AM, Heymann MA. The circulation of the fetus in utero. Methods for studying distribution of blood flow, cardiac output and organ blood flow. Circ Res 1967; 21: 163-84.

Ruseell D, Rubistein L. Pathology of Tumors of the Nervous System 1989.

Russell D, Rubistein L. Pathology of Tumors of the Nervous System 1989.

Sadeghi N, Camby I, Goldman S, Gabius HJ, Baleriaux D, Salmon I, et al. Effect of hydrophilic components of the extracellular matrix on quantifiable diffusion-weighted imaging of human gliomas: preliminary results of correlating apparent diffusion coefficient values and hyaluronan expression level. AJR Am J Roentgenol 2003; 181: 235-41.

Saha GB, MacIntyre WJ, Go RT. Radiopharmaceuticals for brain imaging. Semin Nucl Med 1994; 24: 324-49.

Salcman M, Scholtz H, Kaplan RS, Kulik S. Long-term survival in patients with malignant astrocytoma. Neurosurgery 1994; 34: 213-9; discussion 219-20.

Schaefer PW, Grant PE, Gonzalez RG. Diffusion-weighted MR imaging of the brain. Radiology 2000; 217: 331-45.

Schepers J, Veldhuis WB, Pauw RJ, de Groot JW, van Osch MJ, Nicolay K, et al. Comparison of FAIR perfusion kinetics with DSC-MRI and functional histology in a model of transient ischemia. Magn Reson Med 2004; 51: 312-20.

Scott JN, Brasher PM, Sevick RJ, Rewcastle NB, Forsyth PA. How often are nonenhancing supratentorial gliomas malignant? A population study. Neurology 2002; 59: 947-9.

Sheikine Y, Di Carli MF. Integrated PET/CT in the assessment of etiology and viability in ischemic heart failure. Curr Heart Fail Rep 2008; 5: 136-42.

Shweiki D, Itin A, Soffer D, Keshet E. Vascular endothelial growth factor induced by hypoxia may mediate hypoxia-initiated angiogenesis. Nature 1992; 359: 843-5.

Sinha S, Bastin ME, Whittle IR, Wardlaw JM. Diffusion tensor MR imaging of high-grade cerebral gliomas. AJNR Am J Neuroradiol 2002; 23: 520-7.

Smith JS, Chang EF, Lamborn KR, Chang SM, Prados MD, Cha S, et al. Role of extent of resection in the long-term outcome of low-grade hemispheric gliomas. J Clin Oncol 2008; 26: 1338-45.

Spampinato MV, Smith JK, Kwock L, Ewend M, Grimme JD, Camacho DL, et al. Cerebral blood volume measurements and proton MR spectroscopy in grading of oligodendroglial tumors. AJR Am J Roentgenol 2007; 188: 204-12.

Stewart LA. Chemotherapy in adult high-grade glioma: a systematic review and meta-analysis of individual patient data from 12 randomised trials. Lancet 2002; 359: 1011-8.

Sugahara T, Koroghi Y, Kochi M, Ikushima I, Hirai T, Okuda T, et al. Correlation of MR imaging-determined cerebral blood maps with histologic and angiographic determination of vascularity of gliomas. AJR Am J Roentgenol 1998; 171: 1479-1486.

Sugahara T, Korogi Y, Kochi M, Ikushima I, Shigematu Y, Hirai T, et al. Usefullness of diffusion- weighted MRI with echo- planar technique in the evaluation of cellularity in gliomas. J Magn Reson Imaging 1999a; 9: 53-60.

Sugahara T, Korogi Y, Kochi M, Ushio Y, Takahashi M. Perfusion- sensitive MR imaging of gliomas: comparison between gradient- echo and spin- echo echo- planar imaging techniques. AJNR Am J Neuroradiol 2001; 22: 1306-1315.

Sugahara T, Korogi Y, Shigematsu Y, Liang L, Yoshizumi K, Kitajima M, et al. Value of dynamic susceptibility contrast magnetic resonance imaging in the evaluation of intracranial tumors. Top Magn Reson Imaging 1999b; 10: 114-24.

Szeifert GT, Prasad D, Kamyrio T, Steiner M, Steiner LE. The role of the Gamma Knife in the management of cerebral astrocytomas. Prog Neurol Surg 2007; 20: 150-63.

Tofts P. Quantitative MRI of the brain. 2004.

Tozer DJ, Jager HR, Danchaivijitr N, Benton CE, Tofts PS, Rees JH, et al. Apparent diffusion coefficient histograms may predict low-grade glioma subtype. NMR Biomed 2006.

Tozer DJ, Jager HR, Danchaivijitr N, Benton CE, Tofts PS, Rees JH, et al. Apparent diffusion coefficient histograms may predict low-grade glioma subtype. NMR Biomed 2007; 20: 49-57.

Tzika AA, Astrakas LG, Zarifi MK, Zurakowski D, Poussaint TY, Goumnerova L, et al. Spectroscopic and perfusion magnetic resonance imaging predictors of progression in pediatric brain tumors. Cancer 2004; 100: 1246-56.

van den Bent MJ. Anaplastic oligodendroglioma and oligoastrocytoma. Neurol Clin 2007; 25: 1089-109, ix-x.

van den Bent MJ, Afra D, de Witte O, Ben Hassel M, Schraub S, Hoang-Xuan K, et al. Long-term efficacy of early versus delayed radiotherapy for low-grade astrocytoma and

oligodendroglioma in adults: the EORTC 22845 randomised trial. Lancet 2005; 366: 985-90.

Vick NA, Paleologos NA. External beam radiotherapy: hard facts and painful realities. J Neurooncol 1995; 24: 93-5.

Vlieger EJ, Majoie CB, Leenstra S, Den Heeten GJ. Functional magnetic resonance imaging for neurosurgical planning in neurooncology. Eur Radiol 2004; 14: 1143-53.

Watanabe M, Tanaka R, Takeda N. Magnetic resonance imaging and histopathology of cerebral gliomas. Neuroradiology 1992; 34: 463-9.

Wetzel SG, Cha S, Johnson G, Lee P, Law M, Kasow DL, et al. Relative cerebral blood volume measurements in intracranial mass lesions: interobserver and intraobserver reproducibility study. Radiology 2002; 224: 797-803.

White ML, Zhang Y, Kirby P, Ryken TC. Can tumor contrast enhancement be used as a criterion for differentiating tumor grades of oligodendrogliomas? AJNR Am J Neuroradiol 2005; 26: 784-90.

Wilms G, Demaerel P, Sunaert S. Intra-axial brain tumours. Eur Radiol 2005; 15: 468-84.

Wintermark M, Sesay M, Barbier E, Borbely K, Dillon WP, Eastwood JD, et al. Comparative overview of brain perfusion imaging techniques. Stroke 2005; 36: e83-99.

Wintermark M, Thiran JP, Maeder P, Schnyder P, Meuli R. Simultaneous measurement of regional cerebral blood flow by perfusion CT and stable xenon CT: a validation study. AJNR Am J Neuroradiol 2001; 22: 905-14.

Witwer BP, Moftakhar R, Hasan KM, Deshmukh P, Haughton V, Field A, et al. Diffusion-tensor imaging of white matter tracts in patients with cerebral neoplasm. J Neurosurg 2002; 97: 568-75.

Wong TZ, van der Westhuizen GJ, Coleman RE. Positron emission tomography imaging of brain tumors. Neuroimaging Clin N Am 2002; 12: 615-26.

Wood JR, Green SB, Shapiro WR. The prognostic importance of tumor size in malignant gliomas: a computed tomographic scan study by the Brain Tumor Cooperative Group. J Clin Oncol 1988; 6: 338-43.

Xu M, See SJ, Ng WH, Arul E, Back MF, Yeo TT, et al. Comparison of magnetic resonance spectroscopy and perfusion-weighted imaging in presurgical grading of oligodendroglial tumors. Neurosurgery 2005; 56: 919-26; discussion 919-26.

Yang D, Korogi T, Sugahara T, Kitajima M, Shigematsu Y, Liang L, et al. Cerebral gliomas: prospective comparison of multivoxel 2D chemical- shift imaging proton MR spectroscopy, echoplanar perfusion and diffusion- weighted MRI. Neuroradiol 2002; 44: 656-666.

Young R, Babb J, Law M, Pollack E, Johnson G. Comparison of region-of-interest analysis with three different histogram analysis methods in the determination of perfusion metrics in patients with brain gliomas. J Magn Reson Imaging 2007; 26: 1053-63.

Young RJ, Knopp EA. Brain MRI: tumor evaluation. J Magn Reson Imaging 2006; 24: 709-24.